# Particulate Matter and Gas Phase Emission Measurement of Aircraft Engine Exhaust

# Final Report (04/2012 – 11/2015)

June 2016

## Contributing institutes and authors

*Empa, Advanced Analytical Technologies/ETH Zurich, Institute of Environmental Engineering*

Benjamin Brem, Lukas Durdina, Ari Setyan, Yu-Ying Kuo, Yeon Kyoung Bahk, Jelena Buha, Jing Wang

*ETH Zurich, Institute of Environmental Engineering*

Zeqi Zhu, Melanie Vögtli, Florian Scherrer, Yaorui Hu

*ETH Zurich, Institute for Atmospheric and Climate Science*

Manuel Abegglen, Berko Sierau, Joel Corbin, Amewu Mensah, Ulrike Lohmann

*PSI, Laboratory of Atmospheric Chemistry*

Dogushan Kilic, Rujin Huang, André Prévôt, Jay Slowik, Martin Gysel, Urs Baltensperger

*Empa, Automotive Powertrain Technologies*

Anthi Liati, Daniel Schreiber, Panayotis Dimopoulos Eggenschwiler

*Empa, Air Pollution/ Environmental Technology*

Andrea Fisher

*Missouri University of Science and Technology, USA*

Prem Lobo, Steven Achterberg, Elizabeth Black, Max Trueblood, Don Hagen, Philip Whitefield

*SR Technics Switzerland AG*

Frithjof Siegerist, Peter Beyerle, Kevin Bruderer

*National Research Council, Canada*

Greg Smallwood, Kevin Thomson

*Aerodyne Research, USA*

Richard Miake-Lye, Zhenhong Yu

*Rolls Royce, UK*

Mark Johnson,

*Cardiff University, UK*

Andrew Crayford

*University of Manchester, UK*

Paul Williams

*University of Alberta, Canada*

Tyler Johnson, Jason Olfert

*General Electric Aviation,*

Sara Rocci-Denis, M. Gurhan Andac, Joseph Zelina

*SNECMA, France*

Olivier Penanhoat

*Environmental Protection Agency, USA*

John Kinsey

*AVL, Austria*

Michael Arndt, Barouch Giechaskiel

*Cambustion, UK*

Jonathan Symonds

Table of Contents

# 1. Introduction

Recent development of the non-volatile particulate matter (nvPM) emission standard by the International Civil Aviation Organization (ICAO) signals growing awareness of the aviation impacts. Currently aviation's contribution to global emission inventory of black carbon is estimated to be about 1% (Bond et al. 2004). Civil aviation traffic is growing rapidly, leading to ten times more people traveling by air nowadays than four decades ago. However, commercial aviation remains one of the least characterized man-made sources of air pollution (Masiol and Harrison 2014). The pollutants emitted during landing and take-off operations (LTO) affect the health of airport ground personnel as well as the air quality in the vicinity of airports (Yim et al. 2013, 2015; Schürmann et al. 2007). At cruise altitudes in the upper troposphere and lower stratosphere, jetliner emissions impact the climate and atmospheric environment on a global scale. Therefore, environmentally responsible aviation growth not only necessitates an understanding of the health and environmental impacts from aircraft emissions, but also a detailed quantification and potential reduction of emissions in the future.

We in collaboration with the Swiss Federal Office for Civil Aviation (FOCA) have built a world-unique system in an engine test cell of SR Technics near the Zürich airport. This system allows us to measure emissions from in-service commercial aircraft engines. Thus far our work mainly focused on: test and validate the AIR 6241 system and establish the repeatability and reliability of our measurements; obtain mass- and number- based nvPM EIs for a wide range of aircraft engines; characterize nvPM in terms of size, morphology, effective density and chemical composition; and measure the ICAO-regulated gaseous pollutants. Our study contributes significantly to the ICAO nvPM mass and number standard.

The FOCA project sponsored the international Aircraft Particle Regulatory Experiments (A-PRIDE) campaigns that have taken place at SR Technics (Table 1.1). Empa has become essential in administering and conducting these multi-institutional experiments since the project start in 2012. The early campaigns (A-PRIDE 3, 4, and 5) have focused on the development of the sampling methodology which contributed significantly to the published AIR 6241. The first commercially available sampling system prototype was also tested in a one week campaign (A-PRIDE 6). In 2014, the spatial distribution of emissions in the engine exit plane and the effects of increasing fuel aromatic content on nvPM mass and number emissions were studied (A-PRIDE 7) in a collaborative effort with General Electric and SNECMA. In the A-PRIDE 8 campaign in 2015, more experiments on the fuel aromatic content effects were performed and the volatile organic compounds (VOCs) in the engine exhaust were investigated. The organization and logistics in these dedicated test campaigns have been extensive and overall the campaigns have been more costly than estimated before the project start. However, in particular the help from SR Technics made them possible and overall the outcomes of these campaigns have been essential for the development of the nvPM sampling methodology as

well as for the regulatory agencies. Table 1.1 provides an overview of the campaigns Empa has participated in and their major contributions to research.

**Table 1.1. A-PRIDE campaigns at SR Technics participated by Empa**

| Campaign | Partner Institution(s) | Contributions | Publications/ Reports |
|---|---|---|---|
| **A-PRIDE 3 (SAMPLE III April and May 2012)** | Empa<br><br>SR Technics<br><br>FOCA<br><br>Cardiff University<br><br>University of Alberta<br><br>ETH Zürich<br><br>National Research Council of Canada (NRC) | Assessed the operating parameters of the draft sampling methodology. → Defined 1 µm as the cut off diameter for the cyclone.<br><br>Investigation of particle losses in sampling lines<br><br>   →  Line losses are dominated by diffusive losses of small particles<br><br>Intercomparison of non-volatile particle number instruments<br><br>   →  The lower CPC 50% cut-off diameter has been lowered to 10 nm from 23 nm that is used in the PMP program for vehicle emissions regulation | Crayford *et al.*, 2012<br><br>Johnson, T.J. *et al.* 2015<br><br>Corbin, J.C. *et al.*, 2014<br><br>Boies et al. 2015 |
| **A-PRIDE 4 (Nov. 2012)** | Empa<br><br>SR Technics<br><br>FOCA<br><br>ETH Zürich<br><br>Missouri University of Science and Technology<br><br>National Research Council of Canada (NRC) | Intercomparison of mass and number instruments<br><br>   →  Identified photo-acoustic and laser induced incandescence as the two measurement technologies that will be considered in the proposed standard<br><br>Particle effective density measurements<br><br>   →  The density is strongly dependent on particle size | Lobo et al. 2015 |
| **A-PRIDE 5 (Aug. 2013)** | Empa<br><br>SR Technics<br><br>FOCA<br><br>ETH Zürich<br><br>PSI<br><br>Missouri University of Science and Technology<br><br>Cardiff University<br><br>NRC | Calibration of non-volatile mass instrumentation<br><br>   →  Instruments agree within 10% for diffusion flame soot and with the NIOSH 5040 protocol<br><br>Three systems intercomparison<br><br>   →  Mass instruments agree within 25% and number instruments within 15% for the same engine condition<br><br>Certification like run according to draft standard<br><br>   →  Dependence of nvPM emissions on ambient temperature observed<br><br>Filter measurements for OC/EC and metals (ash) | Durdina *et al.*, 2014<br><br>Liati *et al.*, 2014<br><br>Johnson et al. 2015<br><br>Durdina et al. 2016<br><br>Abegglen et al. 2015 |
| **A-PRIDE 6 (Oct. 2013)** | Empa<br><br>SR Technics<br><br>FOCA<br><br>AVL Graz Inc. | Intercomparison with a prototype of a commercial nvPM mass and number measurement system | Results presented at SAE-E31 meeting, 2013 |

| A-PRIDE 7 (Oct. 2014) | Empa<br>SR Technics<br>FOCA<br>ETH Zürich<br>PSI<br>GE<br>SNECMA | Exhaust plane mapping of emissions<br><br>➜ nvPM mass and number can vary by a factor of two depending on location in the engine exit plane, (data analysis not finished)<br><br>Emissions sensitivity to fuel aromatic content<br><br>➜ nvPM emissions correlate well with fuel hydrogen content | Abegglen et al. 2016<br>Brem et al. 2015 |
|---|---|---|---|
| A-PRIDE 8 (Oct. 2015) | Empa<br>SR Technics<br>ETH Zürich | Characterize engine thrust resolved volatile (VOCs) emissions<br><br>Assess nvPM and VOC emissions sensitivity to fuel aromatic content at engine thrusts below 30%<br><br>Perform a LII instrument applicability check as described in the draft ICAO Annex 16 Appendix 7<br><br>Perform mapping measurement to verify spatial nvPM heterogeneity in exhaust observed in A-PRIDE 7. | Two manuscripts under preparation |

Besides these dedicated campaigns, the exhaust sampling infrastructure has also been used to measure emissions from engines that had a service at SR Technics in so called "piggy-back runs". These runs have been critical for developing and testing sampling procedures intended for the dedicated A-PRIDE campaigns.

# 2. Activities and results in the period 2012/04 – 2012/06 (including A-PRIDE 3/SAMPLE III)

## 2.1. Introduction

A dedicated measurement campaign was carried out from April 17 to May 6, 2012. It was referred to as the SAMPLE III campaign at the time and also known as the A-PRIDE 3 campaign following the convention established later. The campaign successfully compared the Swiss sampling system with the SAMPLE III sampling system, and provided substantial data for particle number and mass measurement in aircraft engine exhaust. Representative results are summarized here and a detailed report of the campaign is available (Crayford et al. 2012).

The participants of SAMPLE III measurement campaign included FOCA, EMPA, ETH Zurich, Rolls Royce plc, Cardiff University, Deutsches Zentrum für Luft- und Raumfahrt e.V., Onera, University of Manchester, Manchester Metropolitan University and Sheffield University. Financial support was mainly from FOCA and EASA (European Aviation Safety Agency). The main objectives of the campaign is to verify the practicability and robustness of the working draft on non-volatile particulate matter (nvPM) AIR (Aerospace Information Report) methodology defined by the SAE E-31 Committee. Following activities were performed during the campaign.

- Assessed the operating parameters of the draft sampling methodology.
- Performed repeated simultaneous penetration measurements using mass and size distribution (with and without volatile removal) instrumentation. (Placed and operated same types of instrument at inlet of nvPM line inside the engine test cell).
- Repeated inter-comparison of two systems for uncertainty analysis.
- Assessment of size cut-off specifications using the newly agreed condensation particle counter (CPC) size cut-off curve and calibration method with CPCs from different manufacturers.
- Assessment of line length influence downstream of first dilutor 12.5 vs 25 m.
- Characterising volatile removal performance of catalytic stripper methodology (OC/EC (organic carbon/elemental carbon) and AMS (Aerosol Mass Spectrometer) measurements).
- Intercomparison of various PM size measurement techniques on engine exhaust and using a carbon particle generator.
- Carbon particle generator based comparison of the CPCs, calibrated by manufacturers to latest E-31 specifications.
- Lab-based assessment of catalytic stripper efficiency using volatile coated carbon particles.

## 2.2. Sampling system intercomparison
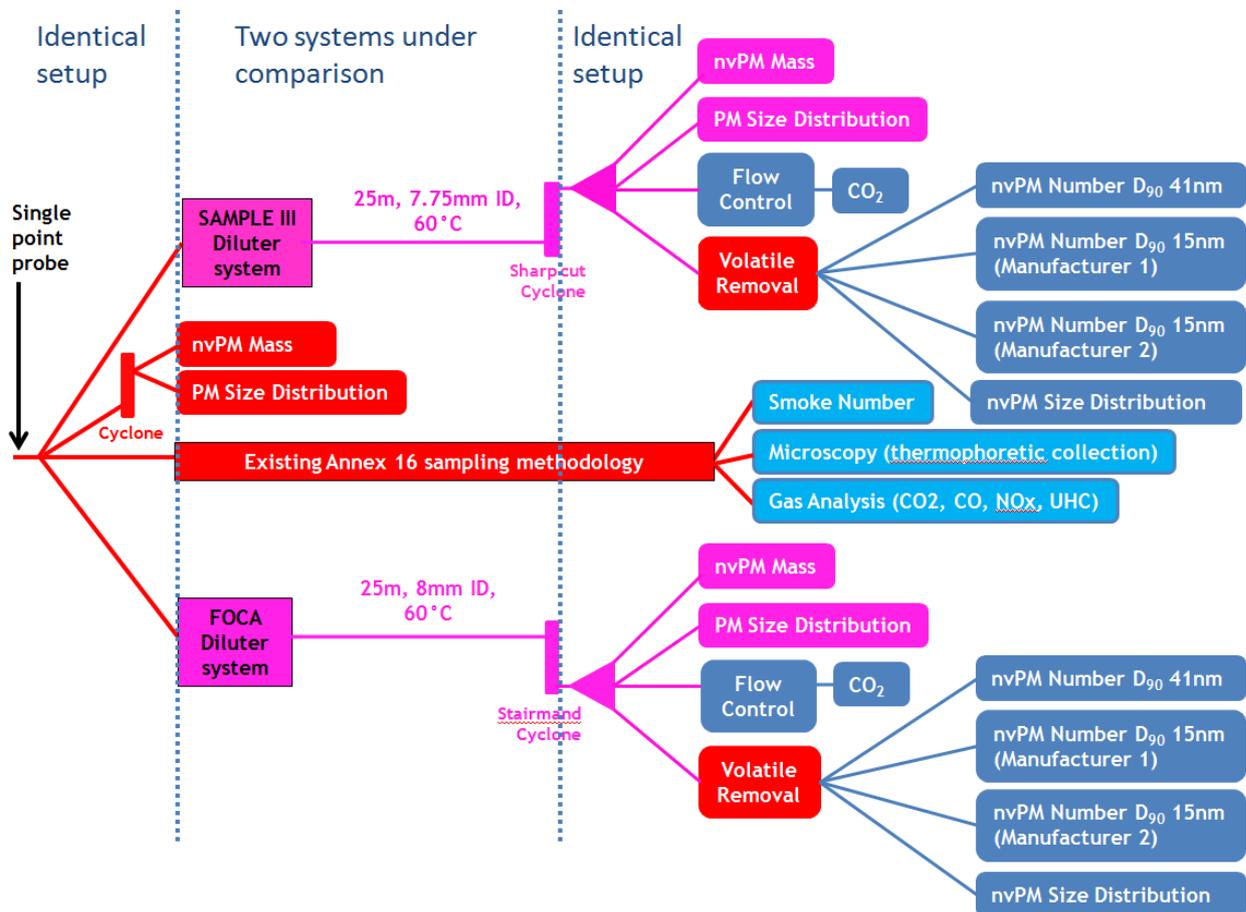


**Figure 2.1. Schematic for the sampling system intercomparison study.**

Figure 2.1 shows the schematic for the sampling system intercomparison study. After the single point sampling probe behind the engine exhaust, the sample flow is divided into several streams. The stream in the Annex 16 line allows measurement of the smoke number, collection for microscopy, and gas ($CO_2$, CO, $NO_x$, unburned hydrocarbon UHC) analysis. Instruments measuring the nvPM mass and size distribution were deployed on the gantry. The major comparison was performed between the SAMPLE III and FOCA sampling systems. The two systems shared similar diluter systems, transport lines, and nvPM instruments. Figures 2.2 – 2.4 show photos of sampling system.
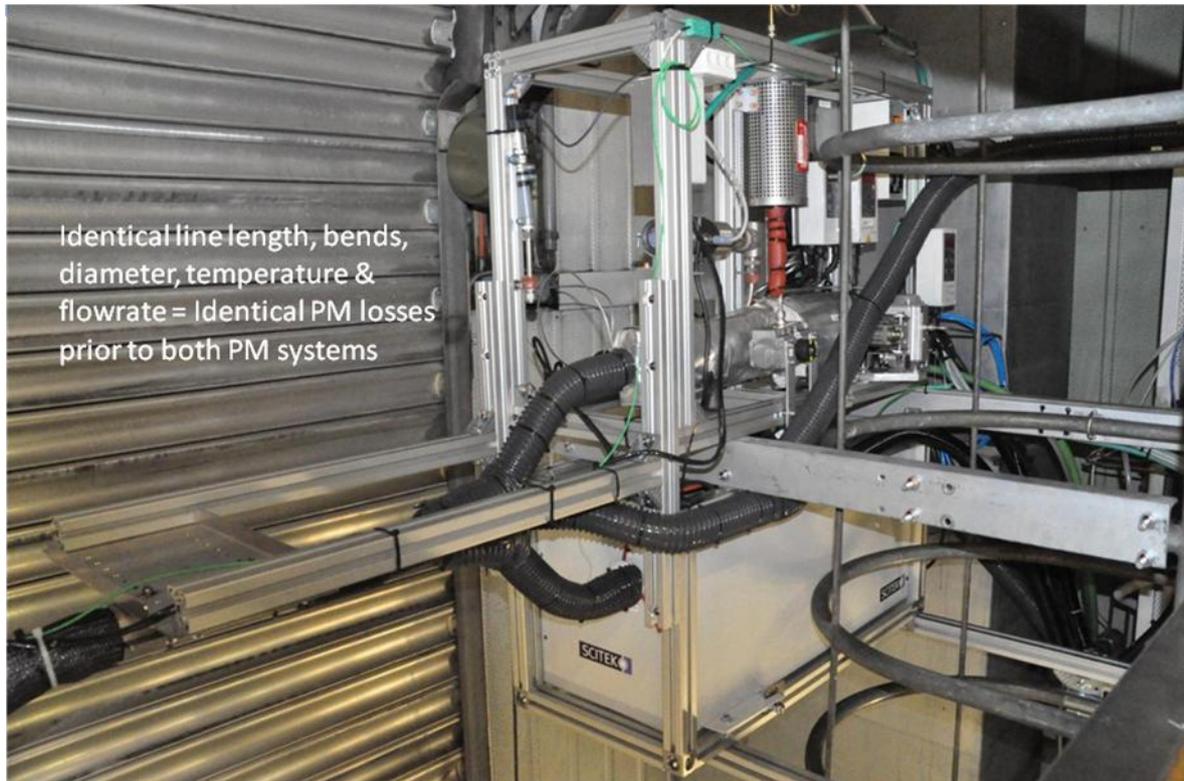
**Figure 2.2. The two diluter systems.**
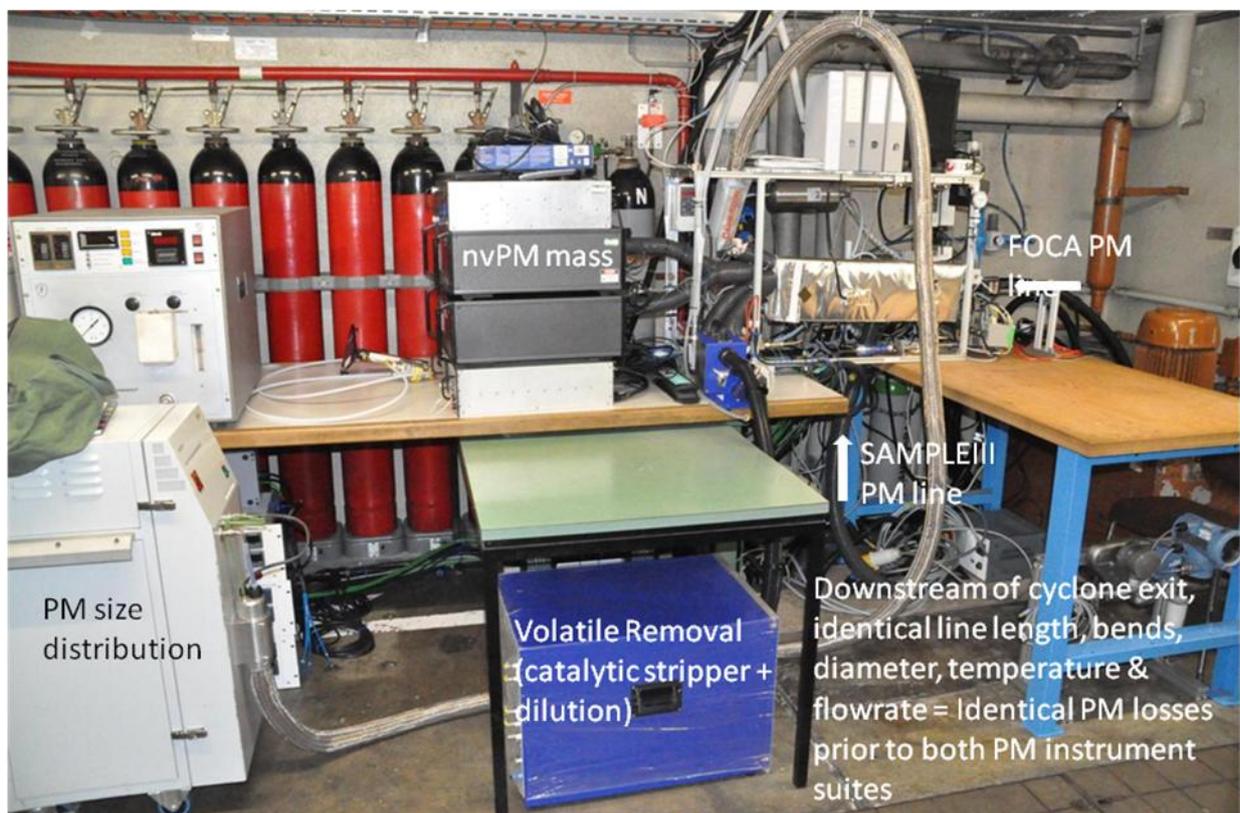


**Figure 2.3. Part of nvPM measurement instruments.**

**Figure 2.4. Annex 16 instrumentation for gas analysis and smoke number.**

Comparison of the two sampling systems was successfully carried out. Figures 2.5 and 2.6 show the nvPM number and mass concentrations respectively, measured on the two sampling systems. The engine condition was stabilized for 5 minutes, followed by 15-minute measurement. It can be seen that the two curves representing the results on the two lines follow each other closely at all the engine conditions. It appears that the concentrations on the FOCA line are consistently higher than that on the SAMPLEIII line.
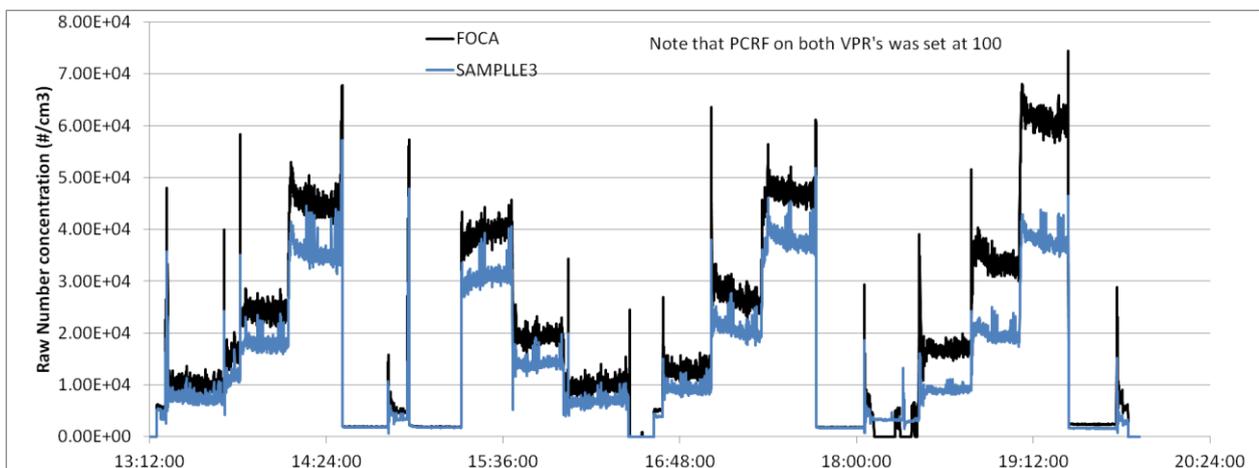


**Figure 2.5. The raw number concentration of nvPM at different engine conditions measured on the FOCA and SAMPLEIII lines.**
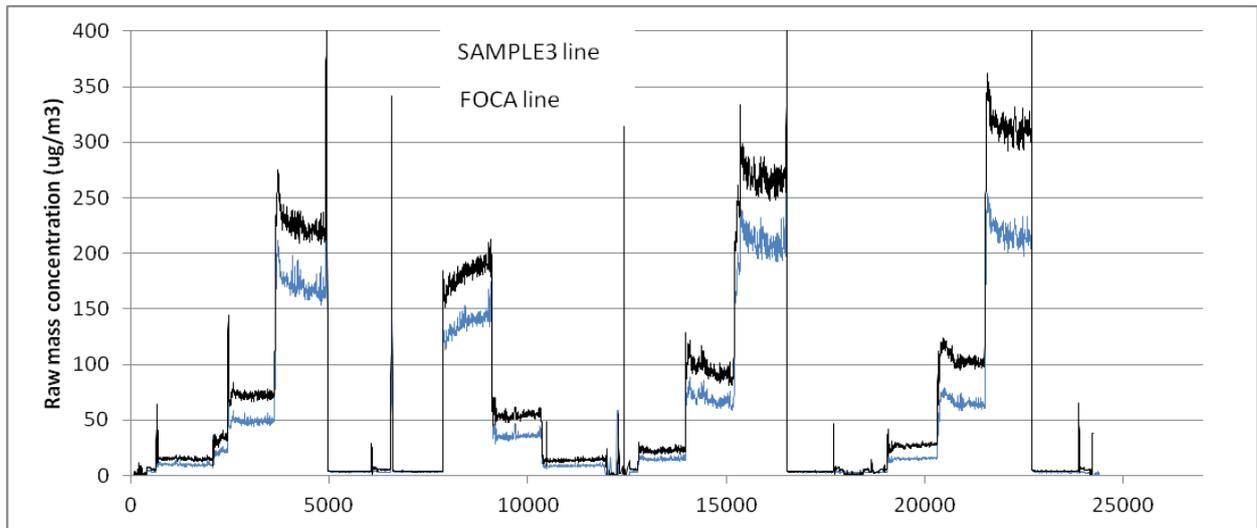
**Figure 2.6. The raw number concentration of nvPM at different engine conditions measured on the FOCA and SAMPLEIII lines.**

## 2.3. Engine source and smoke number (SN)

The selected engine was an excellent source for nvPM system and instrumentation tests. The engine delivered selectable large range of stable nvPM mass and number concentrations at moderate fuel consumption. Its Double Annular Combustor (DAC) provided two burn modes with extremely low nvPM emissions at medium to high thrust, allowing testing the system with very low emissions levels expected for some future engine technologies. Figure 2.7 shows that the SN ranged from 0 to 20 during engine runs.
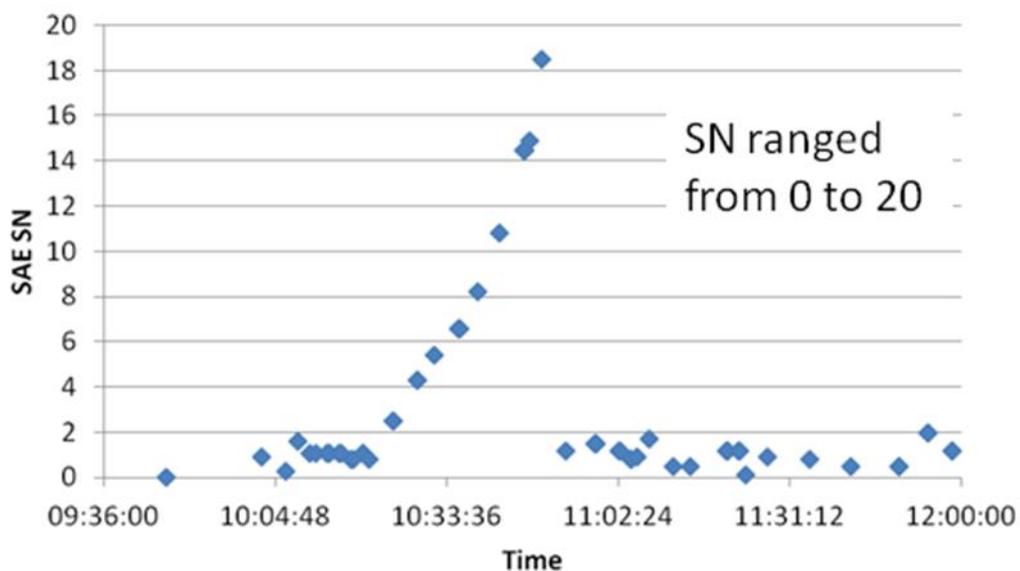


**Figure 2.7. The smoke number results during engine runs.**

## 2.4. Ramp test and nvPM measurement

The fuel flow for the engine was ramped up, which provided the opportunity to find and set four nvPM measurement points. Figure 2.8 shows the fuel flow and combustor inlet temperature during the ramp test. Figures 2.9 and 2.10 show the nvPM number and mass concentrations during the ramp test respectively. It can be seen that with increasing fuel flow, the combustor inlet temperature and the nvPM concentrations increase.  Four measurement points are indicated on Figure 2.8 for possible nvPM measurement: L (low nvPM), ML (medium/low nvPM), MH (medium/high nvPM) and H (high nvPM).
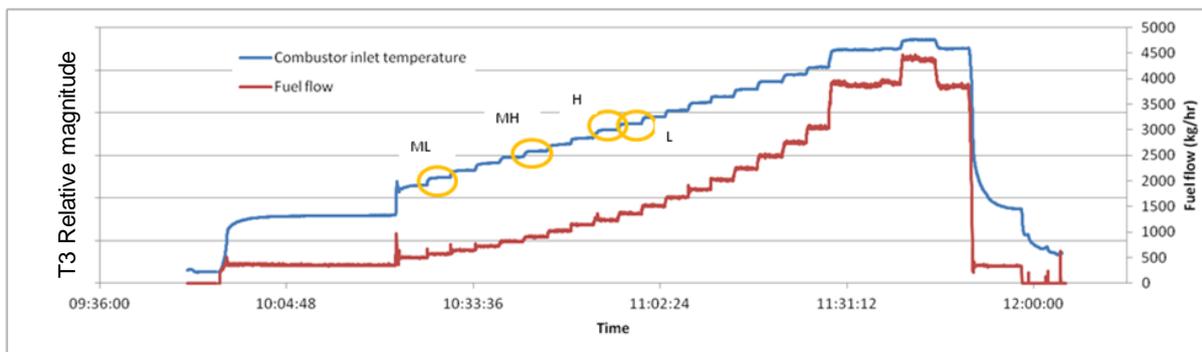


**Figure 2.8. The fuel flow and combustor inlet temperature during the ramp test.**
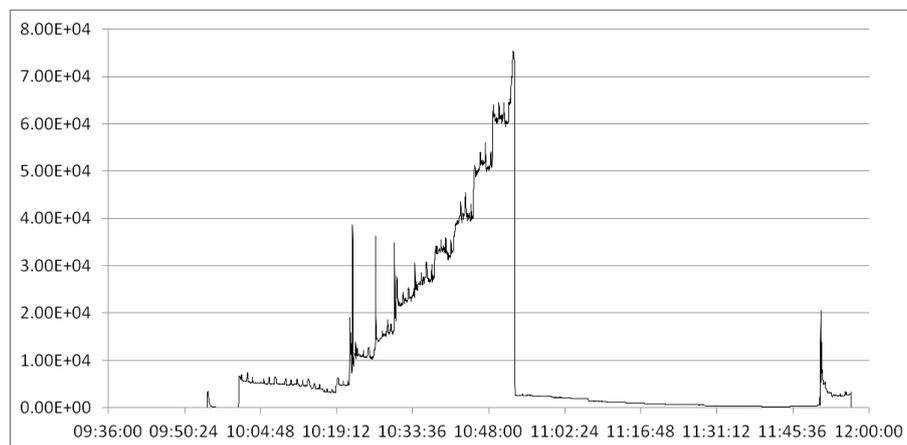


**Figure 2.9. The number concentration (#/cm$^3$) of nvPM during the ramp test.**
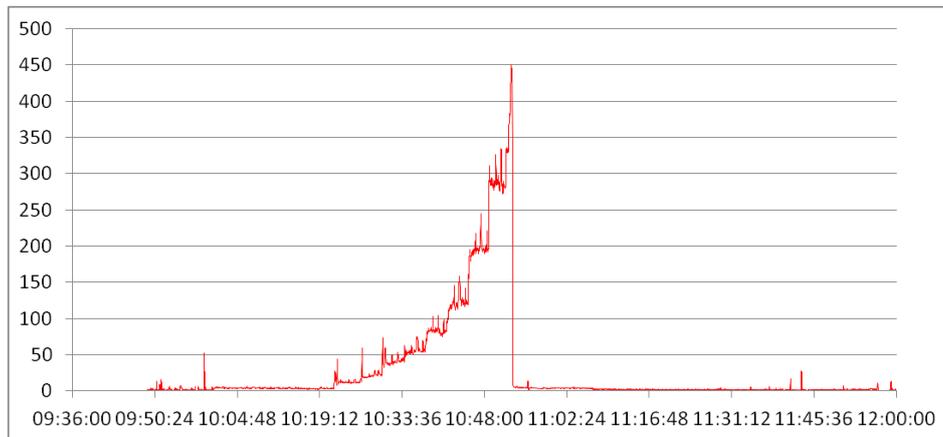
**Figure 2.10. The mass concentration (µg/cm³) of nvPM during the ramp test.**

The particle number-size distribution measured at multiple points during the ramp test is shown in Figure 2.11. The different measurements reflect the increasing nvPM concentrations during the ramp test. Most of the distribution curves show two distinct peaks, one around 10 nm and the other around 30 nm. All the particles are believed to be non-volatile because of the measurement method. It is possible that the 10 nm peak represents primary soot particles, and the 30 nm peak represents soot agglomerates. Electron microscopic images of the soot agglomerates can be seen in Section 2.10. Further measurement and electron microscopic studies will be needed to verify the hypothesis.
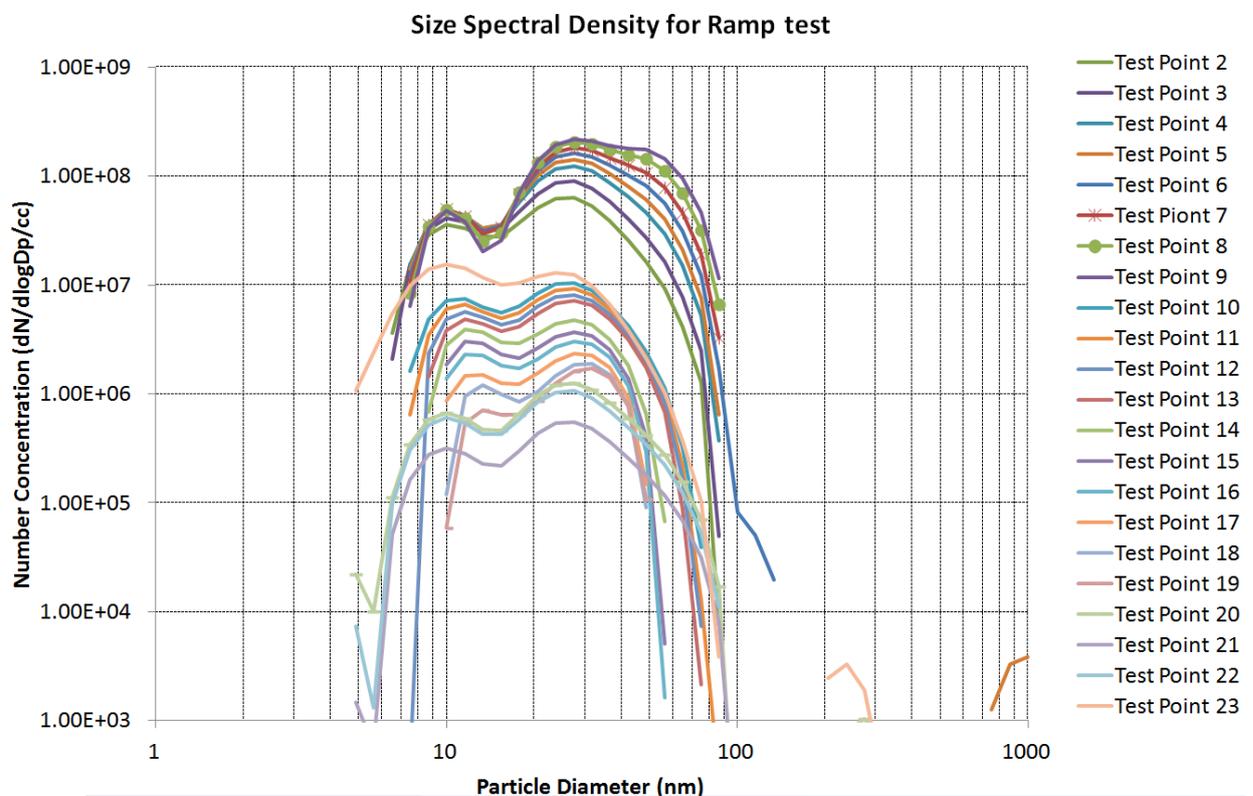


**Figure 2.11. The particle number-size distribution measured at multiple points during the ramp test.**

## 2.5. Catalytic stripper (CS) experiment for volatile particle removal

Filter samples were taken upstream and downstream by University of Cambridge catalytic stripper operated at 8 L/min. Pre-fired quartz filters were used for sample collection at temperature of 60°C. Elemental carbon/organic carbon (EC/OC) filters were analyzed using the EUSAAR_2 protocol and the optical transmittance correction procedures covered by UKAS accreditation. Results were corrected for dynamic blank concentrations – but these values were high (0.8 – 1.98 $\mu g/cm^2$). The European guidance document CEN/TR 16243:2011 states that "typical field blank values are up to 4 $\mu g$ OC/$cm^2$". Mass concentrations shown are averaged for each test condition with standard deviation uncertainty estimates. EC mass concentrations were corrected for solid particle loss in the catalytic stripper. The results shown here were under different engine conditions and they are described qualitatively using relative nvPM concentration.
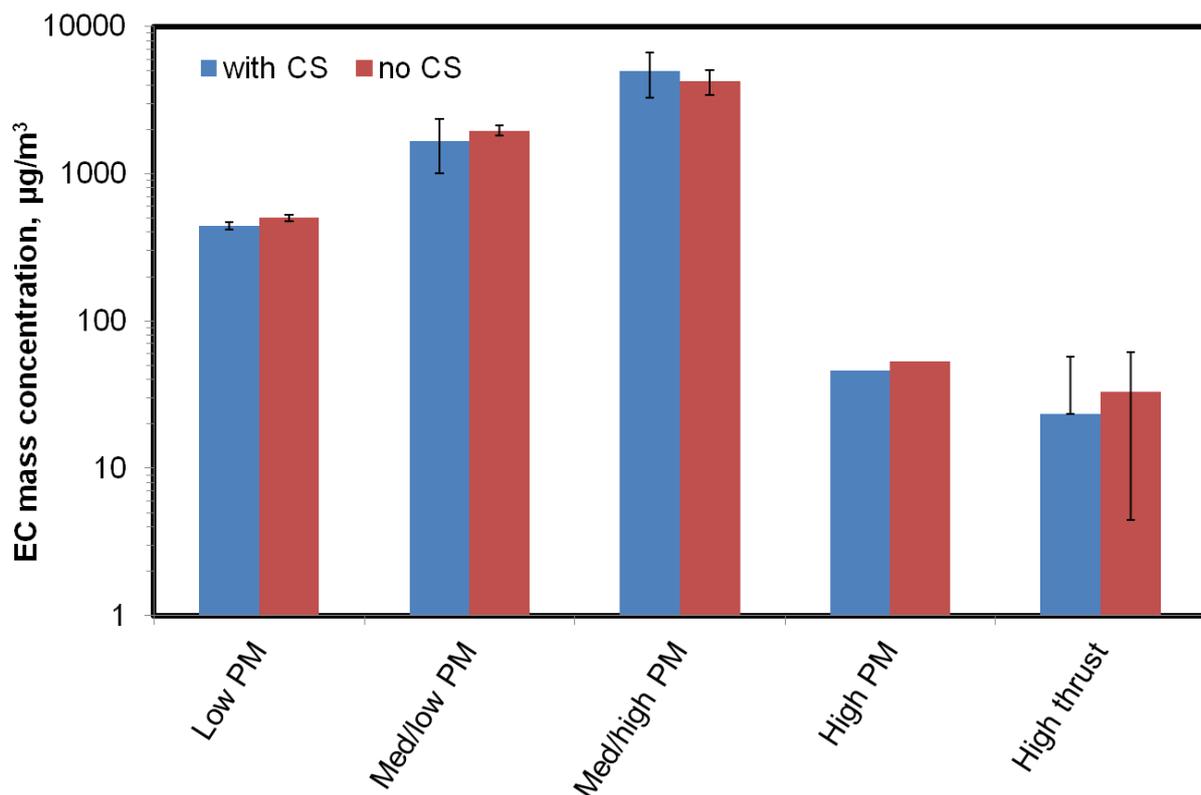


**Figure 2.12. Comparison of the EC mass concentration with and without the CS.**

Figure 2.12 shows the EC mass concentration measured on samples with and without the CS. The differences between them are within the experimental uncertainties under all engine conditions. Figure 2.13 shows the OC mass concentration with and without the CS. All OC values with the CS were

less than zero after blank correction. Thus the results demonstrate the CS removed essentially all the OC whereas it did not change the results on EC measurement. Figure 2.14 shows the EC fraction with and without the CS. The EC fraction was 100% with the CS since all the OC was removed. The EC fraction without the CS varies significantly with the engine condition. It appeared that the EC fraction did not change monotonically with the relative nvPM concentration. The lowest EC fraction was observed under the high thrust engine condition for the tested engine with staged combustion. More studies are needed to fully understand these results.
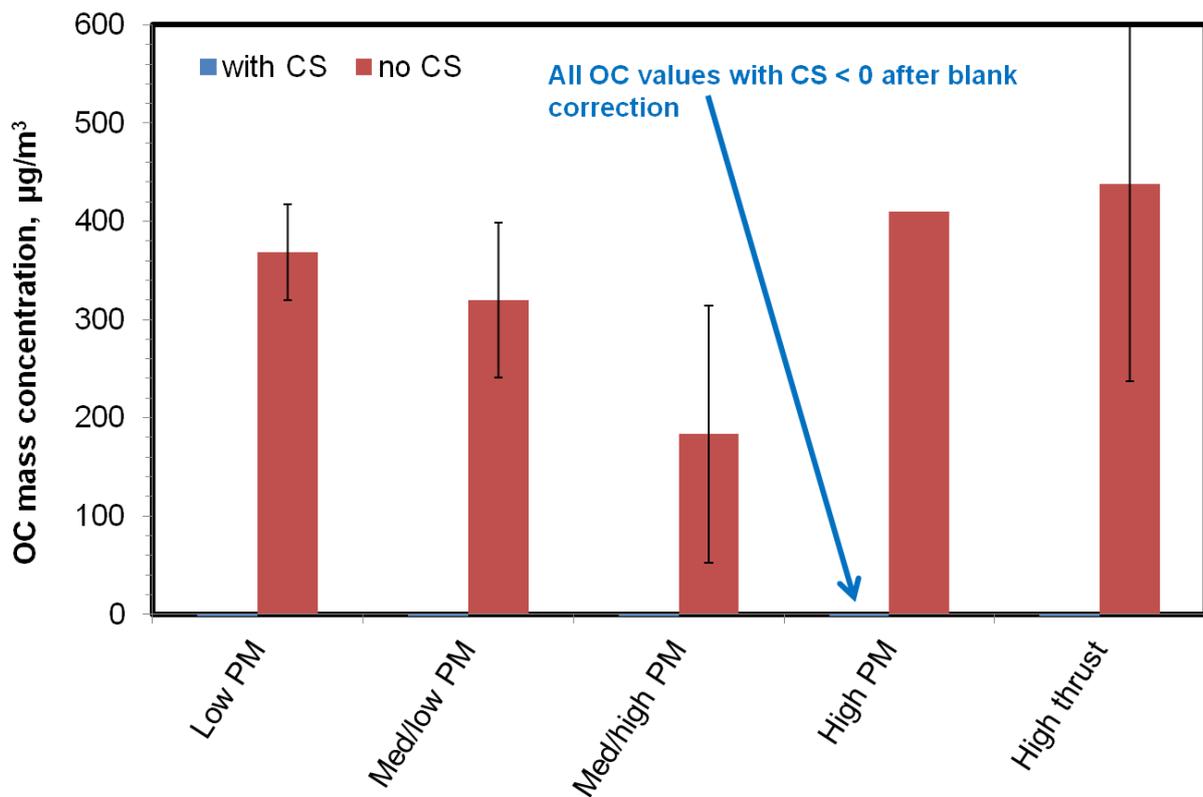


**Figure 2.13. Comparison of the OC mass concentration with and without the catalytic CS.**
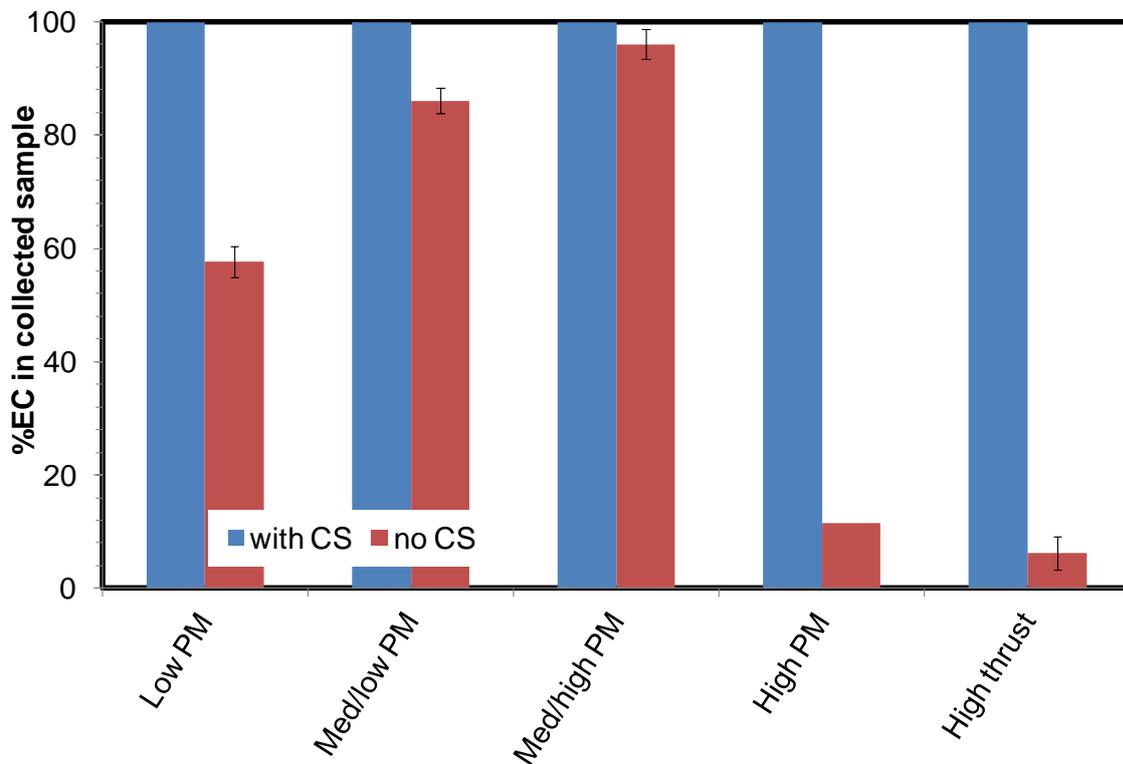
**Figure 2.14. Comparison of the EC fraction with and without the CS.**

## 2.6. Comparison of condensation particle counters (CPCs)

Six CPCs of three different types (2 TSI 3775, 2 TSI 3776 and 2 Grimm) were compared using carbon particles generated by a PALAS Spark Generator. The particle size of 50% counting efficiency is 2.5 nm for TSI 3776, 4 nm for TSI 3775 and Grimm CPC. The ratios of five CPCs to the standard CPC TSI 3776 are plotted in Figure 2.15. The values of the ratios are within the range of about 0.8 to 1.0. As a reference, the specification for TSI 3775 in the single particle counting mode is ±10% error, and in the photometric mode is ±20% error. The comparison results for 2 TSI 3775 and 2 Grimm CPCs during engine runs are shown in Figures 2.16 and 2.17. Four different engine conditions (medium/low, medium/high, high and low nvPM) were used. The raw data are shown in Figure 18 and the data after normalization and dilution correction are shown in Figure 19. It can be seen that the agreement of the two CPCs on the SAMPLE III line was good, whereas the agreement of the two CPCs on the FOCA line was not satisfactory. The CPCs are being checked to identify the reason for the discrepancy.
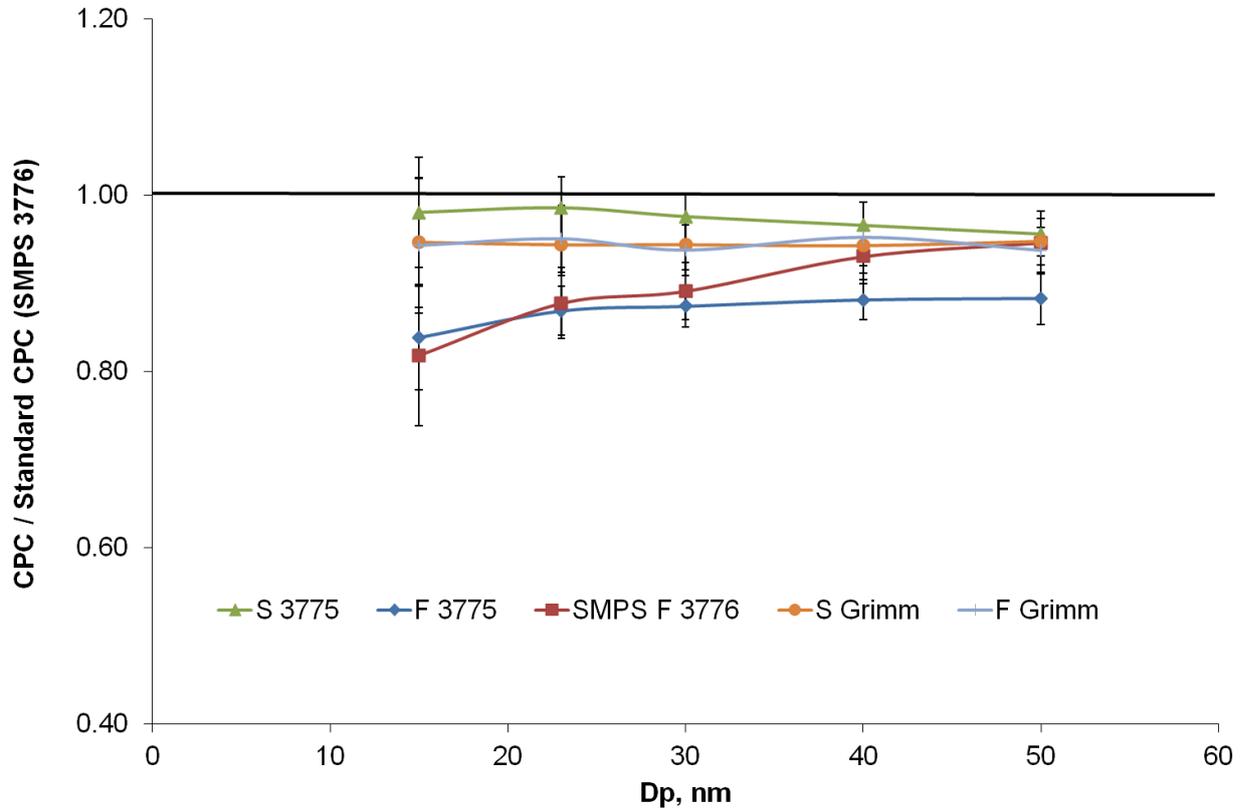
**Figure 2.15. Comparison of the CPCs using carbon particles generated by a PALAS Spark Generator. The designation of "S" in the figure indicates that the CPC was used on the SAMPLE III line, and "F" indicates that the CPC was used on the FOCA sampling line.**
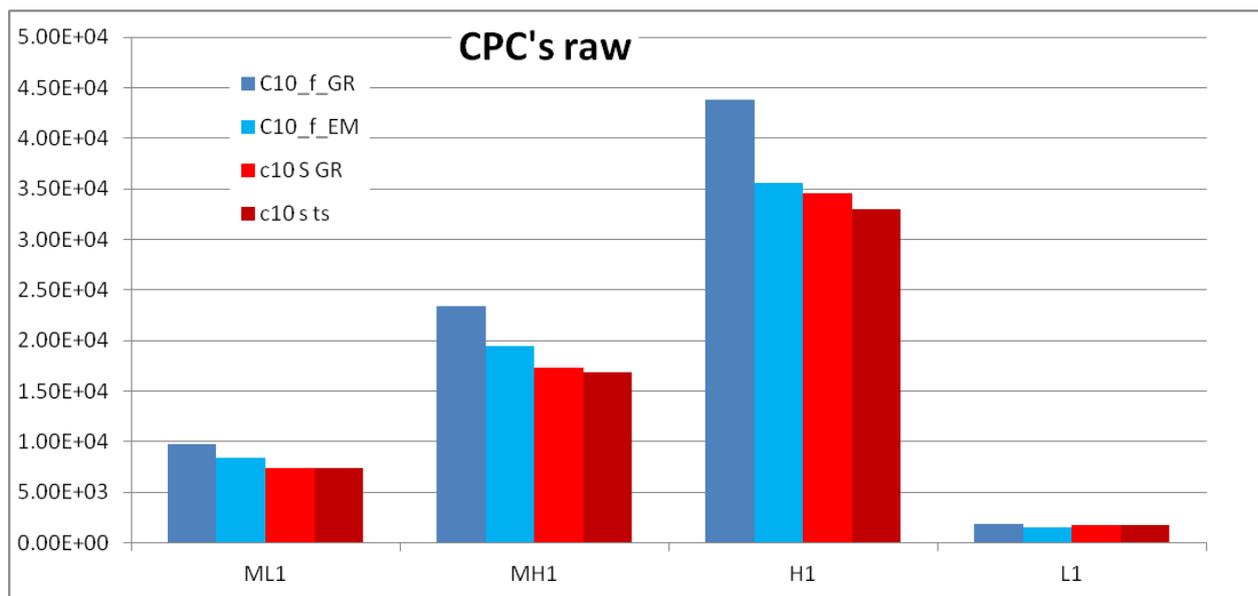


**Figure 2.16. Comparison of the CPC raw data under four different engine conditions (medium/low, medium/high, high and low nvPM). The four CPCs were Grimm CPCs on the**

**FOCA line (C10_f_GR) and SAMPLE III line (c10 S GR), and TSI 3775 CPCs on the FOCA line (C10_f_EM) and SAMPLE III line (c10 s ts).**
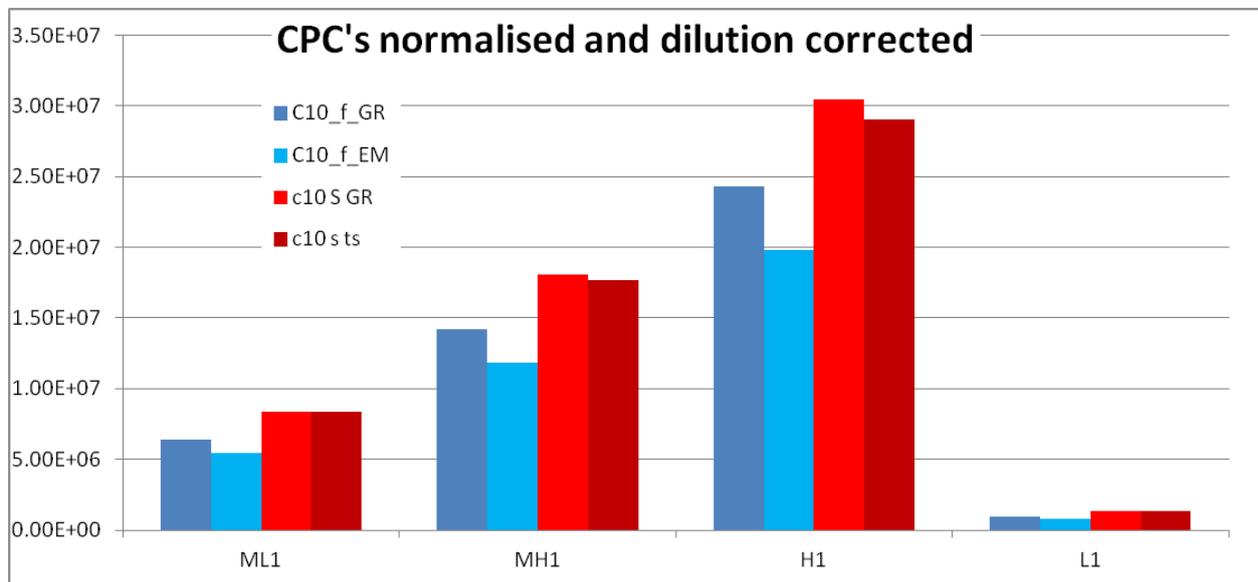


Figure 2.17. Comparison of the CPC data after normalization and dilution correction under four different engine conditions (medium/low, medium/high, high and low). The four CPCs were Grimm CPCs on the FOCA line (C10_f_GR) and SAMPLE III line (c10 S GR), and TSI 3775 CPCs on the FOCA line (C10_f_EM) and SAMPLE III line (c10 s ts).

## 2.7. Effect of the transport line

The effect of the transport line from the diluter system to the cyclone (Figure 1.1) was investigated. Two different line lengths, 12.5 m and 25 m were used. Figure 2.18 and 2.19 show the mass and number concentrations of nvPM, respectively. Three different lines are compared, 25 m on the SAMPLE III line (S 25 m), 25 m on the FOCA line (F 25 m) and 12.5 m on the FOCA line (F 12 m). Comparison between the 25 m and 12.5 m lines on the FOCA line shows that the shorter line resulted in a 5 – 7 % increase in nvPM mass, and a 20 – 25% increase in nvPM number.
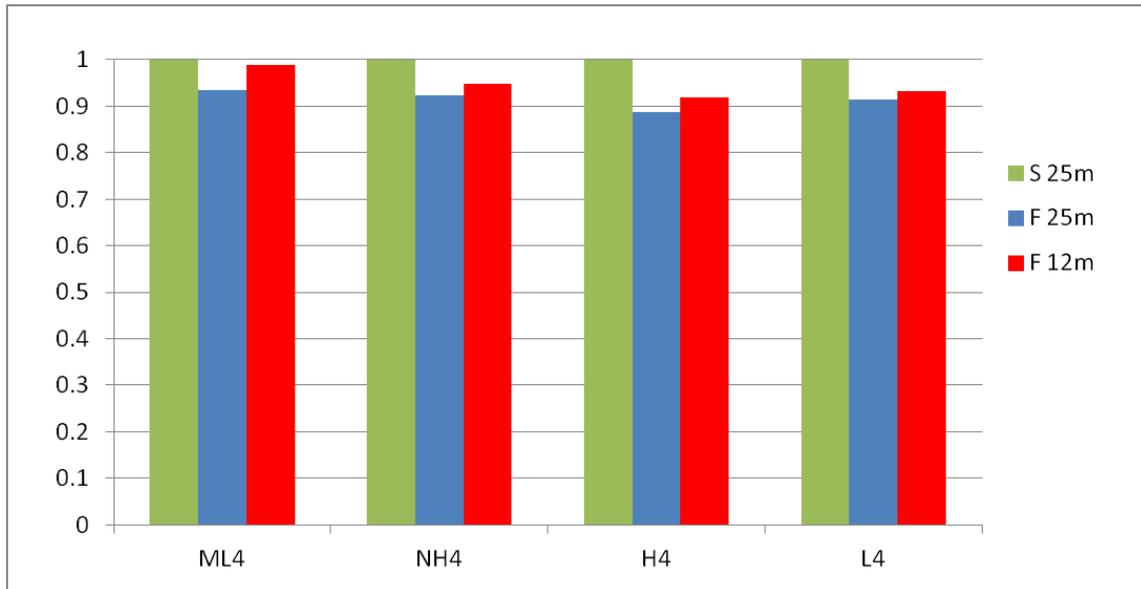
**Figure 2.18. Comparison of the mass concentration of nvPM measured using different transport lines: 25 m on the SAMPLE III line (S 25 m), 25 m on the FOCA line (F 25 m) and 12.5 m on the FOCA line (F 12m). The values are normalized by that of the 25 m transport line on the SAMPLE III line.**
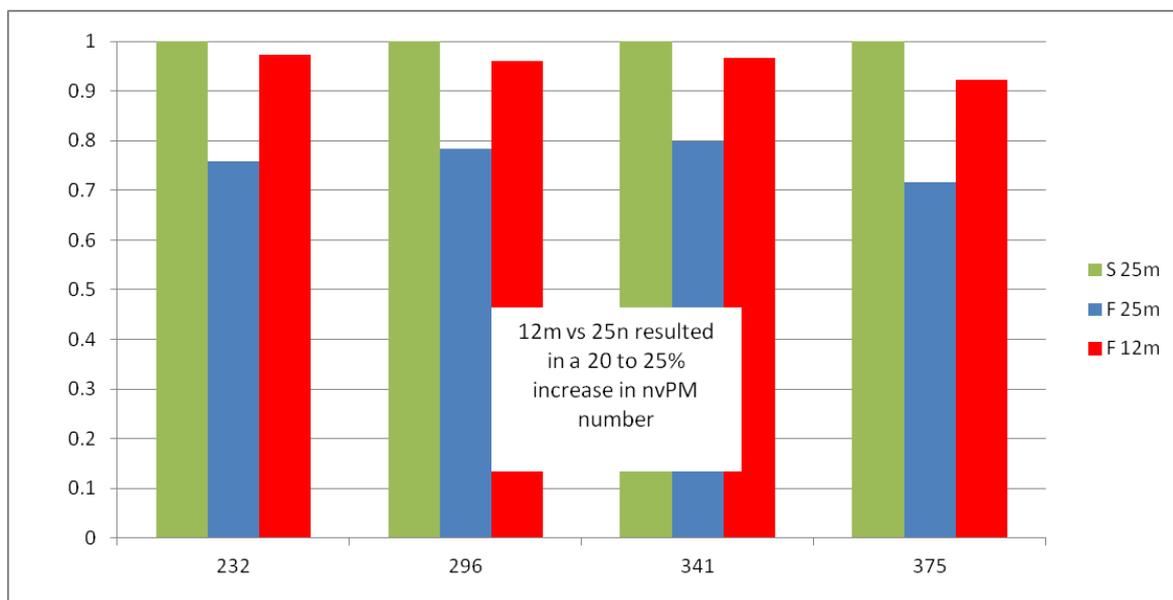


**Figure 2.19. Comparison of the number concentration of nvPM measured using different transport lines: 25 m on the SAMPLE III line (S 25 m), 25 m on the FOCA line (F 25 m) and 12.5 m on the FOCA line (F 12m). The values are normalized by that of the 25 m transport line on the SAMPLE III line.**

The particle number-size distributions were measured using the 25 m and 12.5 m lines. The ratio between these results leads to the penetration through 12.5 m line vs. the particle size, which is shown in Figure 2.20. It can be seen that the penetration was lowest at the smallest particle size around 5 nm, and increases with the particle size up to around 100 nm. The main particle loss mechanism in this size range is diffusion, which is stronger for smaller particles, thus lower penetration for smaller particles. The penetration data under four different engine conditions (low, medium/low, medium/high, and high nvPM) are similar, and they all agree satisfactorily with the model calculation.
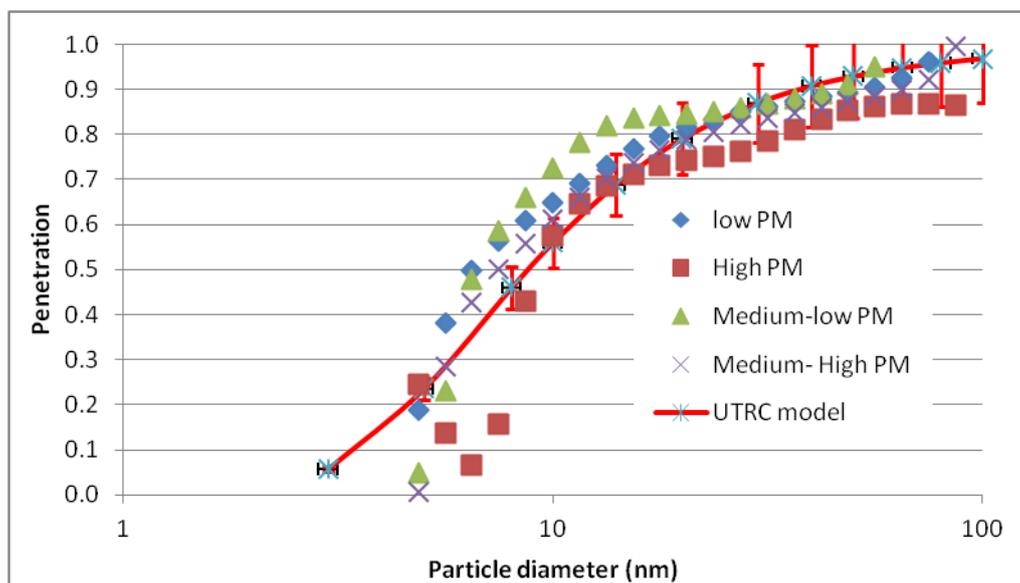


**Figure 2.20. Penetration through 12.5 m line vs. the particle size under different engine conditions. The solid line represents model calculation for the penetration.**

## 2.8. Comparison of different instruments for particle size distribution

Bench experiments were performed using carbon particles generated by the PALAS Spark Generator to test different instruments for particle size distribution. The test setup is shown in Figure 2.21. The EMPA SMPS (Scanning Mobility Particle Sizer) included a TSI 3775 CPC in high flow mode, and the DMA (Differential Mobility Analyzer) was operated with 12 L/min sheath/1.5 aerosol L/min flowrates. The CPC was in photometric mode for all conditions. The data from the fast particle sizer DMS500 M44 (Cambustion) were processed with "bimodal" inversion, and DMS500 M77 (Cambustion) data were processed with both "bimodal aggregate" and "monomodal" inversions. The Fast Aerosol Particle Emission Spectrometer (FAPES, Grimm) was operated by GRIMM. The PALAS particle concentration was varied by changing Ar pressure and to a lesser extent ejector dilutor pressure.
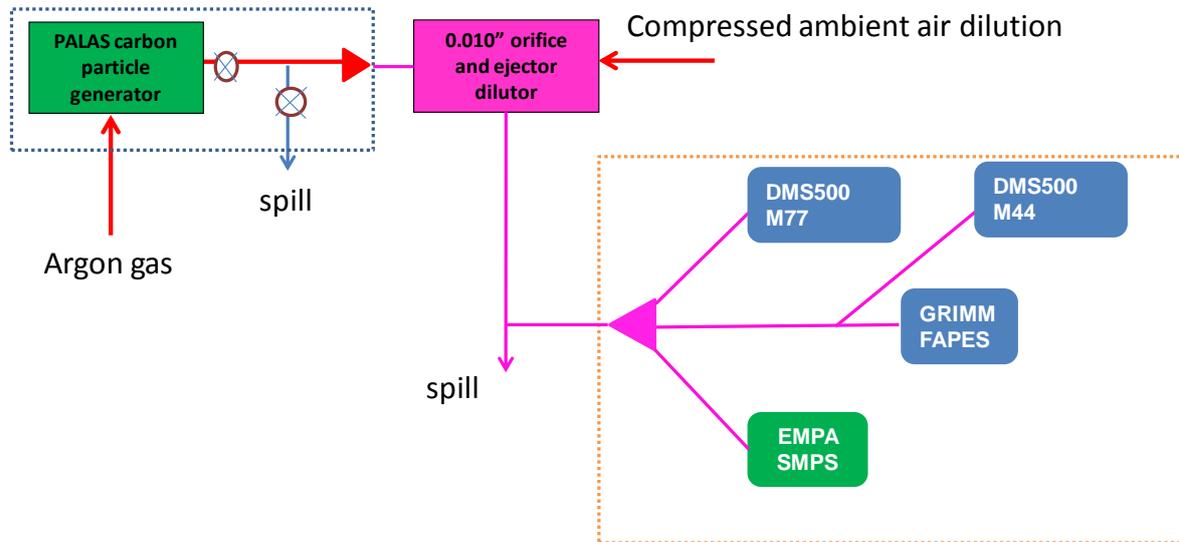
**Figure 2.21. The experimental setup for comparison of different instruments for particle size distribution.**

The particle number-size distributions measured by different instruments are shown in Figure 2.22. All the instruments showed a peak about 30 – 40 nm. The two DMS curves differed slightly in the range of 10 – 20 nm, probably due to different inversion models used. The curve of FAPES was shifted slightly to the larger particle size compared to other instruments. The particle concentration by the SMPS was significantly lower than other instruments. Recent calibration suggested that this discrepancy may be related to the error by the CPC 3775.
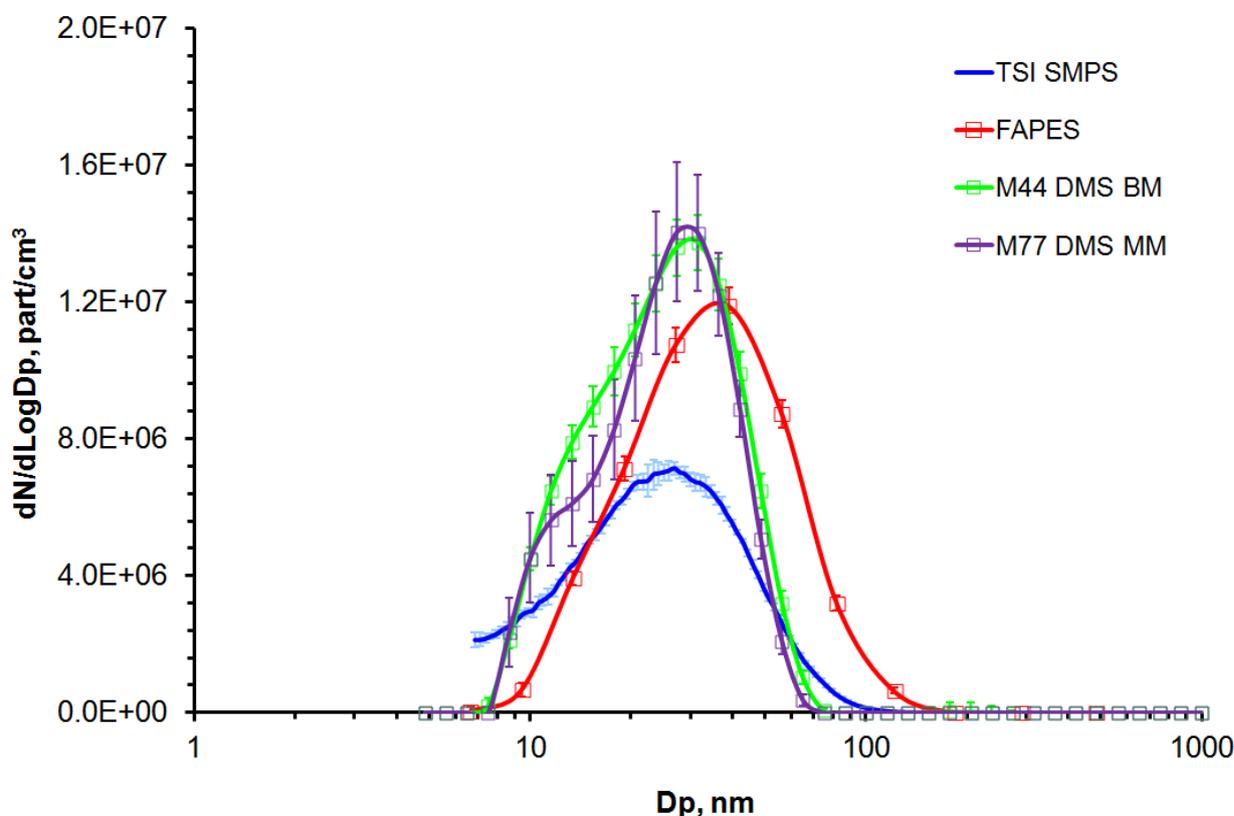
**Figure 2.22. Comparison of different instruments for particle size distribution.**

## 2.9. Effective particle density measurement using CPMA-DMS setup

The Fast Particle Sizer DMS gave the particle size based on electrical mobility, and the Centrifugal Particle Mass Analyzer (CPMA) measured the particle mass. Combination of these data led to the effective particle density based on spherical particles assumption. The measured effective density of exhaust particles in the diluted line against the particle mobility size is plotted in Figure 2.23. At the particle size of about 25 nm, the effective density is highest at around 1000 kg/m$^3$. This density is significantly lower than the amorphous carbon density around 2000 kg/m$^3$. This discrepancy is mainly because that the exhaust particles are not solid spheres, but agglomerates with certain porosity. Thus the volume based on sphere assumption overestimates the particle volume, thus low value of the effective density. As the particle size increases from 25 nm to 40 nm, the effective density decreases to about 700 kg/m$^3$, which indicates that the porosity is increasing in this size range. This is understandable as the number of primary particles in a small agglomerate is low, and the structure is compact; the number of primary particles increases in a large agglomerate, and the structure can be

more open. The effective density is fairly constant for particle sizes larger than 40 nm, indicating that the porosity in this size range is relatively constant.
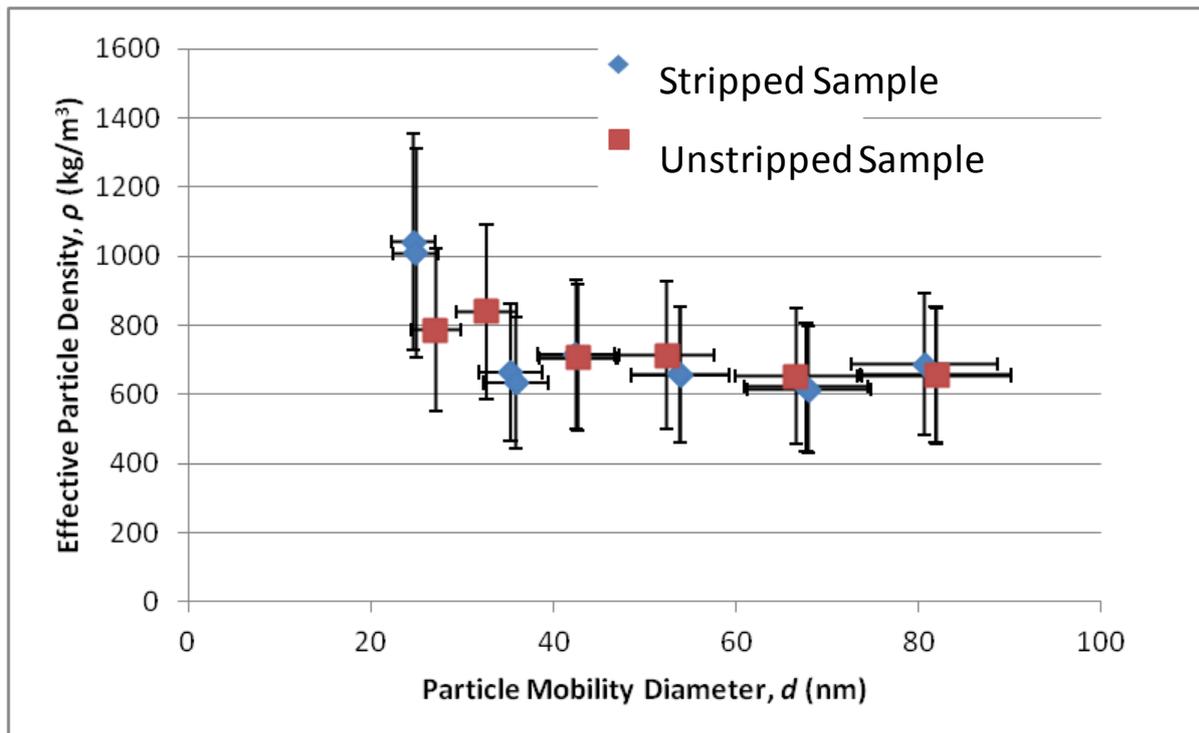


**Figure 2.23. The effective density of exhaust particles in the diluted line measured by the CPMA-DMS setup.**

The effective density was measured for samples in the diluted line with and without the catalytic stripper. The difference was not statistically significant as shown in Figure 2.23. This indicates that the volatile material on the particles in the diluted line is limited. The effective density for samples in the Annex 16 line (undiluted) is shown in Figures 2.24 and 2.25 and compared to the samples in the diluted line. Without the catalytic stripper, the effective density in the Annex 16 line was noticeably higher than that in the diluted line (Figure 2.24). With the catalytic stripper, the effective density in the Annex 16 line was lower and closer to the effectively density in the diluted line (Figure 2.25). These results indicate presence of volatile material on the particles in the Annex 16 line. The volatile material may fill the porous parts of the agglomerated particles, thus increasing the effective density.
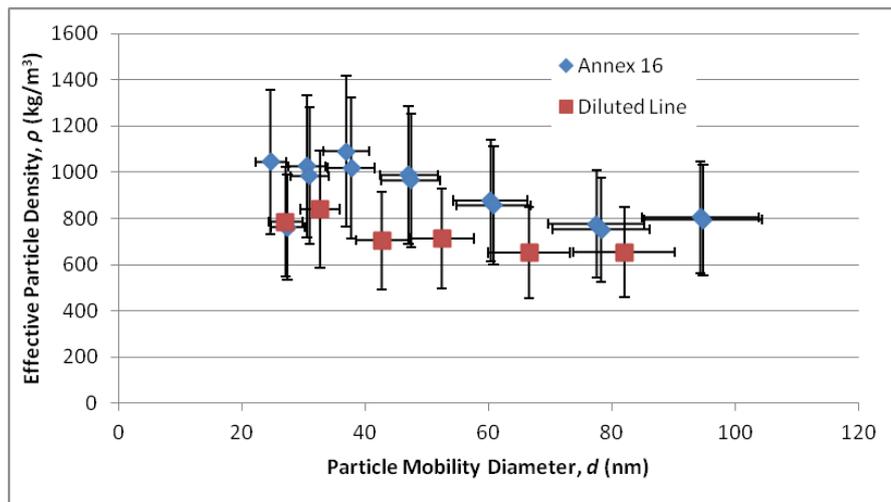
**Figure 2.24. The effective density of exhaust particles in the Annex 16 line and diluted line without the catalytic stripper.**
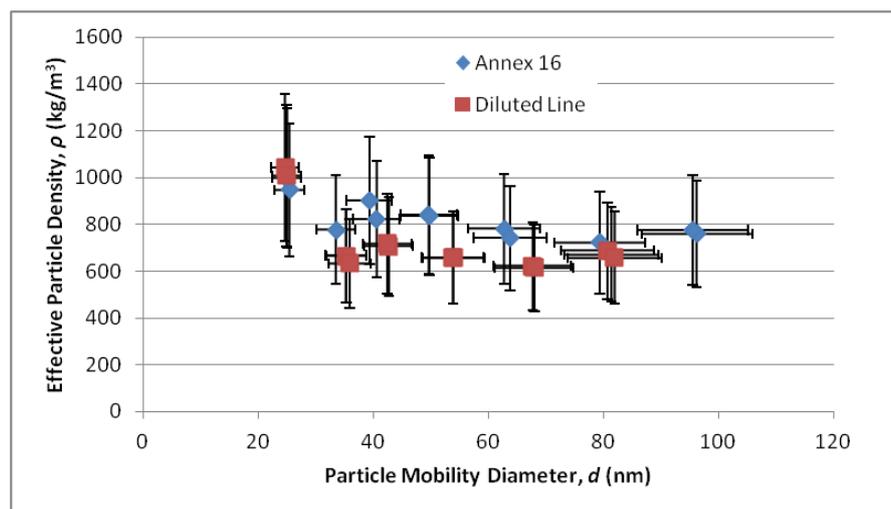


**Figure 2.25. The effective density of exhaust particles in the Annex 16 line and diluted line with the catalytic stripper.**

## 2.10. Particle microscopic analyses

Particles were collected using thermophoretic sampler during the ramp test on the Annex 16 line. The grid holder was at 30-40 $^\circ$C during collection and no water was visible after collection. The sampler was not designed for short samples, thus samples from some engine test points were aggregated on a single sample. Figures 2.26 and 2.27 are example TEM images of the samples from the ramp test. Each of the samples represents particles from two engine test points. The engine power for the samples on

Figure 2.27 was higher than that for Figure 2.26. The pictures show a lot of classic soot. The sample loading of Figure 2.27 was too heavy. Actual aggregates might be only 50-300 nm long.



```
S3UBCD2_11_-45 pan.tif
S3UBCD2_11_-45                    500 nm
Print Mag: 98200x @ 8.3 in       HV=80.0kV
10:51 06/05/12                    Direct Mag: 100000x
TEM Mode: Imaging                 X: 11 Y: -45.3
                                  UBC BioImaging Facility
```
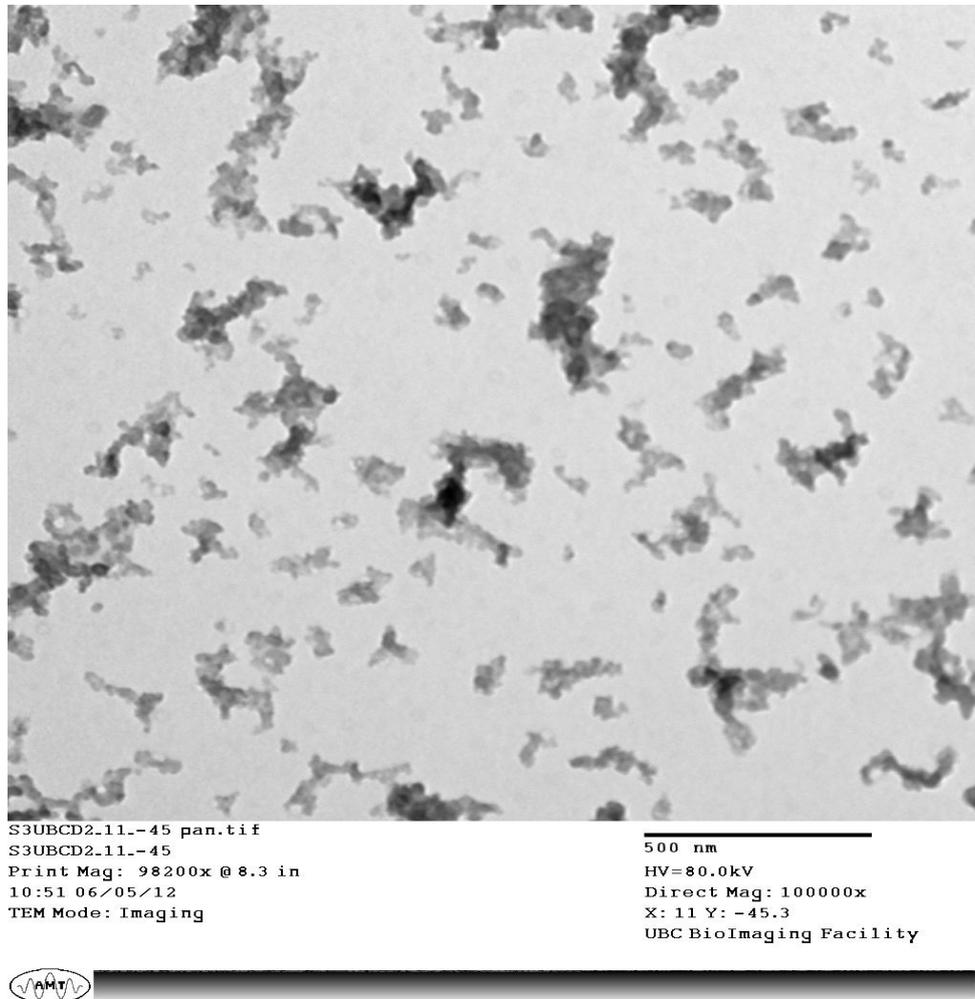
**Figure 2.26. An example TEM image of the exhaust particles during the ramp test.**
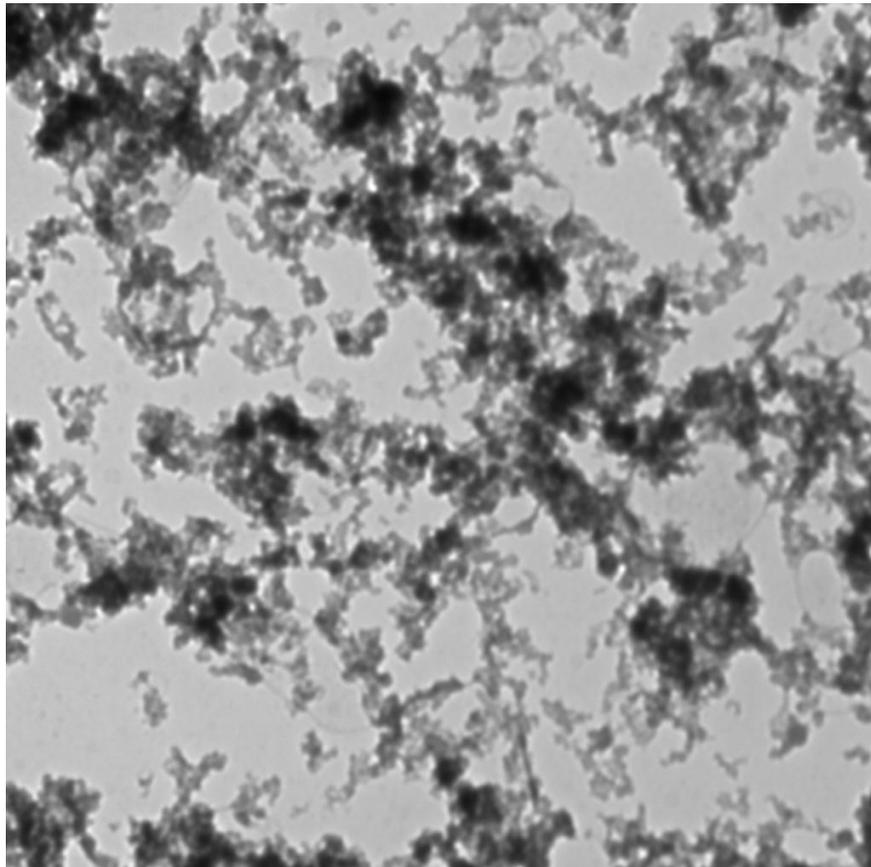
```
S3UBCD3.-500.-493 span.tif
S3UBCD3.-500.-493 span
Print Mag: 78600x @ 8.3 in
13:05 06/01/12
TEM Mode: Imaging

500 nm
HV=80.0kV
Direct Mag: 80000x
X:-500 Y:-493.1
UBC BioImaging Facility
```

**Figure 2.27. An example TEM image of the exhaust particles during the ramp test.**

## 2.11. Summary

The SAMPLE III measurement campaign provided a large amount of data and initiated several topics which were further investigated in later campaigns, such as measurement system intercomparison, particle effective density, line loss, etc. Several peer-reviewed papers based on the SAMPLE III data have been published, including Corbin et al. 2014, Boies et al. 2015 and Johnson et al. 2015.

# 3. Activities and results in the period 2012/07 – 2012/12 (including A-PRIDE 4)

## 3.1. Introduction

During the period between July and December of 2012, activities on four research topics were performed, provided in the subsequent sections. Section 3.2 describes the penetration efficiency testing of two cyclones, one that was originally used in the FOCA emission measurement sampling train (2000-30ENS-1, URG Inc.) and its replacement unit (Model 3800, BGI Inc.). Section 3.3 provides the results of the inter-comparison between mass based instrumentation with the CPMA-electrometer system. Information on the newly constructed and installed Inconel sampling probe suited for dedicated engine tests with long durations and high exhaust temperatures can be found in Section 3.4. A dedicated measurement campaign referred to as Aviation Particle Regulatory Instrumentation Demonstration Experiment 4 (A-PRIDE 4) was conducted from November 5-19, 2012 at SR Technics in Kloten. Representative results and findings from this campaign can be found in Section 3.5.

## 3.2. Cyclone particulate matter penetration tests

### 3.2.1. Introduction

The Aerospace Information Report (AIR) recommends the use of a cyclone to prevent large sized PM from reaching the downstream instrumentation. The following AIR performance specifications have been proposed at a sample flow rate of 25 SLPM:

Cut-point         $D_{50} \geq 1\ \mu m$

Sharpness       $(D_{16}/D_{84})^{0.5} \leq 1.17$

The FOCA sampling system originally utilized a URG cyclone (Model 2000-30ENS-1) which has a manufacturer specified cut-point of 2.5 μm at 10 SLPM which corresponds to an approximate cut-point of 1 μm at 25 SLPM. Issues observed for this cyclone during the SAMPLE III inter-comparison campaign include its 12 mm OD connector sizes which are different from the standard ⅜" OD tubing used in the sampling train, requiring the usage of two reducing unions. In addition the cyclone also has a 90° bend directly attached to its outlet which is not in accordance with the AIR. It was speculated that the differences between the transportation efficiencies of the FOCA line and Rolls-Royce line observed during the SAMPLE III inter-comparison study might be attributed to the two different cyclones employed on the two lines.

In order to address these issues the cyclone utilized in the SAMPLE III design is evaluated here. This cyclone is a sharp cut cyclone by BGI Inc. (Model 3800). The cyclone has ⅜" connectors ensuring an adapter free connection to the sampling system. According to the manufacturer the $D_{50}$ of this model

is 1 μm at 25 SLPM, in compliance with AIR recommendations listed above. The following sections provide the methods and results for the penetration efficiency testing of the two cyclone models at EMPA with diffusion flame generated soot aerosol.

## 3.2.2. Methods

The cyclone efficiency was tested with the setup shown in Figure 3.1 below.
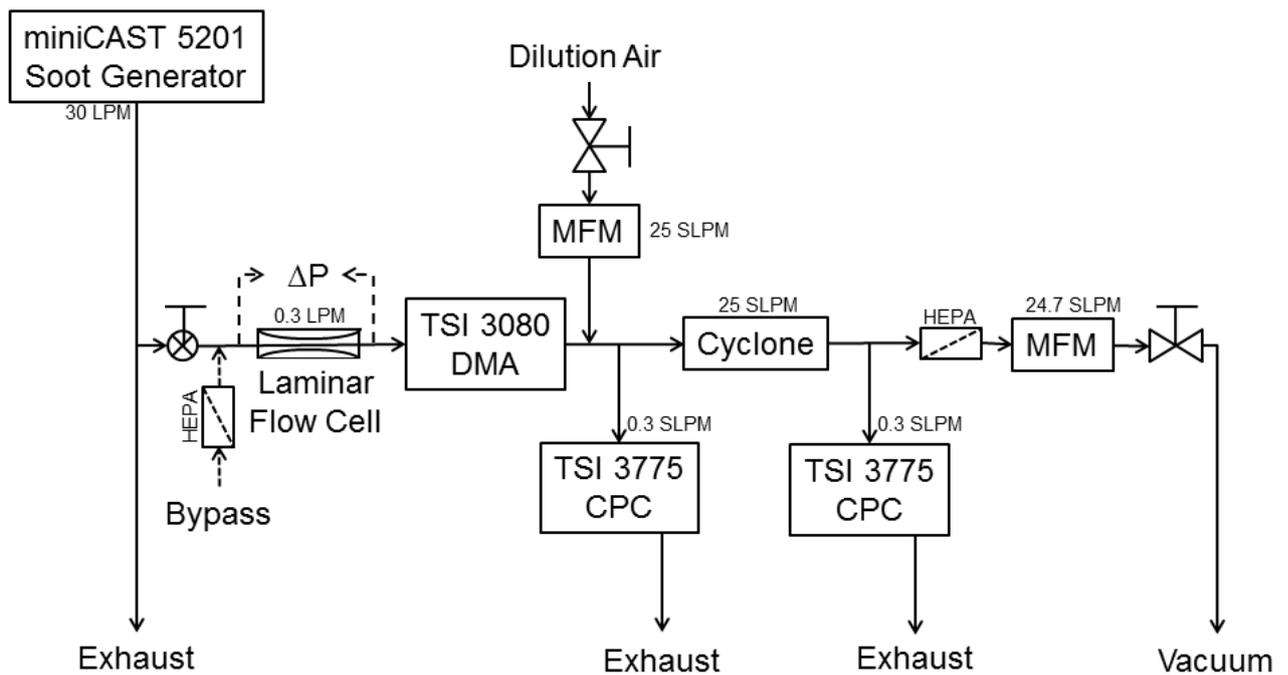


**Figure 3.1. Setup for cyclone efficiency evaluation at EMPA.**

Soot particles were produced with a miniCast Model 5201 soot generator. The generator operated at set point 8 to generate particles in the size range between 20 and 150 nm and at set point 1 for the generation of particles in the size range between 50 and 1000 nm. The use of set point 8 was necessary because set point 1 did not produce a sufficient amount of particles smaller than 50 nm.

A Differential Mobility Analyzer (DMA, TSI 3080) selected particles with equal electrical mobility diameters. The differential pressure over a laminar flow element was used to determine the aerosol flow rate at the DMA inlet (0.3 LPM). The DMA itself was operated with 2.4 LPM sheath flow allowing the selection of mobility diameters between 15 and 1000 nm. After the DMA the quasi mono-disperse aerosol flow was diluted with HEPA filtered dry air and the number concentration of the particles was determined with a Condensation Particle Counter (CPC, TSI Inc. Model 3775). 25 SLPM of the flow was drawn through the cyclone and the downstream particle number concentration was measured with a

second CPC device of the same type. The air flow rates of the dilution and vacuum were controlled with Mass Flow Meters (MFM, TSI Inc., Model 4000) at 25 and 24.7 SLPM in combination with needle valves. A ball valve and bypass upstream of the laminar flow cell allowed particle free background checks and the balancing of the flows before each experiment.

The evaluated particle mobility diameters were selected as 20, 35, 50, 75, 100, 150 for the miniCast set point 8 and 50, 75, 100, 150, 200, 300, 400, 500, 600, 700, 800, 900 and 1000 nm for the miniCast set point 1. Particles generated at these two set points have likely different characteristics in terms of particle shape and density because the set points refer to different fuel to air ratios. Consequently the mobility diameter ranges have been chosen to overlap as much as reasonably possible for all experiments so that the entire size range could be covered and that differences in cyclone penetration could be identified due to the different miniCast set points. Before evaluating the two cyclones the agreement between the two CPCs was evaluated for the same two miniCast settings and mobility diameters by using a 15 cm piece of conductive tubing instead of a cyclone.

CPC counts at each mobility diameter were allowed to stabilize for 3 minutes before taking a measurement. The average concentration up- and downstream for an integration time of one minute were used to calculate the penetration (Equation 3.1)

$$P = \frac{C_{\text{Out}}}{C_{\text{In}}} \; .$$

Equation 3.1

## 3.2.3. Results & Discussion

The following sections describe the CPC agreement, the performance of the URG cyclone and the performance of the BGI cyclone.

### 3.2.3.1. Background Check (CPC Agreement without Cyclone Installed)

The average penetration with no cyclone in line is 0.994 for all mobility diameters selected (Figure 3.2). The overall lower ratio than the ideal ratio of 1 could be caused by losses in the conductive silicone tubing that was used as the cyclone replacement. However, the instruments agree well and the penetration data have a low variability (±0.01) at all mobility diameters. Furthermore, there is no observable difference between the miniCast set point 1 and set point 8.

**No Cyclone**



▲ miniCast set point 1    △ miniCast set point 8
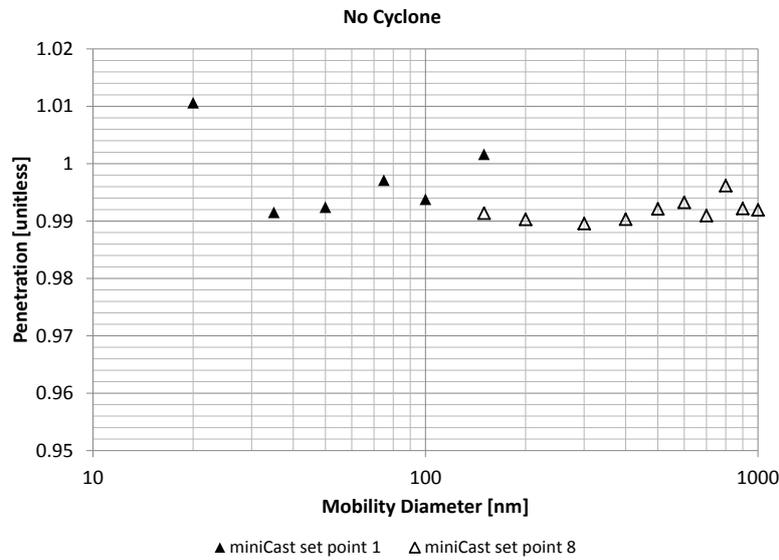
**Figure 3.2. Particle penetration without cyclone in line for soot particles generated with the miniCast set point 1 (solid triangles) and set point 8 (open triangles) for mobility diameters ranging from 20 to 1000 nm.**

### 3.2.3.2. Particle Penetration URG 2000-30ENS-1 Cyclone

The particle penetration through the URG 2000-30ENS-1 Cyclone is shown in Figure 3.3.

**URG Cyclone**



● miniCast set point 8    ○ miniCast set point 1
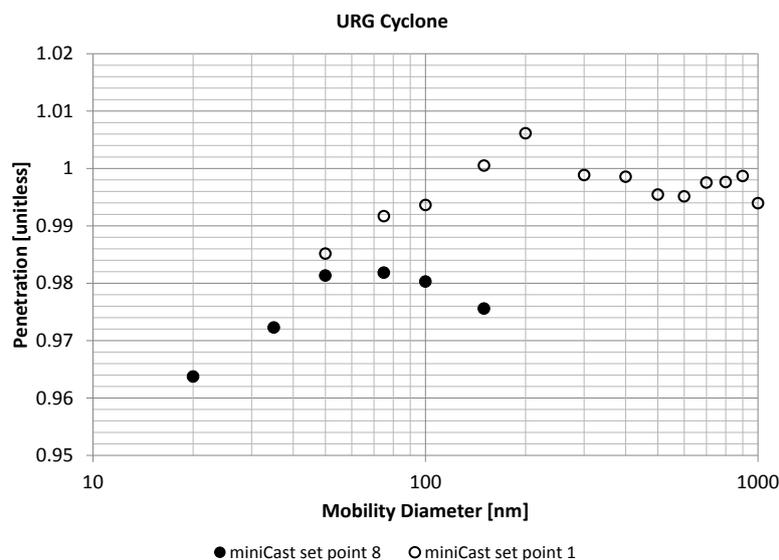
**Figure 3.3. Penetration of soot particles with mobility diameters ranging from 20 to 1000 nm through the URG 2000-30ENS-1 cyclone. Solid circles correspond to a miniCast set point 1 and open circles to a set point of 8.**

The URG cyclone data do not indicate a size cut-off with increasing mobility diameter. At the 1000 nm mobility diameter the penetration is still 0.994. The lowest penetration is observed for the smallest mobility diameters selected from soot aerosol generated with a miniCast set point of 8. The exact reason for the lower cyclone penetration at the smallest mobility diameters is not entirely clear but could be attributed to diffusion losses or to efficient coagulation of these small particles within the cyclone flow during the experiment.

The reason why no size cut-off was observed in the data could be explained by the effective particle density, which decreases with increasing particle size because of the loose morphology of soot agglomerates at larger sizes. Therefore, the electrical mobility diameter is larger than the aerodynamic diameter for such particles and the cyclone cut-off is not observable for the diameter range tested.

There is an observable difference in cyclone penetration for the two different miniCast set points, in particular for the 100 and 150 nm diameters. Due to the order of magnitude lower number concentrations ($10^2$ cm$^{-3}$ comparison to $10^4$ cm$^{-3}$), the miniCast set point 8 data has a penetration uncertainty of ± 0.09 estimated by counting (Poisson) statistics at 150 nm. The uncertainty in the penetration for the miniCast set point 1 data is ± 0.01 based on the same statistics. Therefore, there is more certainty in the miniCast set point 1 data at the 150 nm mobility diameter. However, it is also possible that the soot aerosol generated with the miniCast set point 8 experiences more coagulation within the cyclone which results in a lower particle penetration.

### 3.2.3.3. Particle Penetration BGI 3800 Cyclone

Figure 3.4 shows the soot particle penetration through the BGI 3800 cyclone. The BGI cyclone shows a nearly identical performance to the URG cyclone in terms of penetration fraction. The lowest penetration is again observed for the smallest mobility diameters below 75 nm. There is also no observable size cut-off at the larger mobility diameters near 1000 nm.

**BGI Cyclone**



◆ miniCast set point 8    ◇ miniCast set point 1
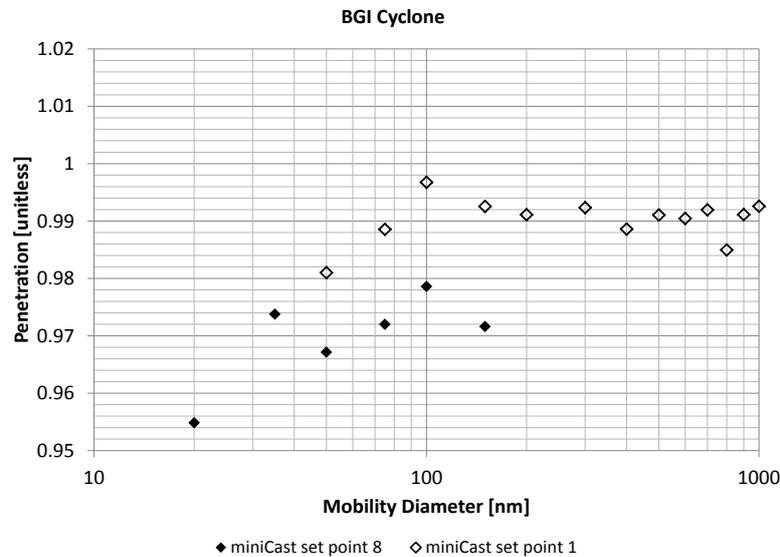
**Figure 3.4. Penetration of soot particles with mobility diameters ranging from 20 to 1000 nm through the BGI 3800 cyclone. Solid triangles correspond to a miniCast set point 1 and open triangles to a set point of 8.**

A difference in particle penetration for the two different miniCast set points is also visible for the BGI cyclone. This difference can likely be explained by the higher uncertainty in the miniCast set point 8 data for the 100 and 150 nm particles and different particle coagulation characteristics within the cyclone as explained previously.

## 3.2.4. Summary and Conclusions

Both the URG and BGI Cyclone models have a soot particle penetration that ranged from 0.95 at a 20 nm mobility diameter to near 1 for diameters greater than 150 nm. No particle cut-off was observed for both cyclone models. Therefore, it can be concluded that URG and BGI cyclones have nearly undistinguishable particle penetration characteristics for diffusion flame generated soot particles with electrical mobility diameters ranging from 20 to a 1000 nm.

## 3.3. Particulate matter mass inter-comparison experiments

This section is a summary of Tyler Johnson's (University of Alberta) report for the experiments conducted in collaboration with EMPA and ETH.

### 3.3.1. Introduction

A CPMA-electrometer system measures the absolute aerosol mass concentration and has the potential to overcome drawbacks of other real time and integrated filter based aerosol mass instrumentation. The purpose of this study was to compare a CPMA-electrometer system to a MSS, an AMS, CPMA-SMPS system and to NIOSH 5040 filters. This comparison was accomplished by comparing the soot mass concentration measured by each system from a common source in the laboratory at EMPA.

### 3.3.2. Methods

**CPMA Operation Principle**

A CPMA classifies aerosol particles by their mass-to-charge ratio. This classification is accomplished by balancing counteracting electrostatic ($F_e$) and centripetal forces ($F_c$) on each individual particle as shown in Figure 3.5.
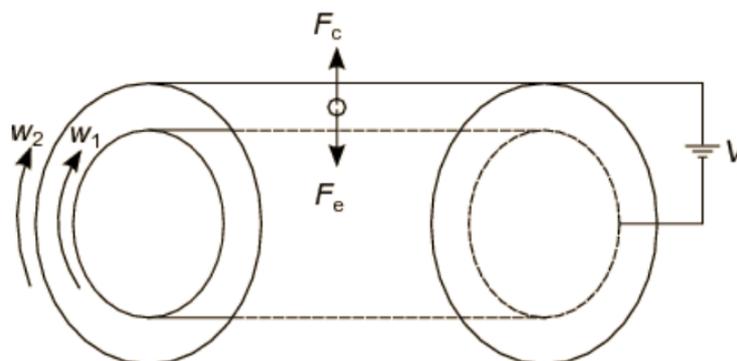


**Figure 3.5 CPMA Principle.**

The electrostatic force is generated by pre-charging the aerosol using a radioactive neutralizer or corona charger and placing a voltage potential (V) between the two classification cylinders. The centripetal force is generated by spinning the cylinders and passing the aerosol between them. By spinning the inner cylinder slightly faster ($w_1$) than the outer cylinder ($w_2$), a stable system of forces is established, improving the transfer function of the instrument significantly.

**Faraday Cup Electrometer Operation Principle**

The Faraday cup electrometer measures the total charge concentration of the aerosol. A HEPA filter is placed inside a Faraday cage, removing the particles (with their charges) from the aerosol stream. By Gauss's Law, the enclosed charge in the filter induces an equivalent charge on the Faraday cage. By measuring the change in the induced charge over time, the current of the aerosol is determined.

## Determination of PM Concentration

The mass concentration of the aerosol classified by a CPMA ($m_{total}$) is equivalent to the summation of the mass concentration of each particle charge state, as shown in Equation 3.2.

$$m_{total} = m_{+0} + Mn_{+1} + 2Mn_{+2} + 3Mn_{+3} + ..... = m_{+0} + M(n_{+1} + 2n_{+2} + 3n_{+3} + .....)$$ Equation 3.2

where $m_{+0}$ is the mass concentration of uncharged particles, M is the CPMA mass-to-charge set point and $n_i$ is the number concentration of particles with i charges. Due to the system of forces within the CPMA, only positively charged and uncharged particles can pass through the instrument and therefore negatively charged particles are not considered in the equations.

The current of the aerosol (I), measured by the Faraday cup electrometer, is also equivalent to the summation of the current of each particle charge state, as shown in Equation 3.3.

$$I = Qe(n_{+1} + 2n_{+2} + 3n_{+3} + .....)$$ Equation 3.3

where Q is the volumetric flow rate of the aerosol, e is the value of the elementary charge and $n_i$ is the number concentration of particles with i charges. Therefore combining Equation 3.2 and Equation 3.3, the mass concentration of the classified aerosol is:

$$m_{total} = m_{+0} + \frac{MI}{Qe'}$$ Equation 3.4

Therefore if the mass concentration of uncharged particles ($m_{+0}$) is negligible or can be quantified, the total mass concentration of an aerosol can be measured with a CPMA-electrometer system.

### 3.3.3. Experimental Setups

The experimental campaign compared different aerosol mass instruments by measuring aerosolized soot mass concentrations and comparing the results. A MSS (AVL, Austria), AMS (Aerodyne, USA), multiple NIOSH5040 filters (thermal-optical method) and two different CPMA (Cambustion, U.K.) configurations were compared. For all of the experimental set-ups a miniCAST 5201 Type C (Jing Aerosol, Switzerland) was used as the aerosol soot source. A spill to a fume hood was used for excess flow from the miniCAST, while a cyclone with an approximately 1 μm cutoff was used to keep the set-up as clean as possible. To achieve the flow rate required for the cyclone, an additional vacuum line was placed just downstream of the cyclone pulling 16 LPM. Since the MSS only measures elemental carbon (EC), a catalytic stripper (Cambustion, U.K.) set to 350°C was used to remove organic carbon (OC) from the soot. Four different experimental set-ups were used to compare the mass concentration instruments.

### CPMA-SMPS System vs. MSS

The first CPMA configuration, shown in Figure 3.6, used a differential mobility analyzer (DMA, Model 3080; TSI, USA) and condensation particle counter (CPC, Model 3775; TSI, USA) with a CPMA to determine the effective density distribution of the soot.
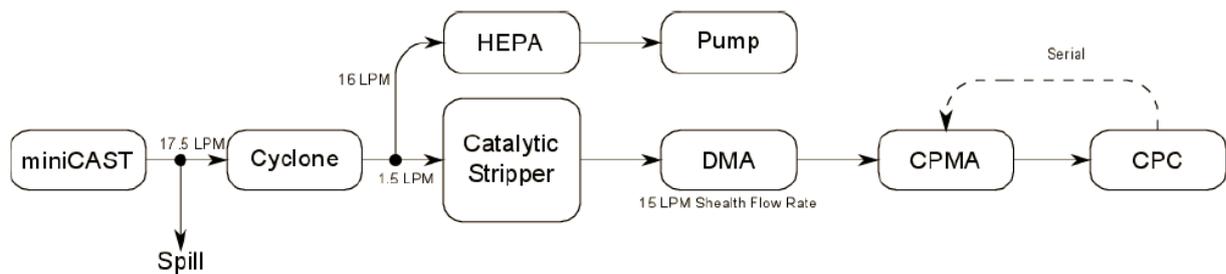


**Figure 3.6. Experimental setup to measure the effective density of miniCast soot aerosol.**

A DMA selected particles based on their electrical mobility size. These particles were further classified by their mass-to charge ratio using a CPMA. By stepping the CPMA operating conditions (i.e. CPMA voltage and rotation speed) and measuring the concentration of classified particles at each setting using a CPC, the average mass for each mobility size was determined. Using the particle mobility size and average mass, the effective density was determined for each DMA setpoint. This process was repeated by stepping the DMA setpoint to determine the entire effective density distribution of the soot.

The aerosol mass concentration can be determined from its effective density distribution if the mobility size distribution is known or measured. The mobility size distribution of the soot was measured using a SMPS (DMA and CPC in tandem). The MSS was placed in parallel with the SMPS, as shown in Figure 3.7, and the mass concentration results of the MSS and CPMA-SMPS system were compared.
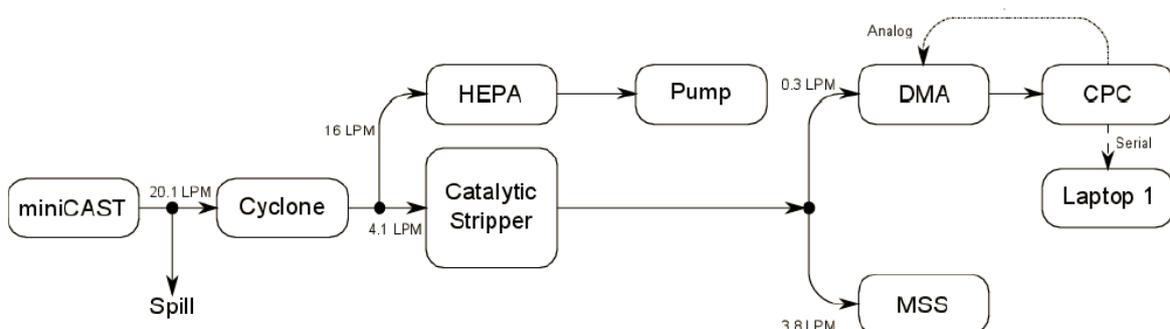


**Figure 3.7. Experimental setup for the MSS and CPMA-SMPS comparison.**

## CPMA-Electrometer System

The second CPMA configuration used was the CPMA-electrometer system as described in the theory section of the report. A Keithley 6517B electrometer was used to measure the aerosol current (I) from the Faraday cup electrometer, while a 0-10 LPM mass flow controller (PR4000F; MKS, Germany) controlled the mass flow rate (Q) through the cup. All of the important experimental parameters (M, I, Q, etc … ) were recorded in real-time electronically via serial connections and a Labview program. To determine the concentration of uncharged particles that passed through the CPMA (or quantify $m_{+0}$), a DMA and CPC were used. The DMA was set to its maximum voltage and no sheath flow, making the instrument an electric precipitator. Since only uncharged would pass through the DMA, a CPC was placed downstream measuring the uncharged particle concentration. Due to the CPMA's transfer function dependence on volumetric flow, all of the mass instruments could not be compared simultaneously. Therefore, multiple experimental set-ups were used to compare the CPMA-electrometer to the other mass concentration instruments.

## CPMA-Electrometer System vs. MSS

The experimental set-up used to compare the CPMA-electrometer system and MSS is shown in Figure 3.8.
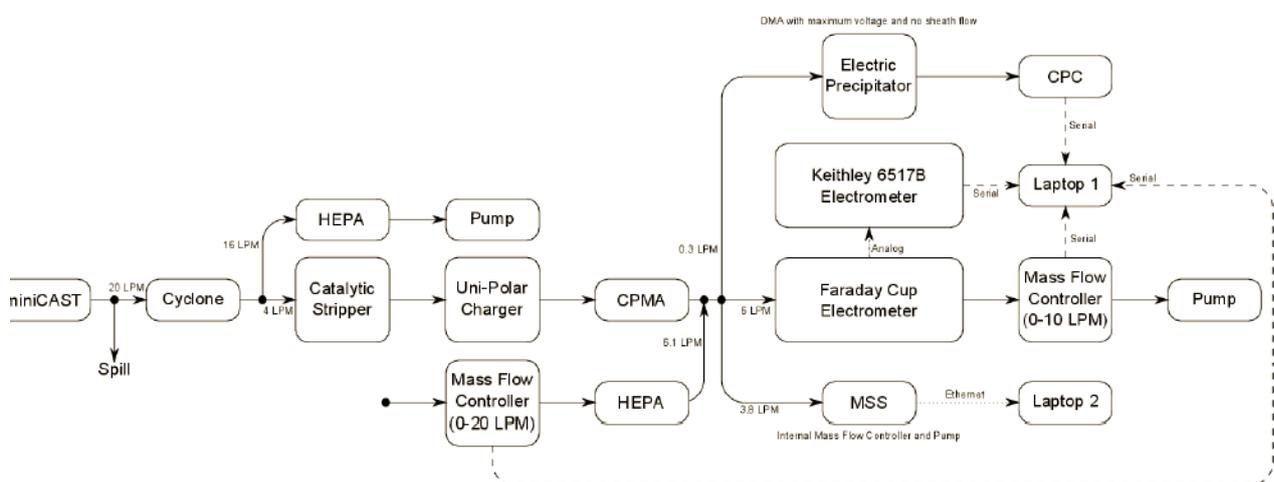


**Figure 3.8. Experimental setup for the MSS and CPMA-electrometer comparison.**

## CPMA-Electrometer System vs. NOISH5040 and AMS

The experimental set-up used to compare the CPMA-electrometer system against NIOSH 5040 filters and AMS is shown in Figure 3.9.
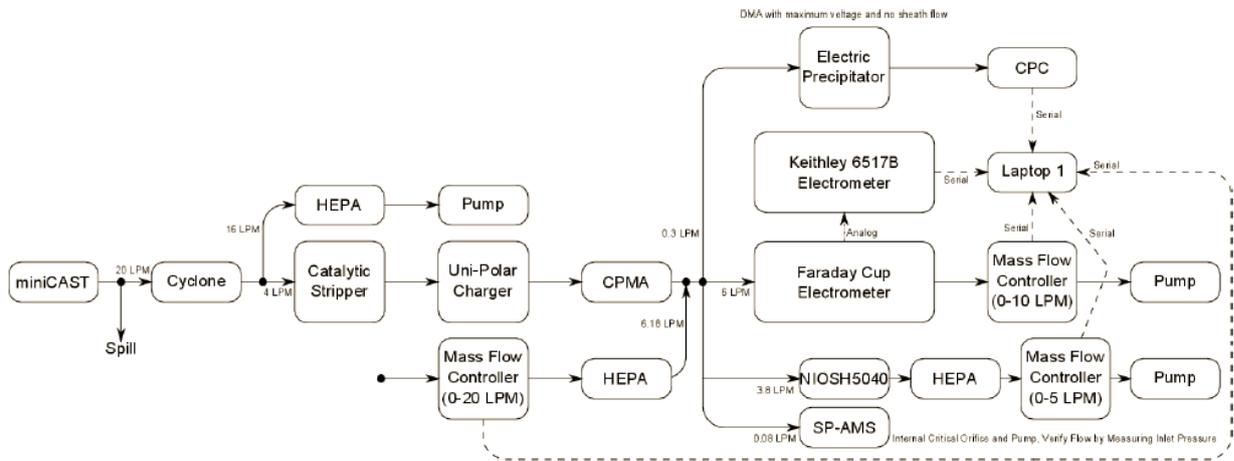
**Figure 3.9. Experimental setup for the AMS, NIOSH5040 and CPMA-electrometer comparison.**

## 3.3.4. Results and Discussions

### CPMA-SMPS System vs. MSS

The effective density distribution from the miniCAST burner at default setting 1 is shown in Figure 3.10 and was determined using the DMA-CPMA-CPC system.
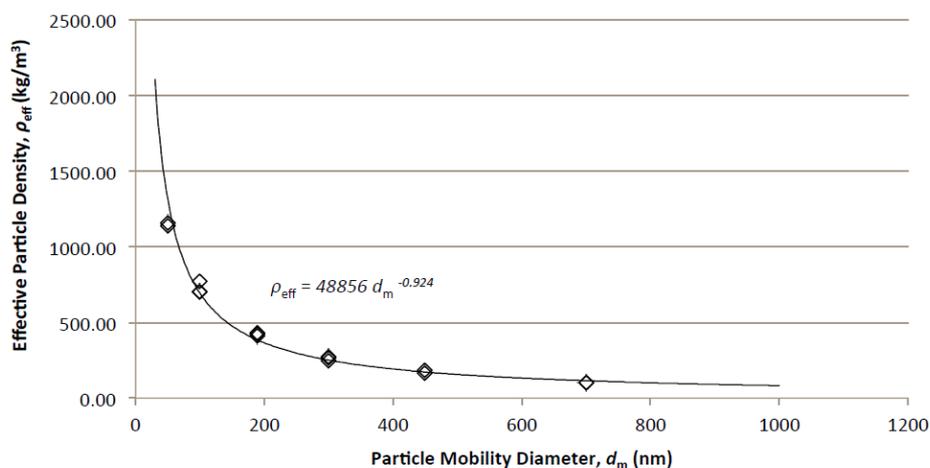


**Figure 3.10. Effective density as a function of mobility diameter of soot aerosol generated using the miniCast soot generator.**

The mass-mobility exponent was determined to be 2.076. As a comparison, diesel soot usually has a mass-mobility exponent of approximately 2.2. Applying this density distribution to the mobility size distributions measured by the SMPS, the total soot mass concentration was determined and compared against the MSS as shown in Figure 3.11.
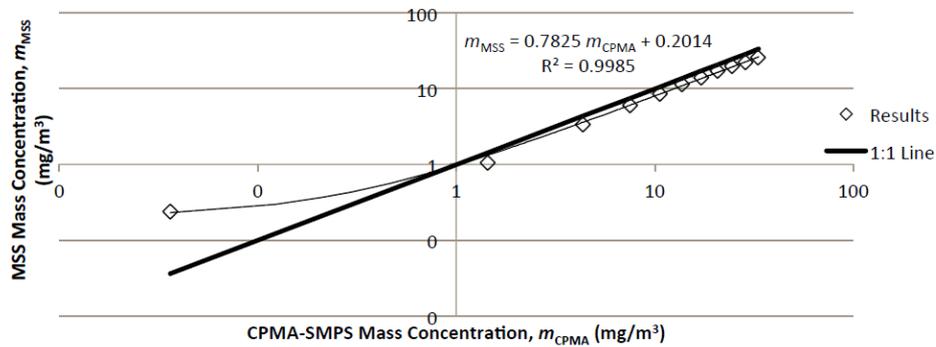
**Figure 3.11. Correlation between the determined MSS and CPMA-SMPS mass.**

The MSS and CPMA-SMPS system agreement was extremely linear above a mass concentration of 1 mg/m$^3$ with a slope of 0.7825. Therefore, the MSS measured 21.75% less mass concentration than the CPMA-SMPS system. One explanation for this discrepancy was the catalytic stripper was not completely removing all of the OC from the aerosol stream. Therefore OC could have been condensing downstream of the CPMA, affecting the size distribution measured by the SMPS and the effective density distribution measured by the DMA-CPMA-CPC system. This hypothesis is supported by the AMS measuring an OC mass fraction of 19% downstream of the CPMA, which is very close to the 21.75% disagreement. However, due to the scanning nature of the DMA-CMPA-CPC system and SMPS, this experimental procedure is limited to steady state sources. This conjecture contradicts previous studies which demonstrated that the catalytic stripper removed more than 99% of OC from engine emission. According to the miniCAST manual, the burner outputs an OC mass fraction of 5% at default setting 1. Further investigation is needed to resolve the difference.

## CPMA-Electrometer System vs. MSS

A CPMA-electrometer system can measure mass concentration from transient sources. Figure 3.12 shows the comparison between the CPMA-electrometer system and the MSS.
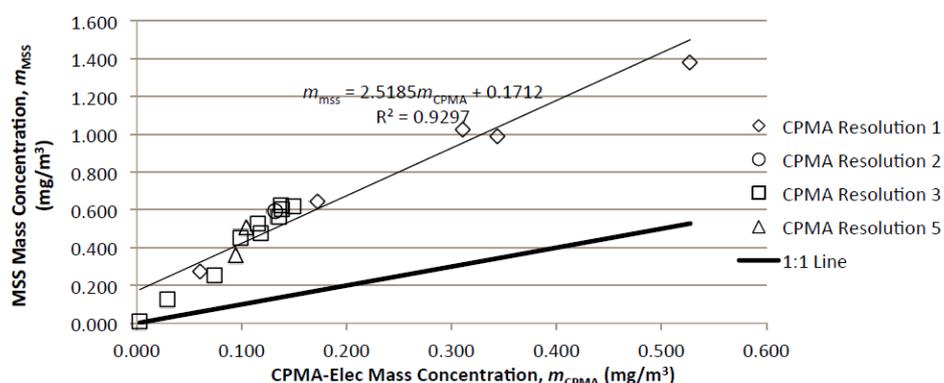


**Figure 3.12. Correlation of the determined MSS and CPMA electrometer masses.**

Contrary to the CPMA-SMPS system, the CPMA-electrometer system was found to measure less mass concentration than the MSS with a disagreement factor of 2.52. This discrepancy is not understood and needs further investigation.

**CPMA-Electrometer System vs. NIOSH5040**

The CPMA-electrometer system measures the aerosol mass concentration, but NIOSH5040 measures the total mass loading on the filter. Therefore, the CPMA-electrometer system mass concentration must be multiplied by the volumetric flow rate through the filter to determine the aerosol mass flow rate through the filter. Finally, to determine the total mass loading on the filter measured by the CPMA-electrometer system, this mass flow rate must be integrated over the exposure time of the filter.

By applying these calculations to every filter trial Figure 3.13 was generated, comparing the CPMA-electrometer system and NIOSH5040 filters.



The chart shows CPMA-Elec Integrated Mass, $M$ (µg) on the y-axis versus NIOSH 5040 Elemental Carbon Mass, $EC$ (µg) on the x-axis, with the fitted line $M = 0.1936\,EC + 2.2798$ and $R^2 = 0.9628$. Legend: Resolution 0.78, Resolution 1, Resolution 3, Resolution 5, 1:1 Line.
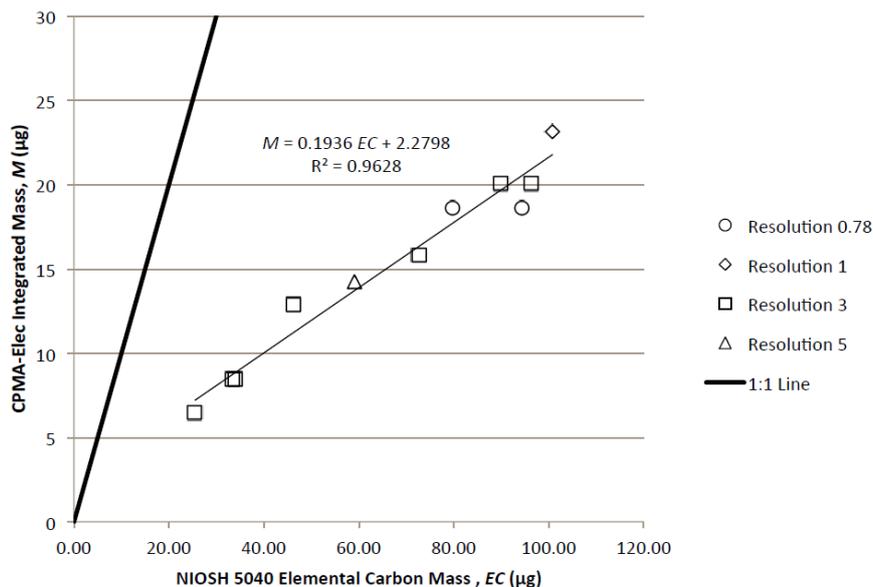
**Figure 3.13. Correlation of the NIOSH 5040 EC mass and the determined CPMA- electrometer mass.**

Similar to the MSS comparison, the CPMA-electrometer system measured less mass concentration than the NIOSH5040 filters. In an attempt to remove the effects of OC previously described, the EC results from the NIOSH5040 filters were used rather than the total carbon (TC) loading. However, the CPMA- electrometer system still measured 80.64% less mass than the EC from the NIOSH5040 filters. The source of this disagreement is unknown. However, the OC mass fraction measured by the NIOSH5040 filters varied from 33% to 59% and supports the theory that the catalytic stripper was not

removing all of the OC from the aerosol stream. Comparing these values to the 19% OC mass fraction measured by the AMS, more OC condensation was taking place on the NIOSH5040 filters than in the AMS. This conclusion makes physical sense as the filter's large surface area and greater temperature drop due to the large metal surface area of the holder caused more OC condensation than the AMS. It should be noted that the AMS results were not fully processed at the time of this report. These results may offer further insights into the disagreement between the CPMA-electrometer system and the other mass concentration instruments.

### 3.3.5.  Recommended Future Work

As with any experiment, many problems arose that should be addressed for further testing with the CPMA-electrometer system. Due to the size and complicated nature of the system, balancing flow rates and finding leaks was challenging. However, accurate flow rates are extremely important as the measured aerosol concentration is inversely proportional to the flow rate through the electrometer. The biggest leaks were the NIOSH5040 holders and an alternate design with a better seal should be used in the future. The Corona charger also had a small leak, but it caused less than a 1% change in the results. Also, to determine the amount of OC that is condensing downstream of the CPMA, two NIOSH5040 filters should be used in series, with the first filter measuring the OC and EC in the aerosol stream and the downstream filter measuring the OC that condenses.

Another significant problem was the instruments becoming extremely dirty due to the high mass concentrations and long run times required. The Corona charger had to be cleaned every hour and a half and the CPMA every three hours as the high voltages in the systems would short circuit. The Corona charger should be modified to avoid this problem or for the cleaning process to be completed faster. Due to the frequent cleanings, the CPMA seal became worn down and began to leak at high CPMA temperatures as the metal cylinders expanded more than the seals. It is believed this seal leak caused the measured mass concentration to fluctuate to zero downstream of the CPMA (verified by multiple mass instruments). The aerosol stream would leak through the CPMA seals and would be pulled through the CPMA case HEPA filter, removing the particles from the aerosol stream, making the aerosol mass concentration zero. This problem has already been addressed by Cambustion by replacing the seals with tapered seals.

Finally, the efficiency of the catalytic stripper at removing OC from the aerosol stream should be addressed. A higher temperature catalytic stripper conversion/catalytic stripper should be used to remove a greater portion of OC from the aerosol stream. Furthermore, cooling coils should be placed downstream of the stripper. By cooling the aerosol stream, any OC that was not removed in the catalytic stripper will condense out and be charged by the Corona charger and classified by the CPMA and therefore accounted for within the CPMA-electrometer system.

### 3.3.6.   Summary and Conclusions

Five aerosol mass instruments were compared by measuring the soot mass concentrations produced by a miniCAST burner. The CPMA-SMPS system measured 21.75% more mass concentration than the MSS. This disagreement could be attributed to the OC mass fraction which was determined to be 19% by the AMS. The CPMA-electrometer system measured 39.7% of the mass concentration measured by the MSS and 19.3% of the mass concentration measured by the NIOSH5040 filters (EC only). The large discrepancies are not understood. To avoid these disagreements between the instruments in the future two NIOSH5040 filters should be used in series to measure the OC that is condensing on the filters. A catalytic stripper set to a higher temperature should be used to remove a greater portion of OC from the aerosol stream, while cooling coils should be placed downstream of the stripper to condense any remaining OC before the CPMA.

## 3.4. The inconel sampling probe

## 3.4.1. Introduction

The sampling probe used in the Sample III campaign was constructed from 1.4816 stainless steel. During the campaign the following issue was identified: thermal material expansion at different rates at high sample temperatures caused stress on welding seams and cracking of seams at certain locations was observed. In addition, the 1.4816 material showed permanent discoloration caused by excessive heat exposure indicating that this material might be not suited for jet engine exhaust sampling.

## 3.4.2. Changes Implemented to the New Design

Based on these observations the following changes were implemented to the original probe design:

1. The material was changed from stainless steel 1.4816 to Inconel 600, which has higher strength at temperatures exceeding 600°C. In addition, the whole structure is now made of one material, which reduces the stress caused by mismatched thermal expansions.

2. The sample tube is no longer welded to the two supporting rips (marked with red circles in Figure 14 below); instead the rips now serve as ring guards, but allow slight tube movement. This releases the thermo-mechanical stress caused by non-uniform heating of the probe during engine runs.

3. At the probe tip, only the central hole was initially drilled (marked with a green circle). However, during the engine test we found the sample temperature was below 160°C. Therefore, the previous design with the two side holes was adopted again, which resulted in a satisfactory sample temperature.

4. A slight change in geometry of the supporting structure was also implemented. This change also reduces the mechanical stress onto the design caused by thermal gradients and rapid temperature changes.

## 3.5. A-PRIDE 4 campaign

## 3.5.1. Introduction

A-PRIDE 4 took place from November 5-19, 2012 at the SR Technics Aircraft engine test cell at the Zürich Kloten Airport. The campaign was a multi-institutional effort from science, government and instrument manufacturers. In addition to the host, SR Technics, scientific institutions included Missouri University of Science and Technology (MST), EMPA and ETH. The governmental agencies included the Swiss FOCA, the United States Environmental Protection Agency (EPA) and The National Research Council of Canada (NRC). Instrument manufacturers present were Aerodyne Research and AVL.

The primary objective of the campaign was the performance evaluation and comparison of two AIR draft working document compliant sampling systems. Secondary objectives were the mass instrument comparison (Laser Incandescence vs. Micro Soot Sensor) and the implementation of an AIR operational checklist. ETH and EMPA further performed particle density measurements using a CPMA in combination with a DMA. Mass and number instruments were compared before and after the aircraft engine tests. Overall, eight engine tests were performed over a period of eight days. From these eight tests four were dedicated tests, three were piggy-back tests and one was a system check.

## 3.5.2. Methods

The following sections provide an overview of the instrumentation used in the campaign, the sampling system and methods used in the pre- and post- mass and number instrument comparison and an overview of the sampling system and methods used for the jet engine tests.

### 3.5.2.1. Instruments Deployed

Table 3.1 shows an overview of all the instrumentation used during the campaign in each sampling line.

**Table 3.1. List of instruments deployed during the A-PRIDE 4 campaign**

| FOCA/EMPA Annex 16 Line | FOCA/EMPA nvPM Line | MST nvPM Line |
|---|---|---|
| $NO_x$ | APC | APC |
| CO | MSS | LII |
| UHC | $CO_2$ | $CO_2$ |
| $CO_2$ | LII | MSS |
| | DMS500 | DMS500 |
| | $SP^2$-AMS | AMS |
| | CPMA | CPMA |
| | Super MAAP | MAAP |
| | $CO_2$ downstream of APC | $CO_2$ downstream of APC |

The Annex 16 line consisted of the standard instrumentation for nitrogen oxides ($NO_x$), carbon monoxide (CO), unburned hydrocarbons (UHC) and carbon dioxide ($CO_2$). The FOCA and MST particulate matter lines included an AVL particle counter (APC) for determining the particle number concentration, an AVL Micro Soot Sensor (MSS) and an Atrium Instruments Laser Induced Incandescence (LII) instrument for determining soot mass, a Cambustion fast particle sizer (DMS500) and a CPMA. Differences in the instrumentation for the two nvPM lines were the use of an Aerodyne Single Soot Particle Aerosol Mass Spectrometer ($SP^2$- AMS) in the FOCA/EMPA line and an Aerodyne AMS in the MST line. In addition the FOCA/EMPA line had a super Multi Angle Absorption Photometer (MAAP) whereas the MST line utilized a standard TSI MAAP.

## 3.5.2.2. Pre- and Post-Campaign Instrument Comparisons

A miniCast 5201 soot particle source was used for the generation of soot particles for the mass and number instrumentation comparison before and after the engine tests. Figure 3.14 shows the setup which was used for these comparison experiments. The miniCast was operated at set point 1 to generate particles with high EC content. The generated aerosol was  then diluted with compressed air and drawn through a flow splitter into the two sampling lines. As it can be seen in Figure 3.14 the position of the MSS and LII mass instruments is not the same in the two sampling lines. In the FOCA/EMPA system the LII is on the dump line whereas in the MST system the MSS is at the same position.
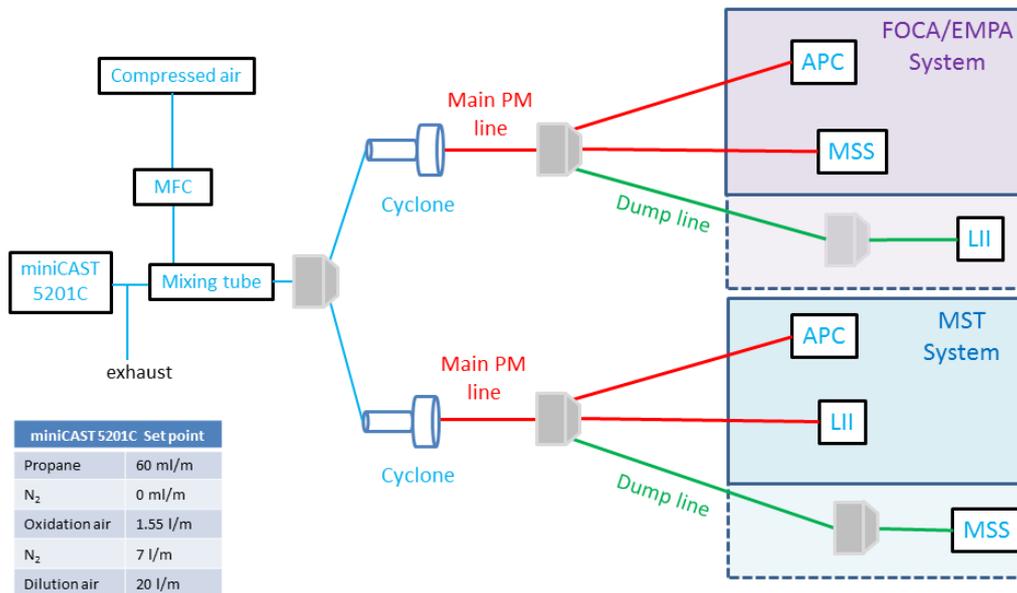
**Figure 3.14. Setup for pre- and post-engine test instrument comparison.**

The tests were performed for nine particle number concentration levels ranging from 0 to $2 \times 10^6$ cm$^{-3}$ and six mass concentration levels ranging from 0.1 to 1 mg cm$^{-3}$. In the post-test nine mass concentration levels were tested in the same range.

### 3.5.2.3 Engine Emission Measurements

The engine tests were performed with the system depicted in Figure 3.15. This configuration has similarities with the ones used in previous campaigns and the two lines after the flow splitter are in accordance with the AIR draft document.
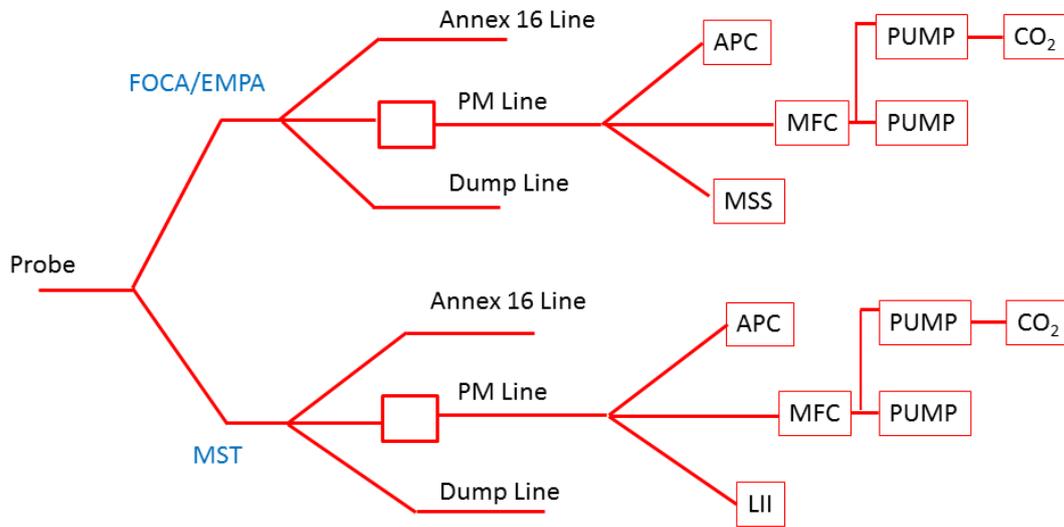
**Figure 3.15. Employed jet engine emission sampling system. The MST and FOCA/EMPA lines are in accordance with AIR.**

In addition to the AIR recommended instrumentation additional instrumentation was employed during the campaign as listed in Table 3.1 and shown in green in Figure 3.16 below.
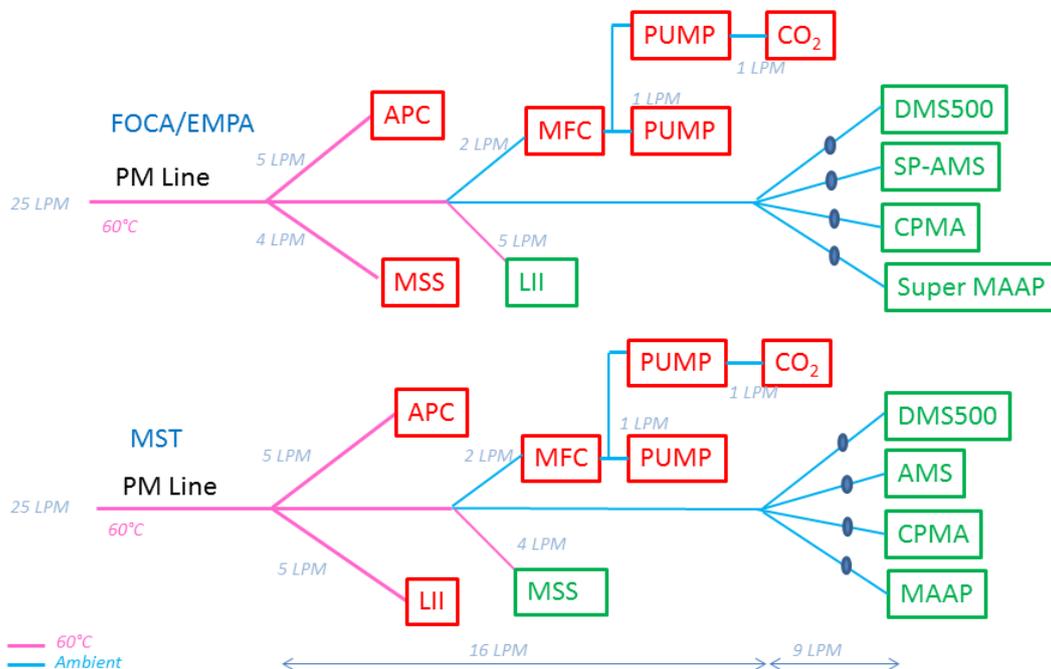


**Figure 3.16. Particulate matter sampling trains for the measurement of jet engine exhaust.**

Similar to the pre- and post-instrument comparison the location of the MSS and LII instrument were switched in the two lines for the emission sampling. The total aerosol flow in each line was 25 LPM of which 13 LPM was used for non-AIR instrumentation.

### 3.5.2.4 Particle Density Measurements

The relationship between mobility diameter measured with a DMA and particle mass measured with a CPMA was used to determine the effective density of the particles. An overview of the system used is shown in Figure 3.17.
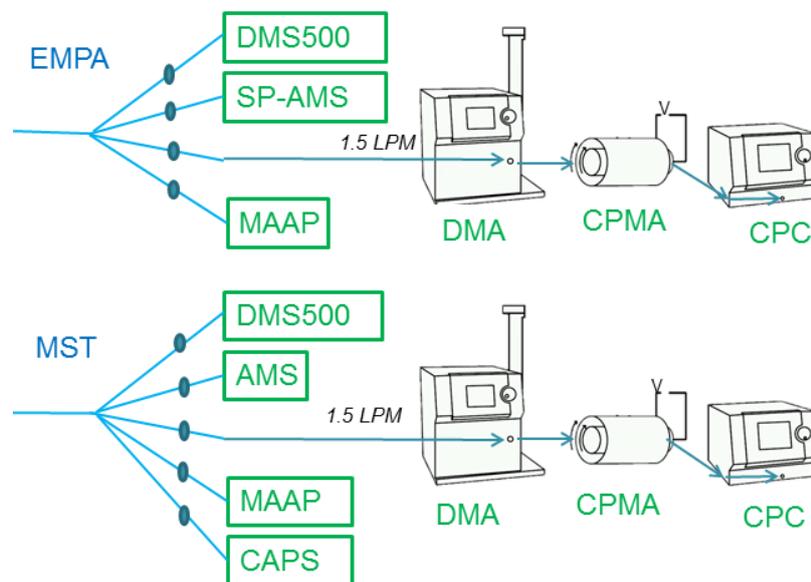


**Figure 3.17. Setup for particle density measurements during engine tests.**

The DMA selected particles of equal electrical mobility which were then passed through the CPMA and CPC which determined their particle mass. Mobility diameter set-points of 20, 30, 40 and 50 nm were evaluated during the engine tests.

### 3.5.3. Results and Discussion

### 3.5.3.1 Number and Mass Instrument Inter-Comparisons

The following two sections provide the results for the pre- and post-campaign comparison for the number and mass instruments.

## Particle Number Concentration Measurements

The comparison of the measured pre- and post-campaign number concentrations determined in the FOCA/EMPA and MST lines with the two APCs is shown in Figure 3.18 and Figure 3.19. The results in both figures are corrected for upstream dilution.
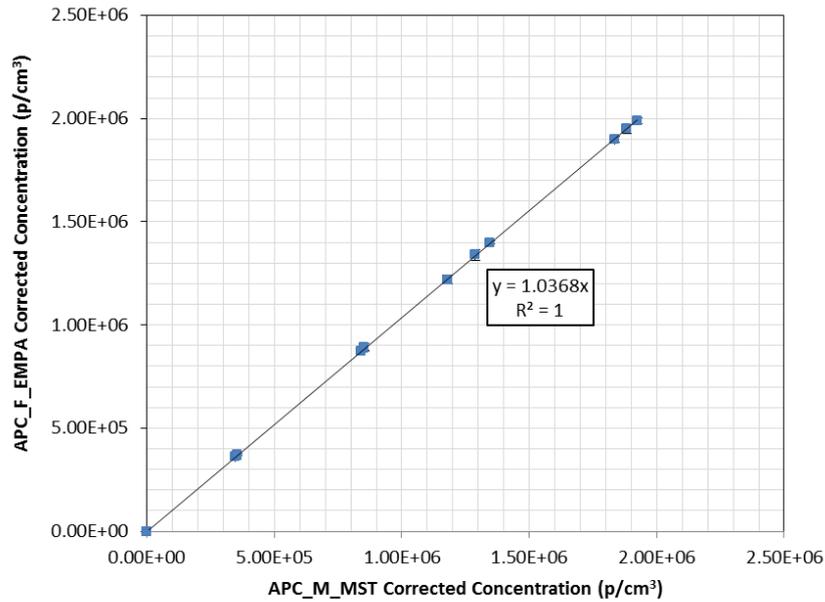


**Figure 3.18. Pre-campaign agreement of the two APCs used for measuring the particle number concentrations in the FOCA/EMPA and MST nvPM sampling lines.**
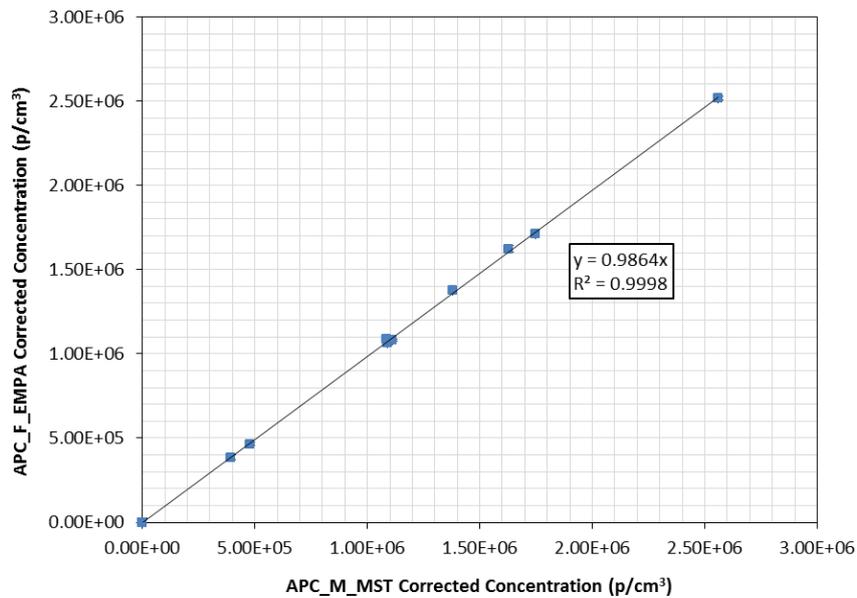


**Figure 3.19. Post-campaign agreement of the two APCs used for measuring the particle number concentrations in the FOCA/EMPA and MST nvPM sampling lines.**

Figures 3.18 and 3.19 show an agreement within ± 4 % between the two instruments. Using the MST APC as the reference, the APC in the FOCA/EMPA line had shown on average a 3.6% higher number concentration before the campaign (Figure 3.18). However, after the campaign the FOCA/EMPA APC number concentration was on average 1.4% lower than the one of the MST line (Figure 3.19). These differences are well within the uncertainty of the two instruments.

## Particle Mass Concentration Measurements

The measured nvPM mass concentrations determined by the 4 deployed instruments before and after the campaign are provided in Figures 3.20 and 3.21, respectively.
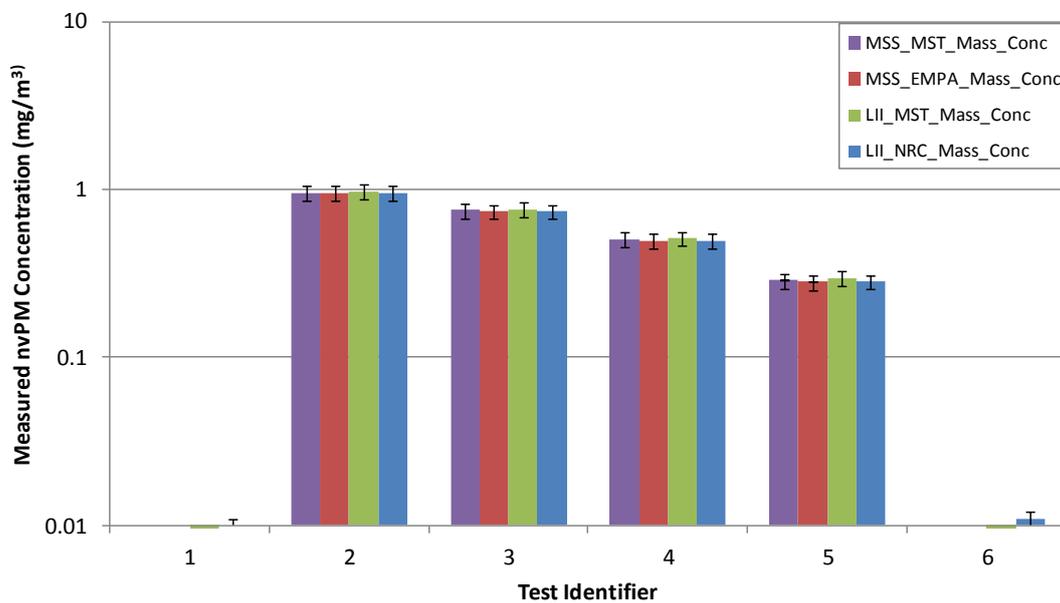


**Figure 3.20. Pre-engine test mass instrument agreement after calibration with NIOSH 5040.**
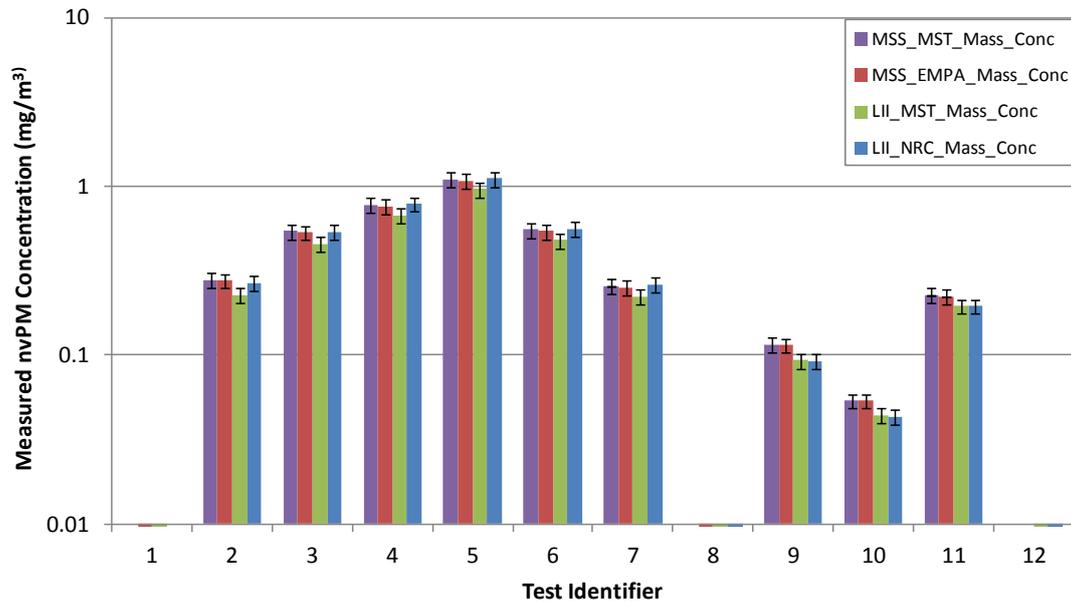
**Figure 3.21. Post-engine test mass instrument agreement.**

These results need to be interpreted carefully since all instruments were corrected before the tests to the MST LII that was calibrated with NIOSH 5040. Therefore, the results do not provide a measure of absolute accuracy but of instrument precision. The results show good agreement between the two sampling lines before the test and a slightly lower mass concentration after the test for the FOCA/EMPA line. There is no observable drift for the different instrument technologies between pre- and post- campaign. The slight difference between the lines in the post-test mass concentrations could be caused by an uncertain dilution factor.

### 3.5.3.2 Engine Emission Measurements

The following two sections provide the results for the agreements of particle number and particle mass for the engine tests.

**Particle Number Concentration Measurements**

The comparison of the determined particle number concentrations by the two APCs located in the FOCA/EMPA and MST line for all eight engine tests is shown in Figure 3.22. The provided results are corrected for dilution and normalized by engine fuel consumption.
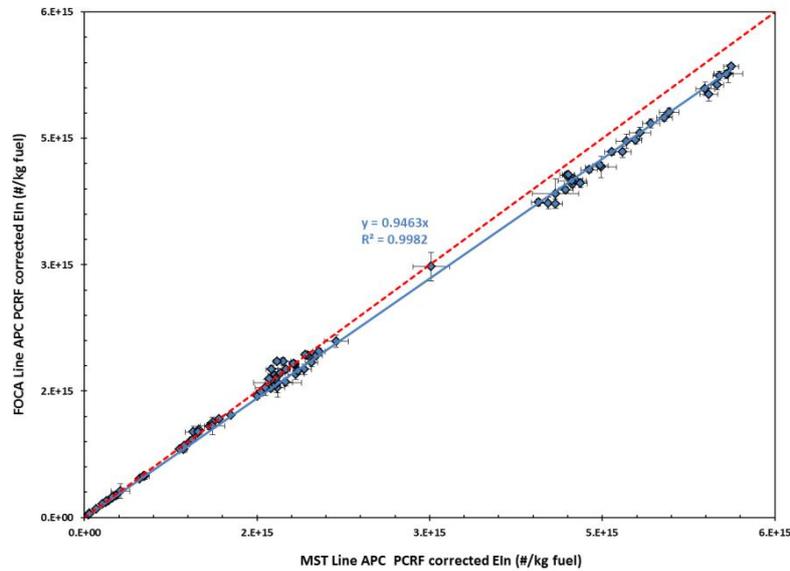
**Figure 3.22. Comparison of particle number concentrations for all engine tests measured by the APCs in the MST and FOCA/EMPA lines corrected for dilution and normalized by engine fuel consumption. The dashed red line indicates the ideal correlation and the solid blue line corresponds to the determined linear regression.**

Figure 3.22 indicates that the MST line measured on average a 5% higher particle number concentration than the FOCA/EMPA line. This agreement is within the accuracy of the instrumentation and indicates that the two sampling lines show a comparable performance in terms of particle losses. The exact reason for the slight disagreement between the instruments is not entirely clear but could be attributed to the uncertainty in the dilution factor.

**Particle Mass Concentration Measurements**

The agreement between the MST LII and FOCA/EMPA MSS determined particle mass concentrations for all eight engine tests are shown in Figure 3.23. The provided results are normalized by engine fuel consumption. The dashed red line indicates the ideal correlation and the blue line shows the determined regression.
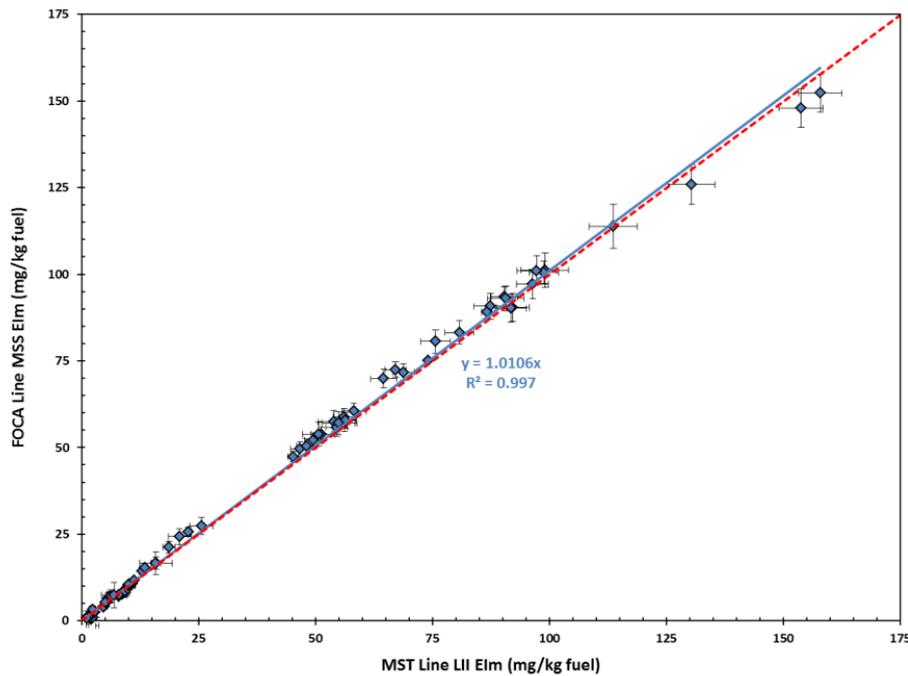
**Figure 3.23. Comparison of soot particle mass concentrations for all engine tests measured by the LII in the MST and the MSS in the FOCA/EMPA lines normalized by engine fuel consumption. The dashed red line indicates the ideal correlation and the solid blue line corresponds to the determined linear regression.**

The FOCA/EMPA line MSS and the MST line LII agree within 1%. Some slight non-linearity is observable in the data, which does not affect the overall result. The FOCA/EMPA MSS was initially calibrated against the MST LII. Therefore, these results do not provide an independent comparison for the two technologies used in terms of absolute accuracy but show the performance in terms of their precision. Furthermore, the results also show that the two sampling lines are comparable in terms of their mass penetration and overall performance.

The correlation between the FOCA/EMPA and MST MSS instruments is shown in Figure 3.24.
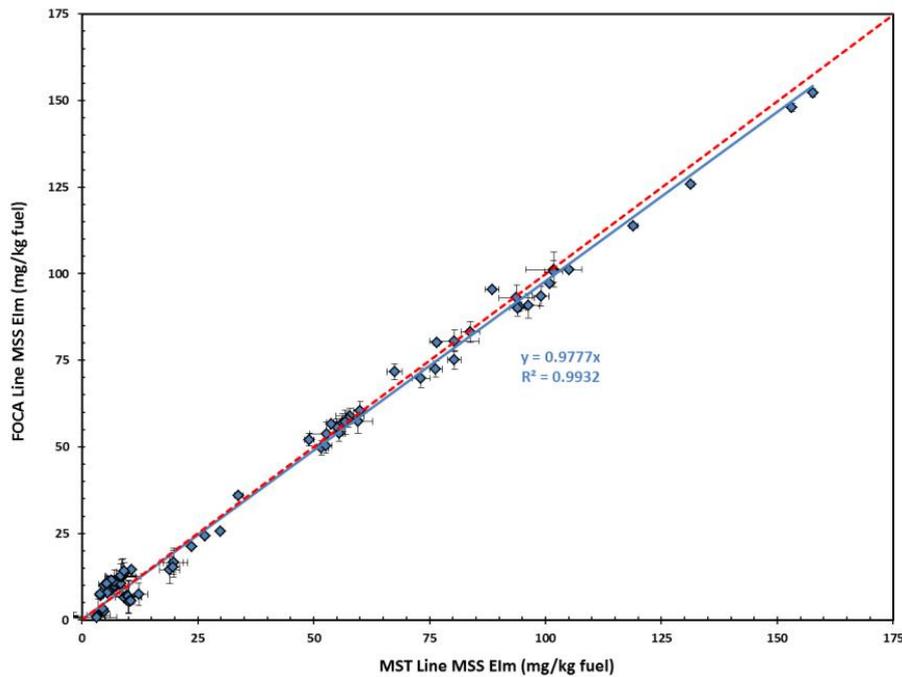
**Figure 3.24. Comparison of particle mass concentrations for all engine tests measured by the MSSs in the MST and FOCA/EMPA lines normalized by engine fuel consumption. The dashed red line indicates the ideal correlation and the solid blue line corresponds to the determined linear regression.**

Both instruments agree within 3%. The data show a slightly higher variability than the one in Figure 3.23. The slight differences in measured nvPM concentration could be caused by the different locations of the two instruments in the two sampling lines. The MST MSS is located in the dump line whereas the FOCA/EMPA MSS is part of the AIR system.

### 3.5.3.3 Effective Particle Density Measurements

The determined particle densities for 20, 30, 40 and 50 nm particles are shown in Figure 3.25 for a dedicated engine test.
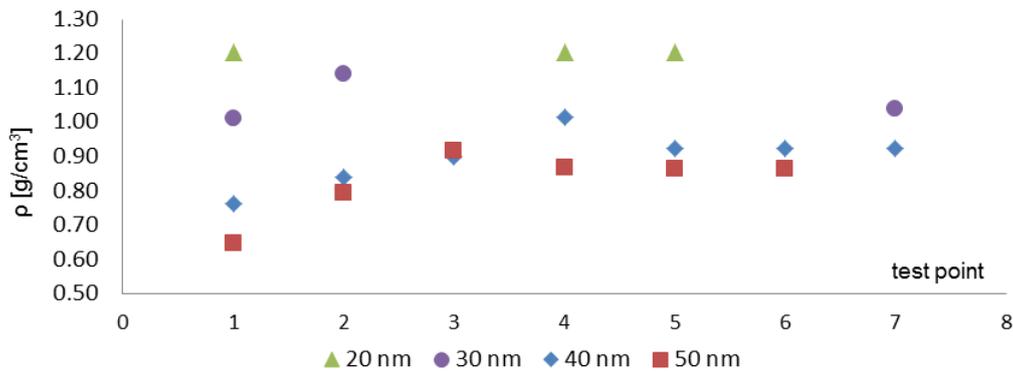
**Figure 3.25. Effective particle density as a function of particle size and engine test point determined during a dedicated engine test.**

The particle density is size dependent and decreases with particle size. The highest densities in the range of 1.2 g cm$^{-3}$ were observed for the 20 nm mobility diameter. The lowest density was in the range of 0.6 g cm$^{-3}$ at 50 nm mobility diameter. The lower density at larger mobility diameters can be explained by the structure of the particles. Large particles are assumed to be loose agglomerates but further research with scanning electron microscopy techniques is needed to prove this.

Figure 3.26 shows all the measured effective density values from Engine Tests 7 and 8 as a function of mobility diameter. In addition, measured density values from the miniCast set point 1 are also provided for comparison.
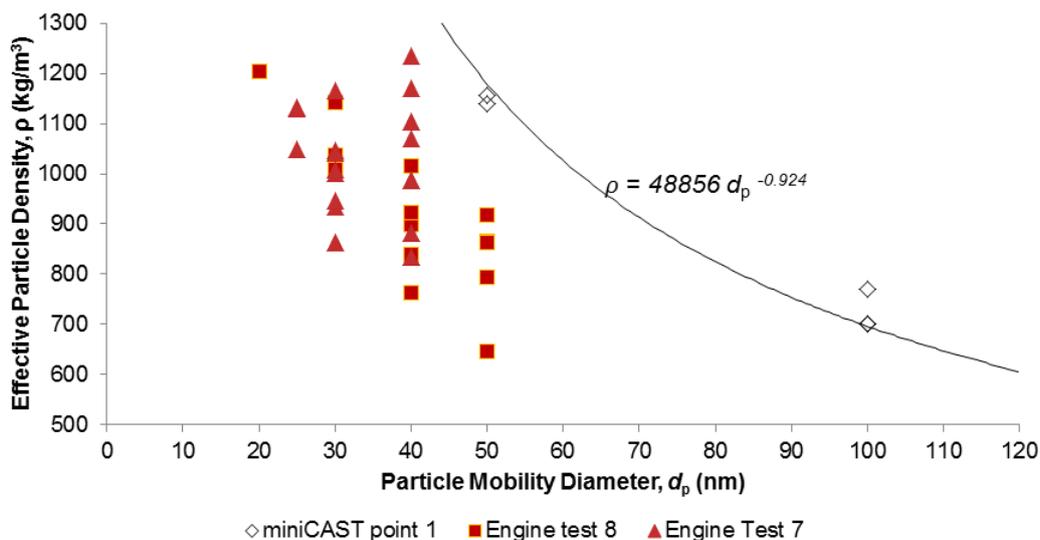


**Figure 3.26. Comparison of effective particle density values as a function of size for jet engine emission nvPM (colored symbols) and soot PM generated with the miniCast set point 1 (black symbols and line).**

The effective density of the jet engine emission nvPM shows a high variability, but as shown in Figure 3.26 a decreasing trend is observable with increasing mobility diameter. The jet engine emission nvPM also has lower density values than the soot PM produced by the miniCast soot generator.

### 3.5.4. A-PRIDE 4 Campaign Data Analysis

Zeqi Zhu, a temporary student helper during the ETH summer break, analyzed all dedicated A-PRIDE 4 engine test data in terms of nonvolatile mass and number emission indices. The analyzed data are shown in Figure 3.27 and uses the SR Technics determined FNK2 value as x-axis.
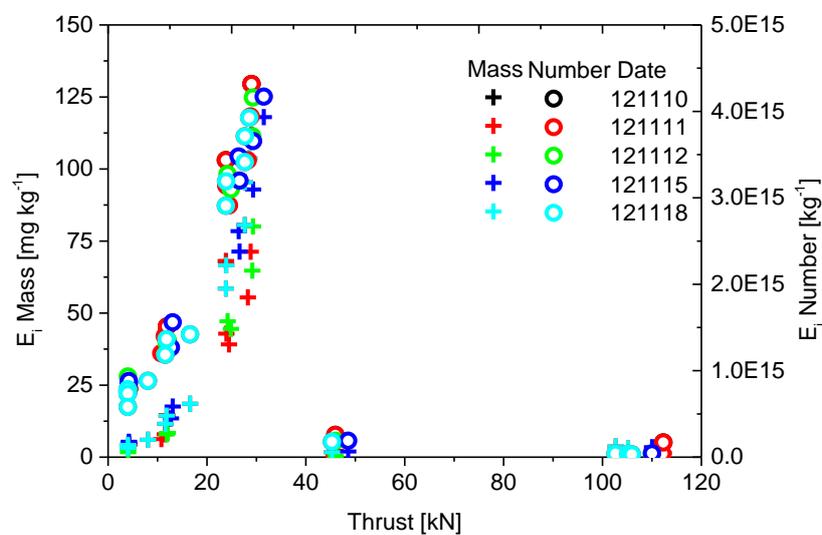


**Figure 3.27. NvPM mass and number emission indices for all the dedicated experiments performed during A-PRIDE 4.**

Figure 3.27 indicates that the nvPM mass and number emission indices increase for thrust levels up to 28 kN. Above 28 kN thrust, a sudden drop in emissions to an index near the detection limit of the mass instrumentation (< 5 mg kg$^{-1}$) is observable. This phenomenon is explained by the staged double annular combustor. This type of combustor is unique with respect to nvPM emissions: at low powers, only a pilot combustor zone is fuelled with a rich fuel mix to ensure combustion stability, resulting in high nvPM emissions; at high powers both the pilot and main combustor zones are fuelled with a lean combustor mix which results in low nvPM emissions. The variability in mass and number emissions indices for different days is relatively low, some variability in the data could have been caused by slightly different meteorological conditions, but further analysis of the data is required.

Along with the nvPM number and mass data, particle effective density was measured on the nvPM line using differential mobility analyzer (DMA), centrifugal particle mass analyzer (CPMA) and

condensation particle counter (CPC) connected in series. In this setup, particles are first pre-classified in the DMA based on their electrical mobility to charge ratio. Particles downstream of the DMA are monodisperse with pre-selected electrical mobility diameter. The range of particle diameters used during A-PRIDE 4 was from 20 to 50 nm. This is the range of the measured particle mode and highest particle number concentration and promised the best signal for particle classification in the CPMA. CPMA classifies particles based on their mass to charge ratio. Assuming singly-charged particles, one obtains mass of the particles with preselected electrical mobility size. Population of these DMA-CPMA-classified particles is then finally counted by the CPC.



Figure with legend: $Rho_{eff} = 0.67156 \cdot Dp^{(2.5774-3)}$ (dashed), 95% confidence interval (red). Axes: particle effective density [kg/m3] vs electrical mobility size [m], color bar engine thrust [kN].
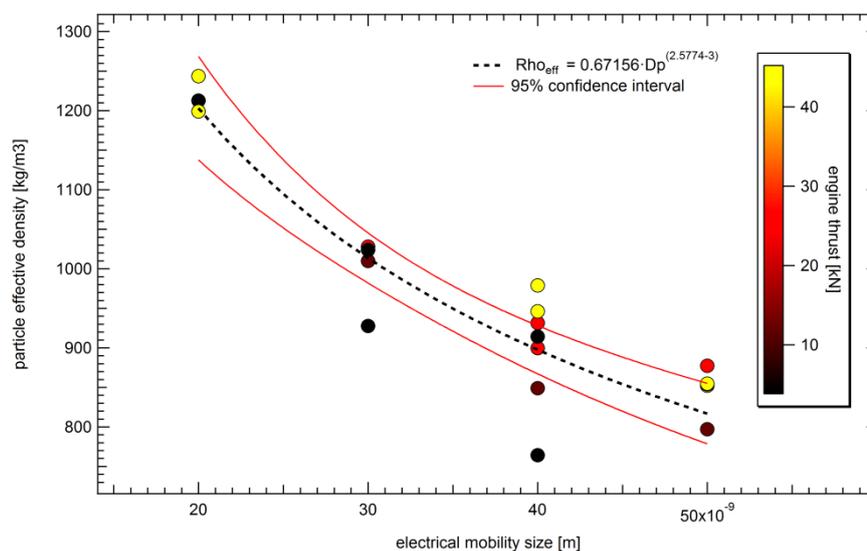
**Figure 3.28. Effective density data fit across all engine test points.**

Successful measurements of effective density during A-PRIDE 4 were possible to a certain extent only during the last dedicated engine run on November 18. During all the previous engine runs DMA-CPMA-CPC setup was operated in low flow mode (0.3 lpm) and no signal could have been obtained. This was probably due to the higher diffusion losses and longer pressure equilibration time between the CPMA classifier and the CPMA box covering the classifier.

Running the instrument by default in high flow mode (1.5 lpm) was not used due to the total flow rate restriction in the nvPM line and flow competition with other ancillary instruments requiring high flow rate like the DMS5000 (8 lpm). These instruments were turned off on the November 18, 2013 and effective density setup was operated in the high flow mode. Results of these measurements are shown in Figure 3.28.

Effective density of the particles follows the so-called fractal-like relationship between particle mass and size using the power law $m_p = C \cdot d_p^{D_m}$ where C is a constant and $D_m$ is the mass-mobility exponent. This exponent is for soot agglomerates usually in the range from 2.2 to 2.8. In case of the effective density fit function in Figure 3.28, $D_m$ equals 2.5774. Further analysis including mass emission calculation using effective density function and particle size distribution data is published in Durdina et al. 2014.

### 3.5.5. Summary and Conclusions

The Aviation Particle Regulatory Instrumentation Demonstration Experiment 4 was conducted from November 5-19, 2012 at SR Technics in Kloten with the main objective to compare two nvPM sampling systems which comply with the aerospace recommended practice draft document. Pre- and post- campaign tests performed with a miniCast soot aerosol generator showed a particle number instrument agreement within ± 4 % and a particle mass agreement within the pooled instrument uncertainties of the two sampling lines. Sampling during four dedicated and three piggy-back jet engine tests had a similar agreement in terms of number and mass, within 5% and within 3% respectively. The measured effective particle density was in the range of 0.6 to 1.2 g cm$^{-3}$. The effective density also decreased with increasing particle mobility diameter. The results of the A-PRIDE 4 campaign are published in Lobo et al. 2015.

# 4. Activities and results in the period 2013/01 – 2013/07

## 4.1. Introduction

This chapter describes the progress of the Swiss Federal Office of Civil Aviation (FOCA) sponsored project entitled "Particulate Matter and Gas Phase Emission Measurement of Aircraft Engine Exhaust" during the period between January and July of 2013. The project time period included activities on the calibration of the micro soot sensor (section 4.2), the evaluation of nvPM losses in the heated sampling line of the aircraft nvPM Sampling system (section 4.3), the design of a new measurement equipment rack (section 4.4) aircraft engine source piggy back measurements and a joint mini campaign with PSI and ETHZ performed at the SR Technics engine test cell (section 4.5), and preparations for the A-PRIDE 5 campaign (section 4.6) which was conducted in July and August 2013.

## 4.2. AVL micro soot sensor (MSS) calibration

### 4.2.1. Introduction

According to the SAE E-31 AIR6241, the MSS and laser induced incandescence (LII) instruments utilized for determining non-volatile soot mass concentrations in aircraft exhaust require an annual calibration using filter collected elemental carbon (EC) mass determined by the thermo-optical NIOSH 5040 protocol as a reference. EMPA's MSS instrument was factory calibrated when the instrument was purchased before the A-PRIDE 4 campaign in October 2012. In the beginning of the A-PRIDE 4 campaign the factory determined calibration constant of 0.475 was adjusted to 0.396, when the instrument was compared to a NIOSH 5040 calibrated LII instrument for mini cast generated soot.

In total four MSS calibrations runs were performed by EMPA for the period between January and May 2013. EMPAs MSS instrument also participated in the July 2013 mass instrument calibration campaign lead by Dr. Gregory Smallwood at the National Research Council (NRC), Canada.

### 4.2.2. Methods

Figure 4.1 and Figure 4.2 provide a schematic overview and an actual picture of the MSS calibration setup installed in the laboratory at Empa.
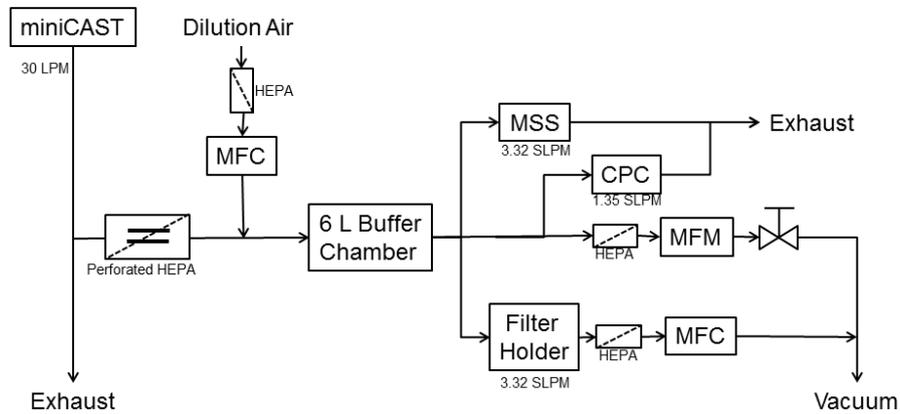
**Figure 4.1. Mass instrument calibration schematic.**
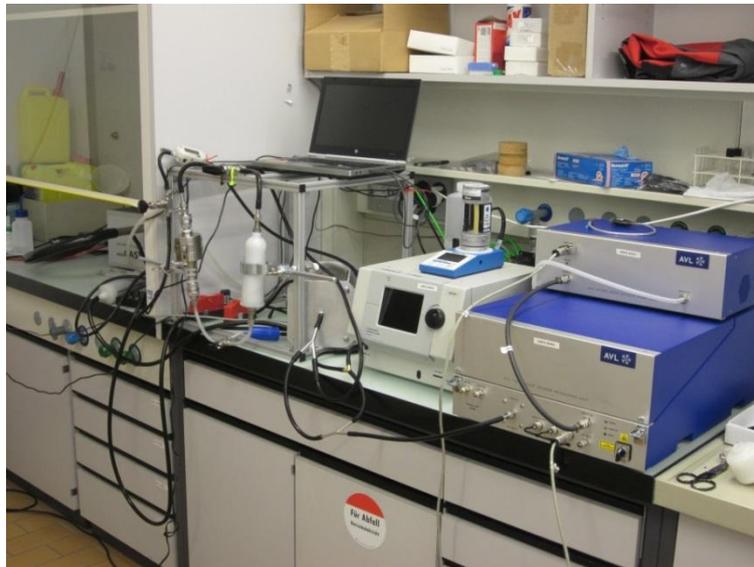


**Figure 4.2. MSS calibration setup installed at Empa.**

A miniCast soot generator (Model 5201, Jing Inc.) generated soot particles. The instrument settings were:

- Fuel (propane): 60 LPM

- Premixing nitrogen: none

- Nitrogen for quenching: 7 LPM

- Combustion air: 1.55 LPM

to produce an EC mass fraction of roughly 80% in the generated soot particles. 0.3 to 2 LPM of the particle laden airflow was then drawn through a perforated HEPA filter. The main purpose of this filter

that contains a perforation of 1.5 mm in diameter is to reduce the particle concentration from 300 mg m$^{-3}$ to approximately 10 mg m$^{-3}$. After the perforated filter the particle flow was diluted with dry HEPA filtered air to the desired mass concentrations, which were approximately 0.25, 0.5, 0.75 and 1 mg m$^{-3}$. A 6L buffer chamber allowed for a uniform mixing of the flows and smoothed potential concentration fluctuations. After the buffer chamber a three way splitter was used to connect the MSS, the filter holder and the excess flow. The ¼" conductive tubing which connected the MSS and filter holder had equal lengths of 0.8 m and equal flow rates of 3.32 SLPM to assure similar PM losses in the two lines. A condensation particle counter (CPC) on the excess flow line was used to monitor the stability and fluctuations in the PM number concentration signal with time.

Quartz fiber filters (Tissuquartz 2500AT-UP, Pall Inc.) were employed to collect PM mass. Sampling times were adjusted to ensure approximately equal mass concentration of approximately 15 µg cm$^{-2}$ on each filter. The sampling times used were 120, 60, 45 and 30 minutes for the 0.25, 0.5, 0.75 and 1 mg m$^{-3}$ concentrations, respectively. The exact integrated standard volume flow for each filter sample was determined by the mass flow controller software and logged for each filter.

The collected filters were analyzed by Dr. Andrea Fisher (Empa Abteilung Luftfremdstoffe) according to the NIOSH 5040 protocol. Two filter punches were analyzed per filter. For one calibration experiment the effect of different OC/EC splits was examined by keeping the filter heating profile unchanged. The OC/EC splits based on laser transmission (NIOSH 5040 standard), reflectance (US EPA IMPROVE Protocol) and operator manual split were investigated.

### 4.2.3. Results and Discussion

The calibration result with the 0.396 calibration constant (determined at A-PRIDE 4) is shown in Figure 4.3. The EC mass concentration determined by the NIOSH 5040 protocol in combination with the integrated filter flow rate is plotted on the x-axis. The average measured BC mass concentration measured with the MSS is shown on the y-axis. Uncertainties in the determined NIOSH 5040 EC mass concentration were determined from the uncertainties in the integrated volume flow (2%) and the reported standard deviation of the OC/EC instrument. The uncertainties for the y-axis correspond to the standard deviation of the MSS reading over the sampling period. The determined regression line takes both the x and y errors into account.
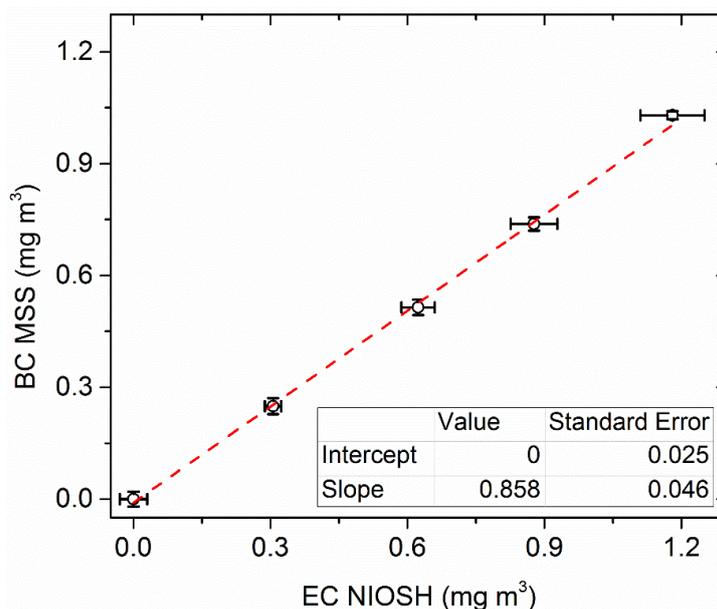
**Figure 4.3. MSS calibration performed at EMPA.**

Figure 4.3 indicates that the MSS calibration constant determined during the A-PRIDE 4 campaign results in 15% lower MSS BC mass concentration readings than the EC concentration readings determined by NIOSH 5040. Therefore the instrument calibration constant was adjusted by the inverse of the found regression slope. The new constant was found to be 0.462 which was within 3% of the factory calibration value 0.475. The following Table 4.1 shows the effect of using different OC/EC split methods on the slope of the regression and the MSS calibration constants

**Table 4.1. Effect of different OC/EC splits on the determination of the MSS calibration constant**

| OC/ EC Split Method | Regression Slope | Calculated MSS Calibration Constant |
|---|---|---|
| Transmission (NIOSH Standard) | 0.858 | 0.462 |
| Reflectance | 0.899 | 0.440 |
| Manual (Dr. Andrea Fisher) | 0.878 | 0.451 |

Due to the relatively low (20%) mass fraction of OC in the generated particles, the use of different OC/EC split points in the OC/EC thermabsogram had a relatively small artifact on the results. All three determined calibration constants agreed within 2% indicating that correction for charring OC in the analysis does not affect the amount of EC significantly.

The calibration performed by NRC with the instrument factory calibration constant of 0.475 is shown in Figure 4.4.
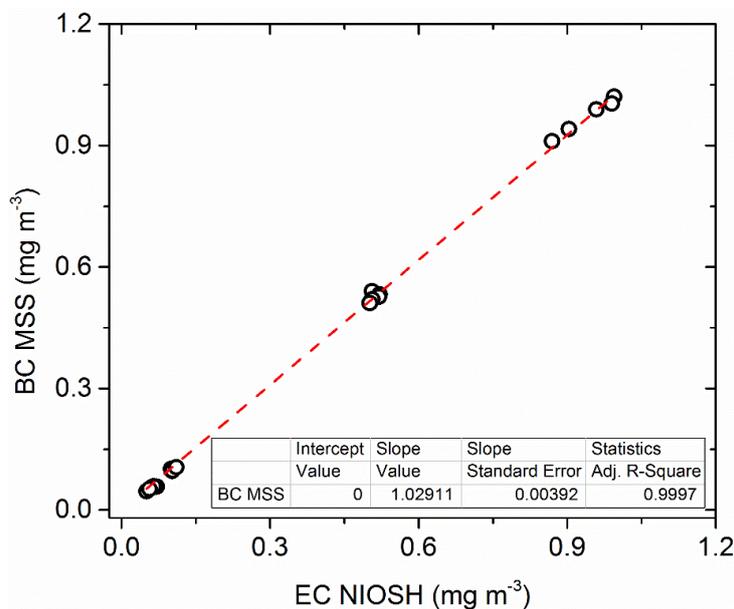


**Figure 4.4. MSS calibration performed at NRC Canada.**

The NRC calibration data shows a good agreement between the BC mass concentrations of the MSS instrument vs. filter determined EC mass concentration determined with NIOSH 5040. The slope value of 1.0291 indicates that the instrument slightly over predicts the EC concentration when using the factory calibration constant of 0.475. The calculated adjusted calibration constant after this calibration is 0.4616, which matches perfectly the value of 0.462 determined by EMPA.

## 4.2.4. Conclusions

The AVL MSS mass instrument was calibrated against filter determined EC mass concentration by the NIOSH 5040 thermo-optical method. Two independent calibrations were performed, one at EMPA and one at NRC. EMPA and NRC report nearly identical calibration constants of 0.462 and 0.4615, respectively, indicating good agreement with the AVL factory calibration value of 0.475. Applying different methods for determining the OC/EC split in the thermabsogram resulted in a calibration factor change of 2% indicating that the correction for charring OC in the analysis does not affect the amount of EC significantly for the used minicast soot aerosol.

Empa has the capability and resources in house to perform future required E31 AIR 6241 calibrations. Since multiple Empa divisions are involved, analyzing and processing the filters and data involves time and requires ahead planning if results are required on specific dates.

## 4.3. Evaluation of sampling line PM losses

### 4.3.1. Introduction

A detailed and accurate characterization of the sampling system with respect to particle losses is essential to relate the measured particle mass and number concentrations to the engine source. Furthermore repeated measurements over longer periods of time could determine if the installed sampling lines need to be exchanged. Empa conducted a line penetration measurement on April 19, 2013, when the engine test cell at SR Technics was available for two days due to maintenance work.

### 4.3.2. Methods

The spill of the Dekati diluter was used as the inlet for the line penetration test. A schematic overview and pictures of the experimental setup are shown in Figures 5 and 6, respectively.
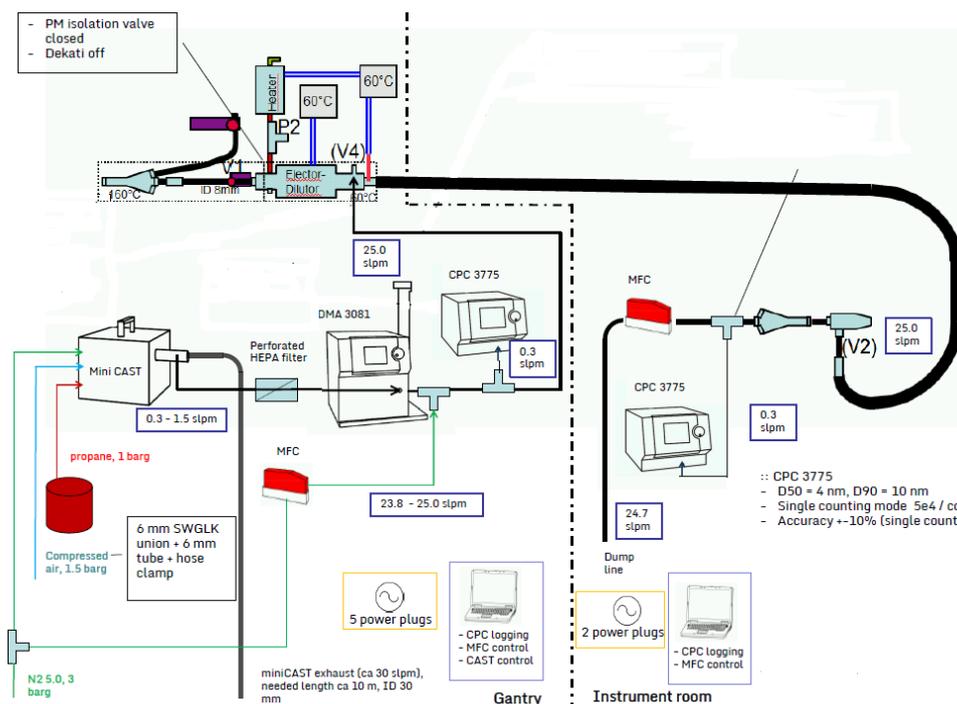


**Figure 4.5. Schematic of the experimental setup for the line penetration measurement.**

**Figure 4.6. Connection to the Dekati spill (left) and monodisperse soot PM generation (right).**

A similar minCast setup with a perforated filter as described in section 4.2.2 was used to generate polydisperse soot PM. There is no single miniCast test point which can generate poly disperse soot PM in the desired electrical mobility diameter range up to 150 nm, therefore test point 8 was used for mobility sizes ranging from 20 to 50 nm and test point 1 for mobility diameters ranging from 40 to 150 nm. Due to the different burner settings the generated particles at test point 8 have a higher pyrolyzed OC content (up to 60%) in comparison to test point 1 which contains around 80% EC and is more representative of emitted aircraft gas turbine PM.

A differential mobility analyzer (DMA, TSI Model 3081) was used to select quasi monodisperse particles of a certain electrical mobility diameter. Due to the relatively small size range (< 200 nm) of the generated polydisperse soot PM the contribution of multiple charged soot particles to the selected mobility diameter was estimated to be negligible. The electrical mobility diameters selected with the DMA tested included 20, 30, 40, 50, 60, 70, 80, 100, 125, and 150 nm. Two CPCs of the same model (TSI Model 3775) were used to measure up- and downstream concentrations. While the upstream concentration was measured as close as possible to the Dekati spill port, the downstream concentration was measured on the MSS port of the sampling system. The two CPC's were adjusted in the laboratory to have the same reading when no sampling line was present. The adjustment was in the range of 3%. The sampling line was operated in its usual configuration (60°C and 25 SLPM flow). To reach the 25 SLPM a dilution flow of dry nitrogen after the DMA was necessary.

The line penetration model developed Liscinsky et al. from the united technologies research center (UTRC) was utilized for modeling the theoretic line penetration. The penetration was modeled for a simplified sampling system with 4 sub-sections:

- 1.5 m unheated 1/4" conductive tubing between the CPC and the Dekati spill

-   24.5 m 60°C 8mm ID heated line from Dekati to Cyclone

-   Cyclone (penetration values taken from last progress report)

-   0.75 m 60°C 8mm ID heated line section between the Cyclone and the CPC

No thermophoretic losses were modeled; the gas, particle and tubing wall temperatures were assumed to be in equilibrium at 60°C.

### 4.3.3. Results and Discussions

The following figure 4.7 shows the measured and modeled penetration values for the 60° heated section of the sampling system between the Dekati and the MSS connection. Penetration uncertainties were calculated from the measured standard deviations, sizing uncertainties were assumed to be 5%.
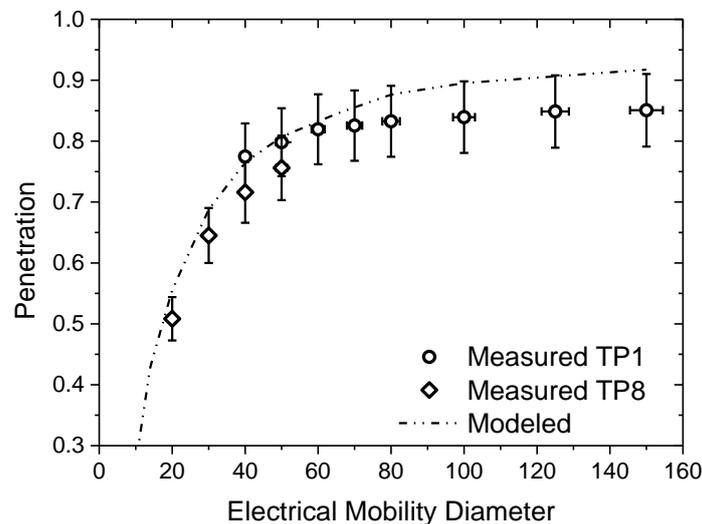


**Figure 4.7. Measured (symbols) and modeled PM penetration as a function of PM electrical mobility diameter for miniCast soot generated with setting 1 (circles, 20 to 50 nm) and setting 8 (diamonds 40 to 150 nm).**

The observed penetration shows the expected modeled behavior. Diffusion to the tubing walls is the dominant loss mechanism which results in almost 50% particle loss at the 20 nm mobility diameter. The line loss decreased with increasing particle electrical mobility diameter. The measured penetration was roughly 5% lower than the modeled values at mobility diameters greater than 80nm. Furthermore the measured penetration seems to plateau earlier than suggested by the model. The exact reason for this behavior is unclear. More losses in the sampling system in comparison to the model are somewhat expected because the model does not resolve the geometries inside the Dekati dilutor or the two splitters. A further reason for the difference could also be more coagulation due to the higher PM concentration for the larger mobility diameter experiments. For the 80 to 150 nm mobility

diameters the inlet CPC concentrations ranged from 13000 to 22000 cm$^{-1}$, whereas for the other experiments the concentrations were in the range of 700 to 5000 cm$^{-1}$.

### 4.3.4. Conclusions

The line penetration was measured and modeled for the section of the sampling system installed at SR Technics, namely between the Dekati diluter and the MSS connection port. A soot generation and aerosol particle size selection system was installed on the balcony in the test cell. Line penetrations were measured for soot particles with mobility diameters ranging from 20 to 150 nm. An expected line penetration that qualitatively agrees with modeled values was observed.

## 4.4. Planning and design of a new instrumentation rack

### 4.4.1. Introduction

Until the publication of the AIR6241 by SAE-E31, the sampling system installed at SR Technics was under constant development. While the sampling system and lines in the test cell were constructed to fulfill SR Technics guidelines, the downstream instrument placement was designed for the quick change of equipment. Due to all the necessary power, gas and data acquisition lines, the arrangement of the equipment became complex and is hard to maintain and requires skilled personnel to operate. A picture of the current instrumentation setup is provided in Figure 4.8.
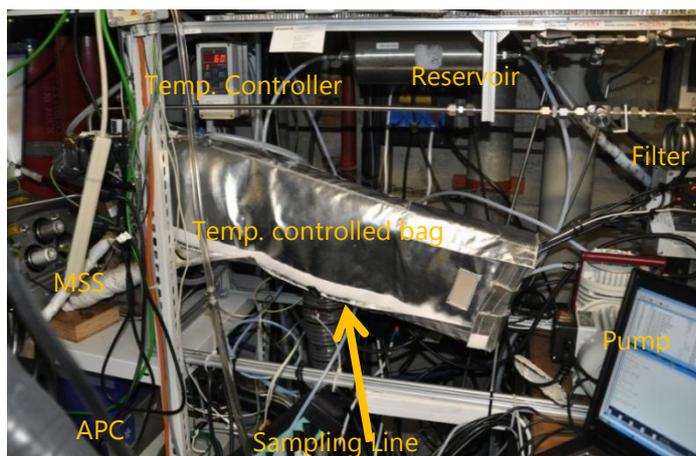


**Figure 4.8. Equipment setup at SR Technics in 2013.**

Since the publication of the AIR the measurement equipment is specified and no drastic changes in the downstream sampling equipment are expected in the future. FOCA furthermore would like to potentially use the sampling system in the field on a mobile platform in the future. Therefore a safe

and user-friendly placement of the measurement instrumentation is a long-term goal. While this is not part of the scientific proposal that was submitted to FOCA, Empa developed an initial rack design. Empa believes that the time and effort spend will pay off for them by having a system that is safer and easier to maintain and operate.

## 4.4.2. Developed Design

Based on the instrument specifications, a rack design was developed by Empa and a specification was written for a potential contractor. A snapshot of the design is shown in Figure 4.9.
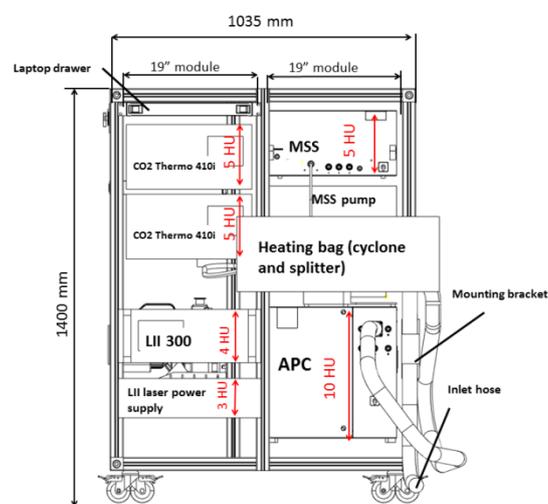


**Figure 4.9. Frontal view of the developed instrument rack design.**

## 4.4.3. Status

The execution of the rack building was delayed several times, first the favored contractor NBN-Electronics was not willing to perform the specified work. Then the preparations for the A-PRIDE 5 campaign started and the work was put on hold. A new contractor was found with the apprentice shop of SR Technics who updated the rack specifications and submitted an offer for building the designed rack at the beginning of October 2013. The installation of the equipment on the new rack started around February 2014.

## 4.5. Piggy back measurements and joint mini campaign at SR Technics

### 4.5.1. Introduction

From the beginning of March until the end of June Empa performed piggy back measurements of customer engines at SR Technics. Table 4.2 shows an overview of all piggy back measurements including ambient meteorological conditions such as barometric pressure ($P_A$), temperature range ($T_A$) and relative humidity (RH) range during the tests. In addition the corresponding fuel sample for each test is also presented in Table 4.2.

**Table 4.2. Overview of piggy back experiments performed at SR Technics**

| Date | $P_A$(mbar) | $T_{Amin}$(°C) | $T_{Amax}$(°C) | $RH_{min}$(%) | $RH_{max}$(%) | Fuel Sample | Comment |
|---|---|---|---|---|---|---|---|
| 13.03.2013 | 951 | 1.1 | 3.2 | 85 | 88 | 03.04.2013 | |
| 19.03.2013 | 953 | 8.2 | 8.5 | 45 | 49 | 03.04.2013 | |
| 22.03.2013 | # | # | # | # | # | 03.04.2013 | No Engine Data |
| 26.03.2013 | 955 | - 1.2 | 1.8 | 77 | 87 | 03.04.2013 | |
| 27.03.2013 | 957 | -2.2 | 0.1 | 74 | 82 | 03.04.2013 | |
| 24.04.2013 | 975 | 18.8 | 21.8 | 23 | 29 | 03.05.2013 | |
| 03.05.2013 | 965 | 12.5 | 13.3 | 81 | 83 | 03.05.2013 | |
| 03.05.2013 | 964 | 11.1 | 13.6 | 76 | 93 | 03.05.2013 | |
| 15.05.2013 | 952 | 14.1 | 17.3 | 53 | 79 | 03.05.2013 | |
| 15.05.2013 | 952 | 18.1 | 19.1 | 47 | 56 | 03.05.2013 | |
| 21.05.2013 | 963 | 10.6 | 12.7 | 73 | 83 | 03.06.2013 | |
| 24.05.2013 | 961 | 6.6 | 9.2 | 58 | 75 | 03.06.2013 | |
| 03.06.2013 | 973 | 10.4 | 11.6 | 68 | 71 | 03.06.2013 | Joint Campaign |
| 04.06.2013 | 968 | 15.5 | 19.0 | 47 | 56 | 03.06.2013 | Joint Campaign |
| 06.06.2013 | 967 | 21.7 | 24.0 | 22 | 29 | 03.06.2013 | Joint Campaign |
| 07.06.2013 | 969 | 21.0 | 23.7 | 29 | 45 | 03.06.2013 | Joint Campaign |

A one week measurement campaign jointly with the PSI and ETH teams was also a part of this piggy back effort. The joint campaign was performed in calendar week 23 at the beginning of June 2013. In terms of ambient conditions the March tests had some temperatures at freezing conditions. The highest ambient temperature (24°C) was observed for the joint piggy back campaign at the beginning

of June. While the ambient temperature changed typically not more than 4°C during a test, RH changed more than 20% in some cases. The ambient temperature is expected to have effect on the PM emission levels.

## 4.5.2. Methods

For all tests the single point probe was operated at the specific position determined by FOCA. The setup was operated in its standard configuration. During the piggy back campaign additional instrumentation was connected by PSI and ETH on the dump line (Section 4.6, Figure 4.17). For some measurements the particle size distribution was either measured with a scanning mobility particle sizer (SMPS) or a fast mobility particle sizer spectrometer (FMPS). Fuel samples were drawn by Erwin Roduner (SR Technics) each time when a new fuel batch was present in the tank. Typically SR Technics consumes a batch of fuel (85000 L) every three to four weeks depending on testing activities. The fuel samples were analyzed for the Annex 16 parameters aromatics, naphtalenes, total sulfur, hydrogen, density, viscosity, specific energy and volatility (distillation initial and end boiling points). All the fuel samples were analyzed by Urs Debrunner and his team at Intertek AG in Schlieren.

NvPM emission indices ($E_i$) were calculated according to equations 7.15 and 7.16 from the SAE E31 6241 AIR document. 30 second averaged nvPM mass and number concentrations and gas data were used as inputs. Generally periods right before the engine conditions changed were used for the calculations, which allowed for longest possible time of the engine and the sampling system to equilibrate in terms of temperatures and pressures. No line loss corrections are applied to the data shown in this report. The variables named FNK2 (CFM Engines) and FNC_LBS (Pratt and Whitney) were used in the data analysis for describing the Engine thrust. These two variables describe the engine thrust corrected for deviations from the international standard atmosphere (ISA, 15 °C/ 1013.25 mbar) and for engine test cell air flow. Fractional engine powers were calculated by dividing this corrected thrust value by the rated take off engine thrust of each engine type.

## 4.5.3. Results

### Fuel Specifications

The fuel specifications for the three analyzed fuel samples are shown in Table 4.3.

**Table 4.3. Fuel specifications.**

| Parameter | Unit | Annex 16 LOW | Annex 16 HIGH | 03.04.2013 | 03.05.2013 | 03.06.2013 |
|---|---|---|---|---|---|---|
| Aromatics | % (V/V) | 15 | 23 | 18.4 | 17.9 | 17.8 |
| Sulfur, total | % (m/m) | 0 | 0.3 | 0.066 | 0.06 | 0.065 |
| Initial boiling point | °C | NA | NA | 149 | 152 | 150 |
| 10 Vol % recovered at | °C | 155 | 201 | 169 | 170 | 169 |

| | | | | | | |
|---|---|---|---|---|---|---|
| 20 Vol % recovered at | °C | NA | NA | 176 | 176 | 175 |
| 50 Vol % recovered at | °C | NA | NA | 195 | 195 | 194 |
| 90 Vol % recovered at | °C | NA | NA | 235 | 235 | 234 |
| End point | °C | 235 | 285 | 260 | 258 | 260 |
| Residue | % (V/V) | NA | NA | 1 | 1.2 | 1.1 |
| Loss | % (V/V) | NA | NA | 0.5 | 0.6 | 0.4 |
| Density at 15 °C | kg/m³ | 780 | 820 | 802.4 | 801.3 | 798.7 |
| Viscosity at -20 °C | mm²/s | 2.5 | 6.5 | 3.74 | 3.723 | 3.654 |
| Specific energy, net | MJ/kg | 42.86 | 43.5 | 43.2 | 43.2 | 43.2 |
| Smoke point | mm | 20 | 28 | 20 | 20 | 20 |
| Naphthalenes | % (V/V) | 1 | 3.5 | 1.11 | 0.92 | 0.78 |
| Hydrogen | % (m/m) | 13.4 | 14.3 | 13.74 | 14.38 | 14.3 |
| H/C ratio (calculated) | NA | 1.84 | 1.99 | 1.90 | 2.00 | 1.99 |

All Annex 16 specifications were met besides for the naphthalenes for the samples of May 3rd and June 6th and for Hydrogen on May 3rd. While the level of naphthalenes did not meet the lower level specified by Annex 16 (1%) at this time (it met the future specifications), the total aromatic content did. Aromatics content is known to have an impact on nvPM emissions; the exact role of its naphthalene subspecies required further research.

## Raw Data Results of a Typical Engine Test Run

A raw data example of the June 4th piggy back test is displayed in Figure 4.10. The undiluted gaseous concentrations measured on the Annex 16 line are shown in the top graph and the roughly tenfold diluted nvPM mass and number concentrations are shown on the bottom.

The gaseous emissions show the typical behavior of a combustion process at different stages; carbon dioxide ($CO_2$) nitric oxides ($NO_x$) concentrations increase with increasing engine power, oxygen ($O_2$) decreases. Carbon monoxide (CO) and unburned hydrocarbons (UHC) are present at low combustion efficiencies i.e. ground idle (at the beginning and the end of the time period shown in Figure 4.10). The nvPM number concentration is the highest after the startup of the engine, but the concentration is unstable and decreases with time. The highest mass and number concentrations are found at the highest engine powers for this type of engine where the emissions of $NO_x$ and $CO_2$ are also the highest.
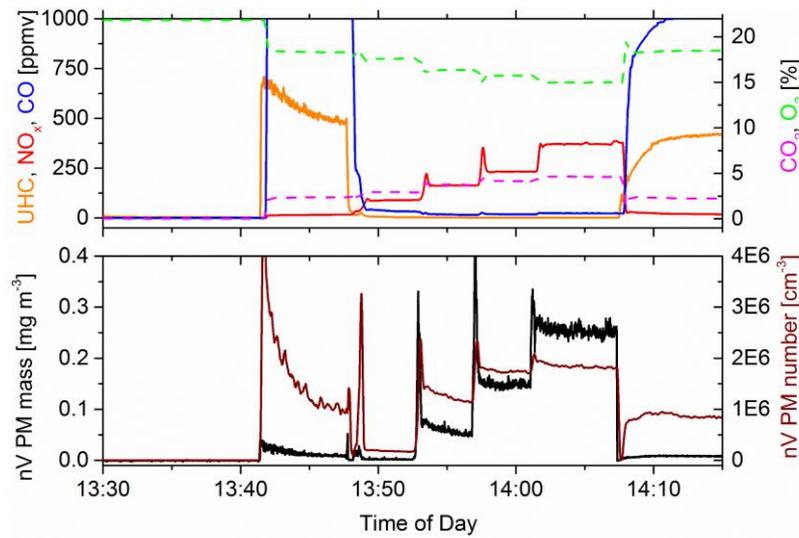
**Figure 4.10. Raw data from the June 4th piggy back test. The undiluted gaseous concentrations measured on the Annex 16 line are shown in the top and the diluted nvPM mass and number concentrations are shown on the bottom graph.**

## Calculated Emission Indices

Figure 4.11 shows the calculated nvPM mass and number emission indices for the June 4th piggy back test.
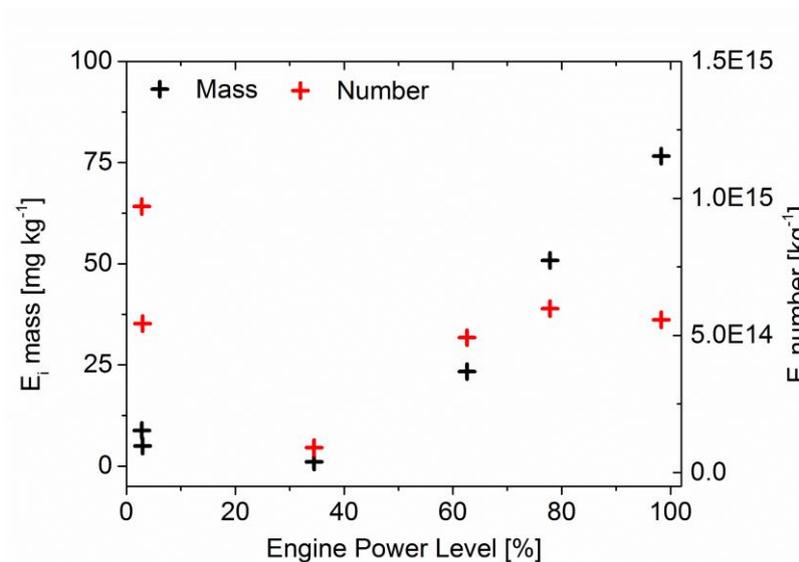


**Figure 4.11. Calculated nvPM mass and number emission indices of an engine source measured on June 4th, 2013.**

The mass emission index ranges from nearly zero at 35% engine power to 78 mg kg$^{-1}$ at 98% engine power. A slightly higher than zero mass $E_i$ is observed at ground idle (approximately 3%) engine power. For the nvPM number emission index the highest value is observed at ground idle while the lowest nvPM number emissions were observed near 35% engine power. An interesting feature is that the nvPM number emissions seem to level off at engine powers above 80%, while the mass is still increasing. This indicates that the size distribution is also changing as it can be seen in Figure 4.12.
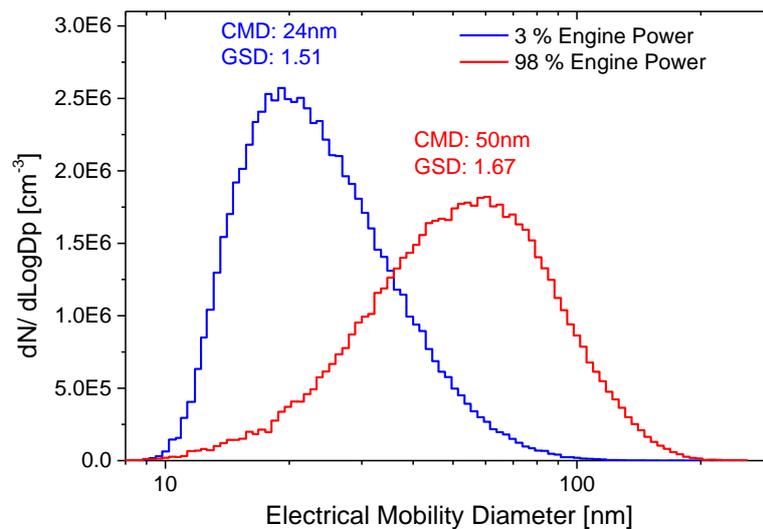


**Figure 4.12. Particle size distributions measured of near idle and take-off thrust settings.**

The determined emission indices of another engine source measured on March 13th, 2013 are shown in Figure 4.13.
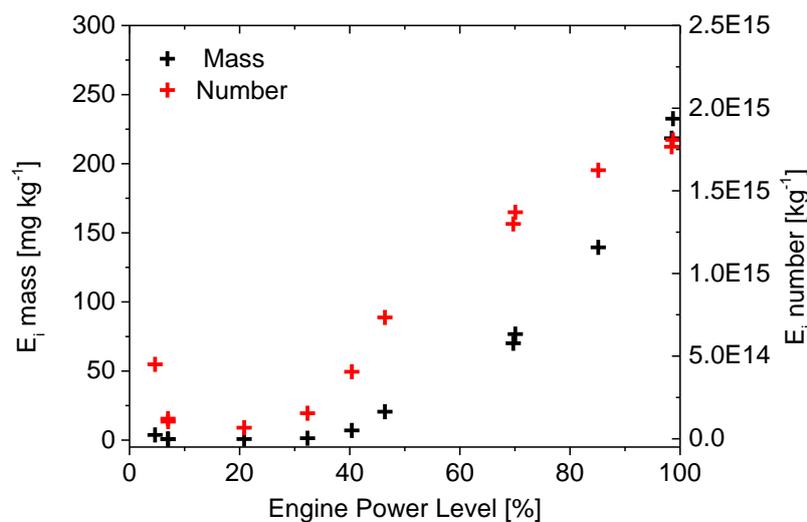


**Figure 4.13. NvPM mass- and number emission indices of an engine source measured on March 13th, 2013.**

Generally a similar emission index behavior as for engine source measured on June 4th 2013 (Figure 4.11) is observed in Figure 4.13. However, both, the mass and the number emission indices in Figure 4.13 are about twice as high in comparison to the ones in Figure 4.11. The high number emissions at low throttle settings are also less obvious than for the engine in Figure 4.11, however the lowest power setting of the two engines are not exactly identical.

### 4.5.4. Conclusions

In total 16 piggy back engine emission measurements were performed by Empa between March and July 2013 with the nvPM sampling system installed at SR Technics. Various engine types and meteorological conditions were encountered with these experiments providing the building blocks for a robust engine emissions database for emissions modeling.

## 4.6. Preparations for the A-PRIDE 5 campaign

The A-PRIDE 5 campaign was the biggest measurement campaign of its type ever conducted at SR Technics. Empa prepared and coordinated the resources for this campaign in coordination with SR Technics and FOCA. Further planning and preparations were also required for experiments conducted by Empa itself.

### 4.6.1. Floor Space

Together with Frithjof Siegrist from SR Technics, the best locations for the placement of the four involved sampling systems were found. A detailed CAD drawing (Figure 4.14) was provided by Empa to the leads of the individual teams. At the time the Rolls Royce team was expected to participate.
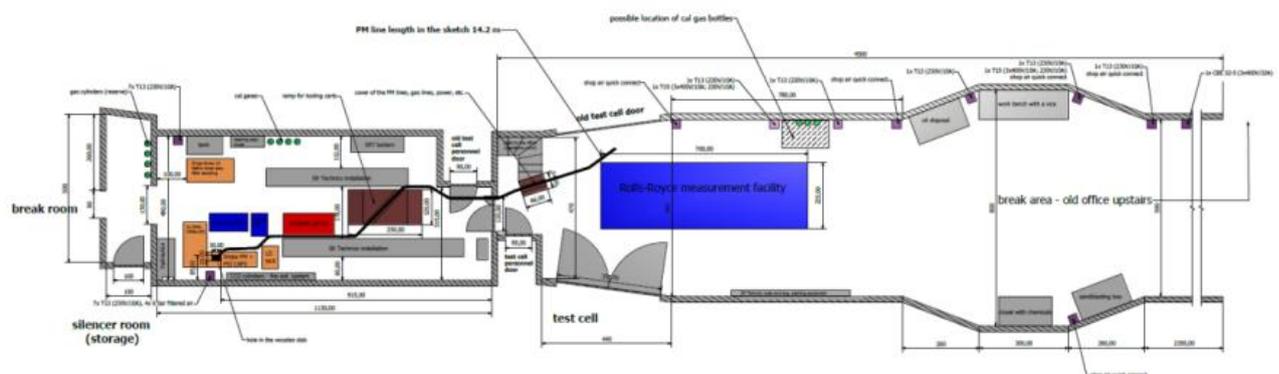


**Figure 4.14. Floor plan of the SR Technics facility for planning the placement of the setups of the individual A-PRIDE 5 teams.**

### 4.6.2. Organizing Compressed Gases and other Consumables

The participating teams required pressurized gases and electricity. Together and in coordination with Frithjof Siegerist gas lines were installed into the hallway and to the dilutor box locations.

Utmost time consuming was the organization of the pressurized gases from Carbagas. Empa required special certified gases for the planned certification like run. Other teams changed their minds multiple times and required special attention and additional orders, which almost could not been carried out in the timeframe before the campaign.

### 4.6.3. Organizing Reliable Communications

During the joint piggy back campaign with PSI and ETHZ radio frequency interference of the handheld radios with the signals of the deployed aerosol mass spectrometers were observed. An elegant solution was found by Empa with analog ASCOM two wire induction bunker phones formerly utilized by the Swiss armed forces. Erwin Roduner helped with the wall installations of the phones. Empa installed all the necessary lines to get the engine operators room connected with individual teams and the break room/ office area.

### 4.6.4. Instrumentation on the nvPM and Annex 16 Lines

The additional temporary campaign measurement setups on the FOCA/ Empa sampling line had to be coordinated and planned. Empa produced the following drawing shown in Figure 4.15 based on the experiences from the joint piggy back campaign and organized a pre- campaign briefing for ETH and PSI.
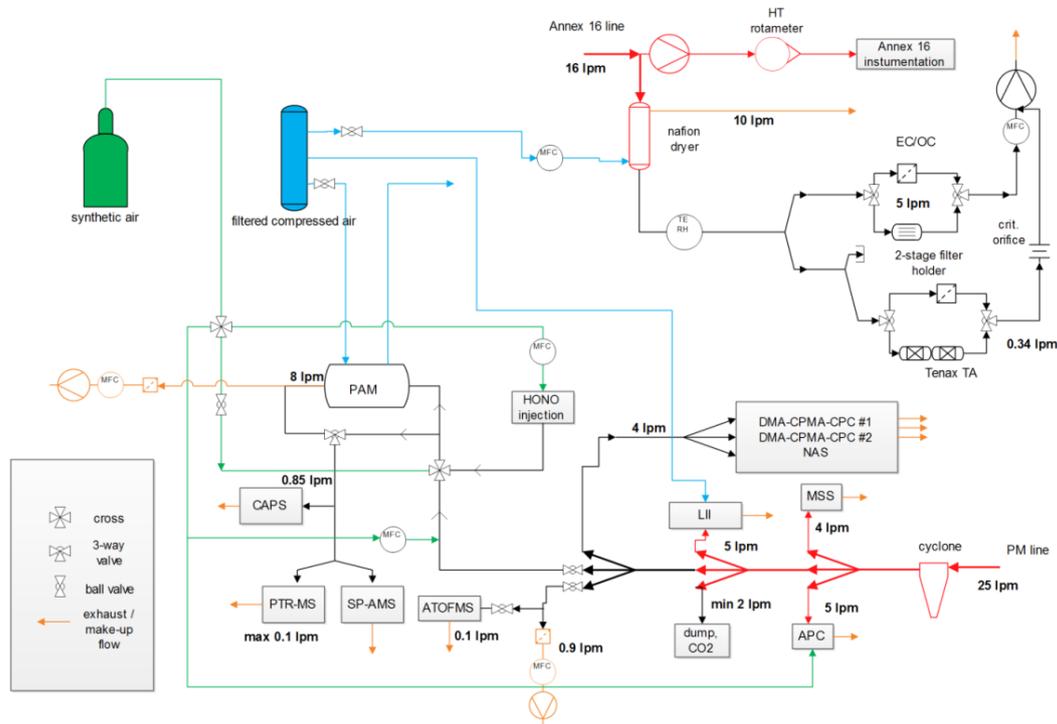
**Figure 4.15. Planned A-PRIDE 5 temporary measurement setups on the nvPM and Annex 16 lines.**

A membrane dryer system shown at the top right in Figure 4.16 and below in Figures 4.17 was designed, built and tested before the campaign to dry the flow of the Annex 16 line without diluting it. The dryer system was furthermore designed that it could be operated in parallel to the standard Annex 16 instrumentation without affecting its performance.
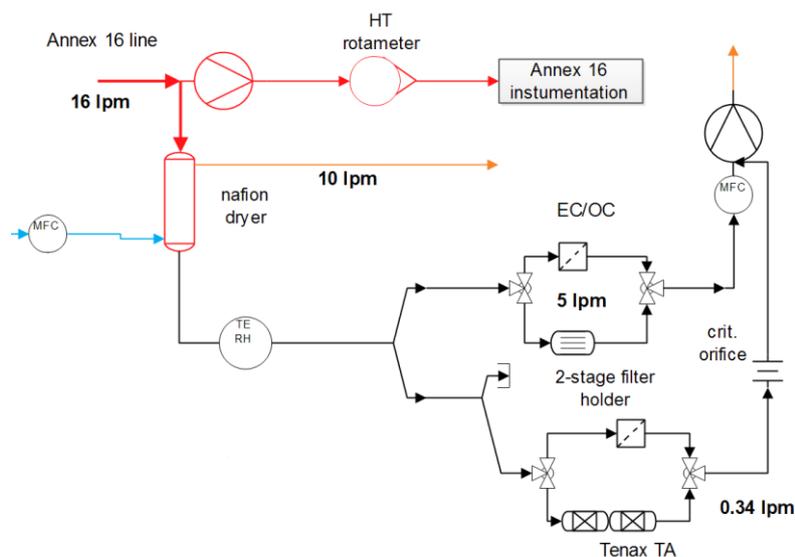


**Figure 4.16. Dryer system to perform undiluted filter measurements on the Annex 16 line.**
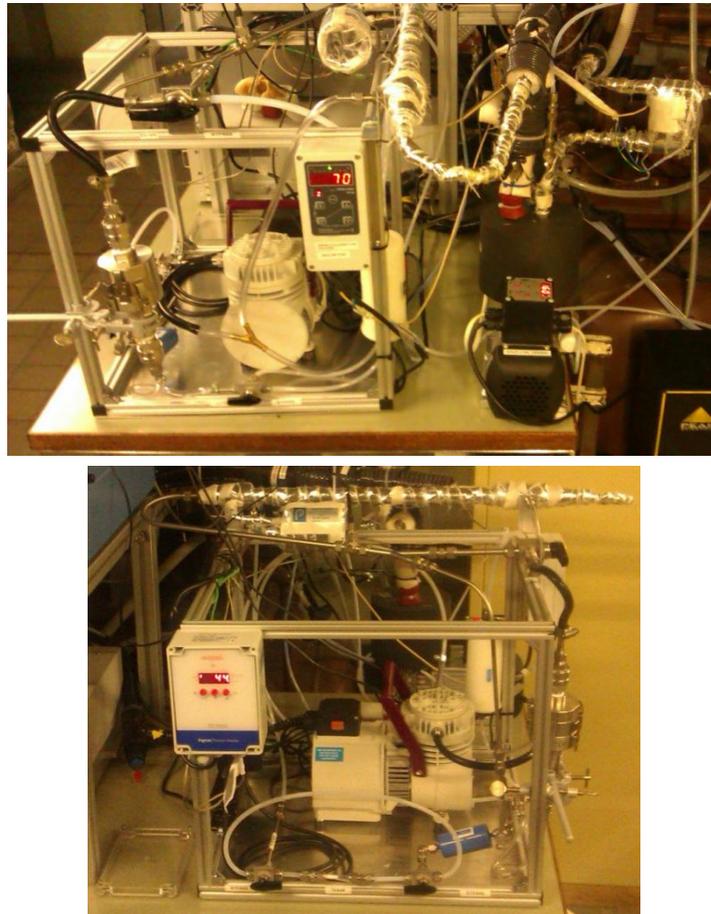
**Figure 4.17. Side and front view of the dryer system as built at SR Technics.**

The design utilizes a commercially available nafion-membrane dryer which requires compressed dry air for operation. The RH and temperature are monitored downstream of the dryer before the filter holder.

# 5. Activities and results in the period 2013/08 – 2014/06

This chapter describes the progress of the Swiss Federal Office of Civil Aviation (FOCA) sponsored project entitled "Particulate Matter and Gas Phase Emission Measurement of Aircraft Engine Exhaust" during the period between August 2013 and June 2014.

**Time plan August 2013 – June 2014**

| ID | Task Name | Start | Finish |
|----|-----------|-------|--------|
| 1 | ⊟ A-PRIDE 5 | 25/7/2013 | 28/2/2014 |
| 2 | Measurement campaign | 25/7/2013 | 28/8/2013 |
| 3 | Data Analysis - certification like runs and EC/OC | 30/8/2013 | 29/11/2013 |
| 4 | Effective density and line loss analysis | 1/10/2013 | 28/2/2014 |
| 5 | A-PRIDE 6 campaign with AVL | 18/10/2013 | 28/10/2013 |
| 6 | Automated EI calculation tool development in Matlab | 1/1/2014 | 1/5/2014 |
| 7 | ICAO CAEP PM VDB Sheets | 20/11/2012 | 20/11/2012 |
| 9 | New rack fabrication and testing | 1/3/2013 | 1/7/2014 |
| 10 | LD research visit at Missouri S&T | 14/3/2014 | 13/6/2014 |
| 11 | ⊟ A-PRIDE 7 preparations | 20/11/2012 | 4/5/2015 |
| 12 | meeting with GE representative | 10/12/2013 | 10/12/2013 |
| 13 | Traversing probe specifications and technical work | 20/12/2013 | 20/3/2014 |
| 14 | Fuel doping specification and technical work | 31/1/2014 | 4/5/2015 |
| 15 | ⊟ E-31 meetings | 20/11/2012 | 6/6/2014 |
| 16 | Tullahoma | 3/12/2013 | 5/12/2013 |
| 17 | Annual meeting at Aerodyne | 2/6/2014 | 6/6/2014 |
| 18 | ⊟ Conferences | 20/11/2012 | 25/6/2014 |
| 19 | Aerosol Technology Karlsruhe | 16/6/2014 | 18/6/2014 |
| 20 | ETH conference on combustion generated nanoparticles | 23/6/2014 | 25/6/2014 |

## 5.1. A-PRIDE 5 campaign

### 5.1.1. Overview

The measurement campaign A-PRIDE 5 took place at SR Technics from 25 July to 28 August 2013. Its main objective was the intercomparison of three draft standard measurement systems: the Swiss fixed system (Empa/FOCA), the North American mobile system (Missouri S&T), and the European mobile system (Sample III) (Figures 5.1 and 5.2).
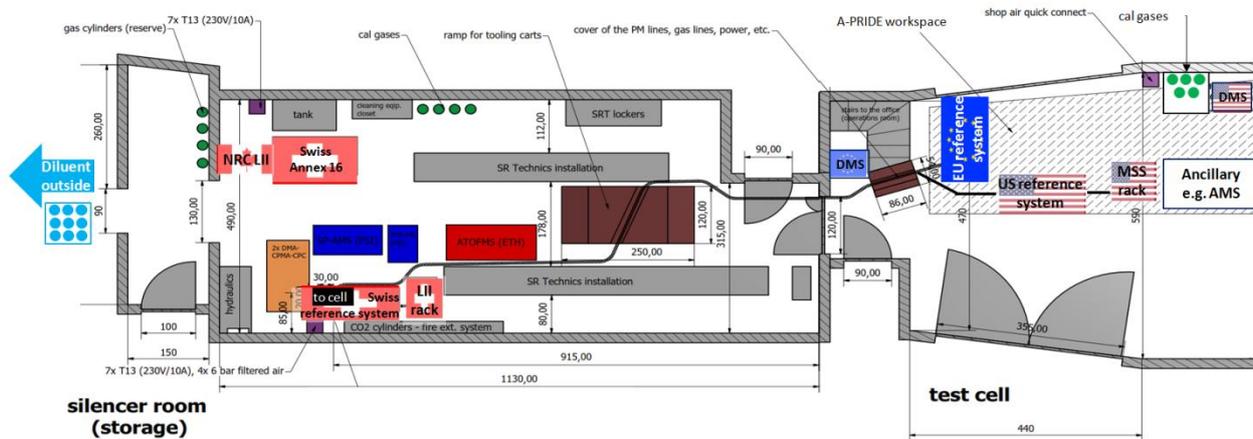
**Figure 5.1. Layout of the experimental setup at SR Technics.**
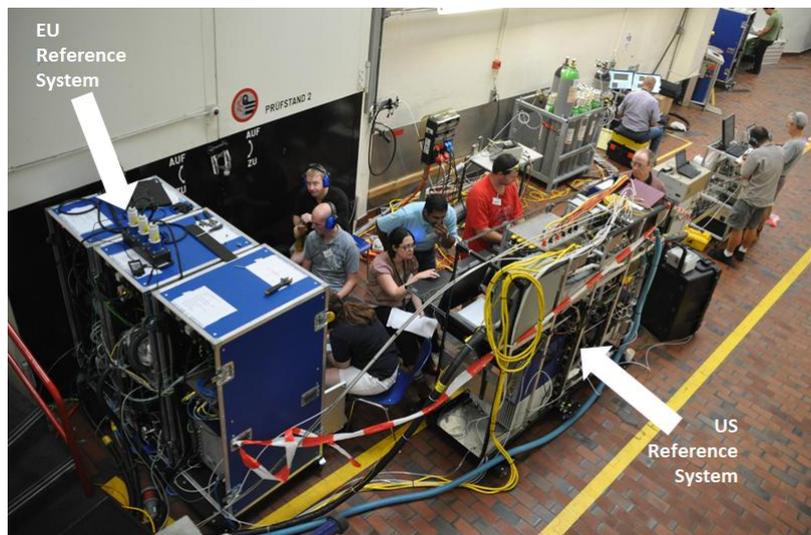


**Figure 5.2. The guest mobile measurement systems in the hallway.**

The experiments in the campaign were performed on a leased engine as well as on other customer engines during piggy-back measurements. During most of the dedicated engine tests, we deployed a new multi-orifice probe compliant with the current emissions certification requirements (ICAO Annex 16 vol. 2). A significant amount of time was also dedicated to intercomparison of the mass-based instruments. Three intercomparisons were performed during the campaign using the miniature combustion aerosol standard generator (miniCAST, Jing Ltd. model 5201C).

Empa's main objectives in this campaign were:

-   Certification-like measurements using the multi-orifice probe
-   Collection of particles for electron microscopic analysis

The data from A-PRIDE 5 on particle effective density of aircraft exhaust PM applied to determine PM

mass and correction factors for sampling losses are presented in Durdina et al. 2014. The results of the transmission electron microscopic analysis of the soot particle morphology are presented in Liati et al. 2014.

## 5.1.2. Certification-like measurements

The certification-like measurements for a leased engine were performed based on an engine certification test plan developed with FOCA based on ICAO Annex 16 Volume II and AIR6241. FOCA provided the engine sea level performance data for the engine and the geometry and basic design of the certification multipoint probe, which was built by Brunner GmbH, Lauterbrunnen. The test runs were carried out on August 17th and 18th, 2013, witnessed by FOCA in the role of the certification authority. To our knowledge, these were the first ever certification-like nvPM measurements of an aircraft gas turbine, complying with AIR6241 to test out the developed protocols and measurement methodology. The measurements followed strictly AIR6241. The gaseous emission indices for NOx, CO and UHC (unburned hydrocarbon) vs. the engine thrust at the ISA conditions are shown in Figure 5.3. The circular and triangular symbols represent our results and the crosses represent the ICAO database values for this engine. Our results are in excellent agreement with the ICAO values. Figures 5.4 and 5.5 show the nvPM mass and number emission indices vs. the engine thrust at the ISA conditions, respectively. The nvPM mass EI increases with the increasing thrust level. The nvPM number EI first decreases with the increasing thrust level and then increases and peaks near 85% thrust. The high nvPM number EI when the thrust is below about 7% is attributed to the very small particle sizes at this thrust level.
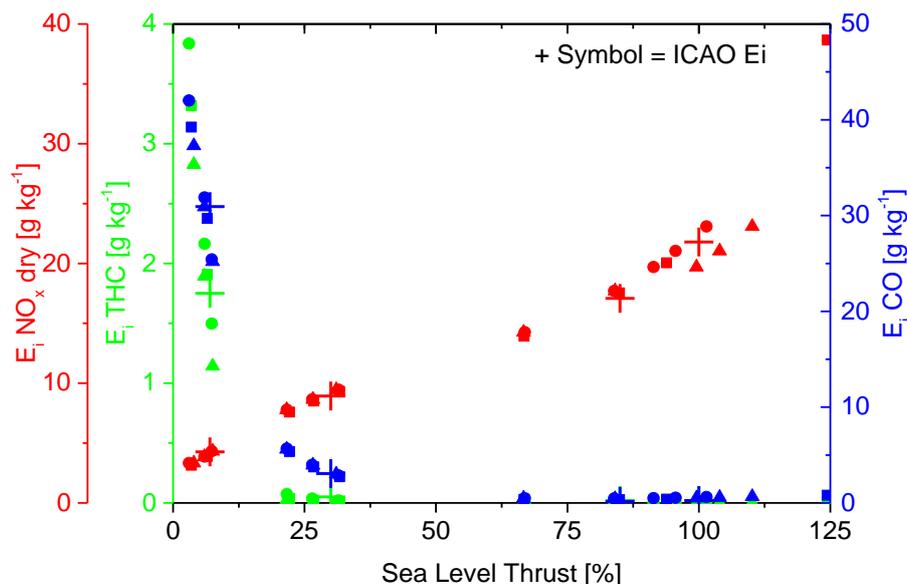


**Figure 5.3. The gaseous emission indices for NOx, CO and UHC vs. the engine thrust at the ISA conditions.**
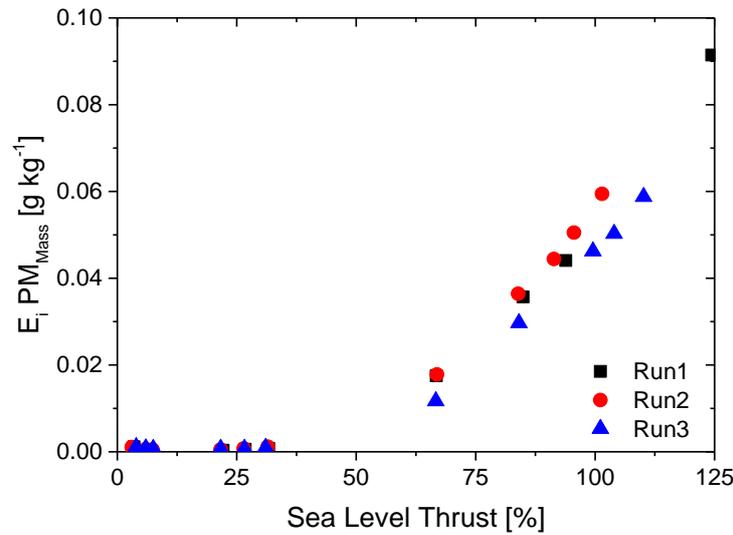
**Figure 5.4. The nvPM mass emission index vs. the engine thrust at the ISA conditions.**
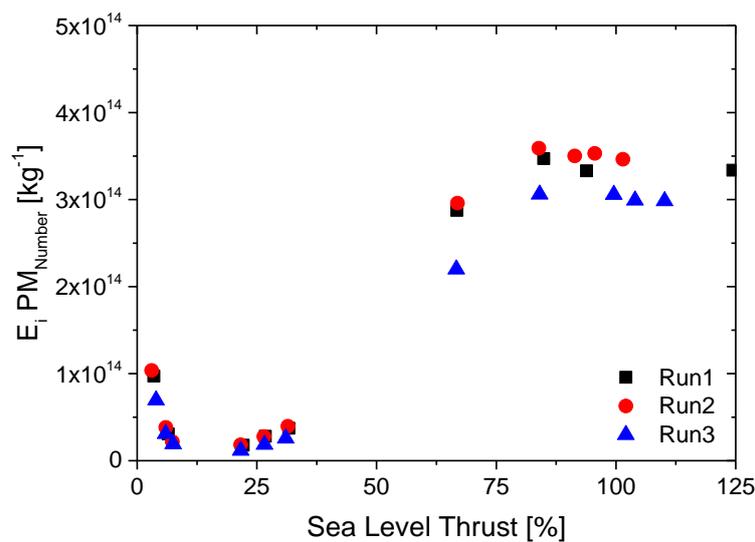


**Figure 5.5. The nvPM number emission index vs. the engine thrust at the ISA conditions.**

## 5.1.3. Examples for emission indices measurements

The nvPM mass and number emission indices of a number of different types of aircraft engines were measured during A-PRIDE 5. As an example, the results for a 90s technology mid-size turbofan engine are shown in Figures 5.6 and 5.7. Here the emission indices are plotted as functions of the fuel flow rate which correlates with the engine thrust. The general trends are similar to those shown in Figures 5.4 and 5.5. The high number emissions at low engine fuel flow do not correlate with mass emissions which is attributed to the very small particle sizes at low fuel flow rate. Temperature effect is visible in the number emissions.
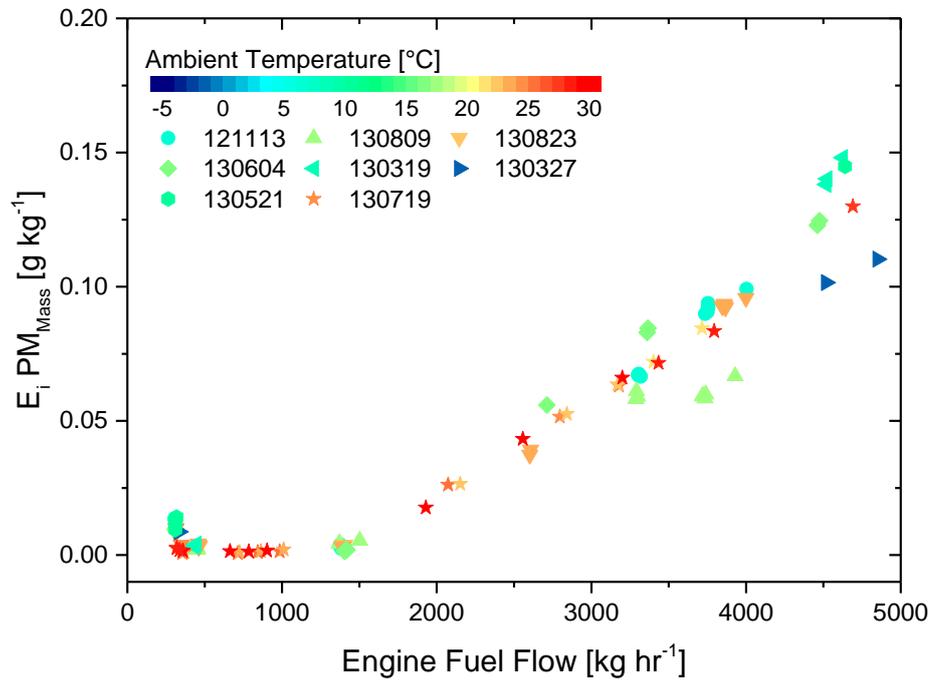
**Figure 5.6. The nvPM mass emission index vs. the engine fuel flow.**
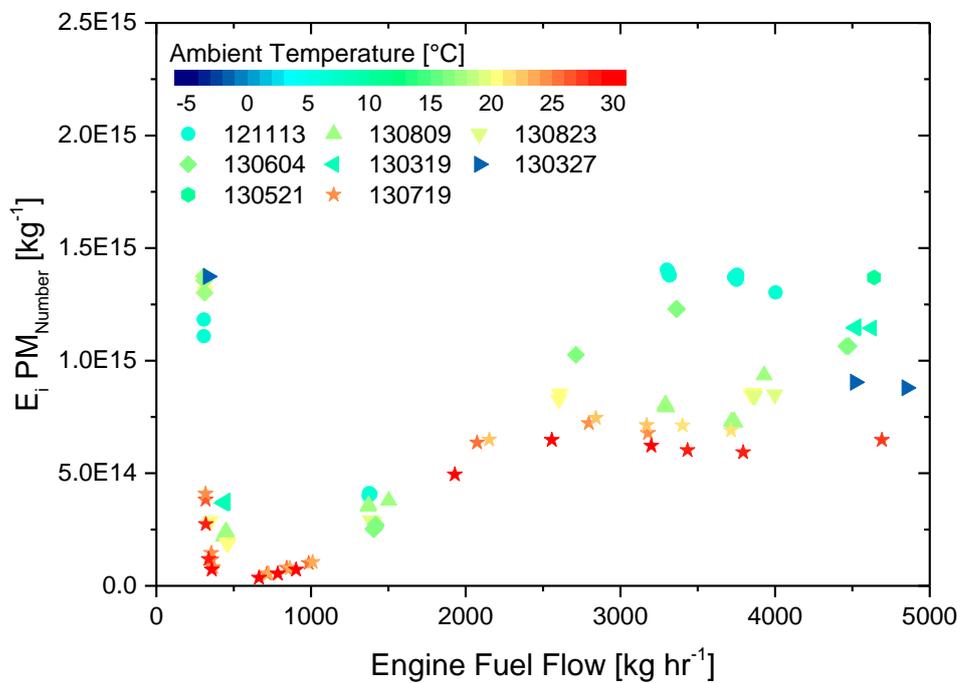


**Figure 5.7. The nvPM number emission index vs. the engine fuel flow.**

## 5.1.4. Effective density

The effective density is important for understanding the particle morphology and can be used to calculate the mass emission and particle line loss correction. The data of thrust-dependent effective density for in-use aircraft engines were not available before our project. The effective density of the particles emitted from a commercial turbofan engine was determined using a differential mobility analyzer and a centrifugal particle mass analyzer. The effective density increased from engine idle to take-off by up to 60%. The determined mass-mobility exponents ranged from 2.37 to 2.64 (Figure 5.8). The mean effective density determined by weighting the effective density distributions by PM volume was within 10% of the unit density (1000 kg/m$^3$) that is widely assumed in aircraft PM studies. We compared the measured black carbon (BC) mass and the total PM mass determined from particle size distributions (PSD) and effective density. We found ratios close to unity between the PM mass determined by the integrated PSD method and the real-time BC mass measurements, and the integrated PSD method achieved higher precision at ultra-low PM concentrations at which current mass instruments reach their detection limit. The detailed results can be found in Durdina et al. 2014.
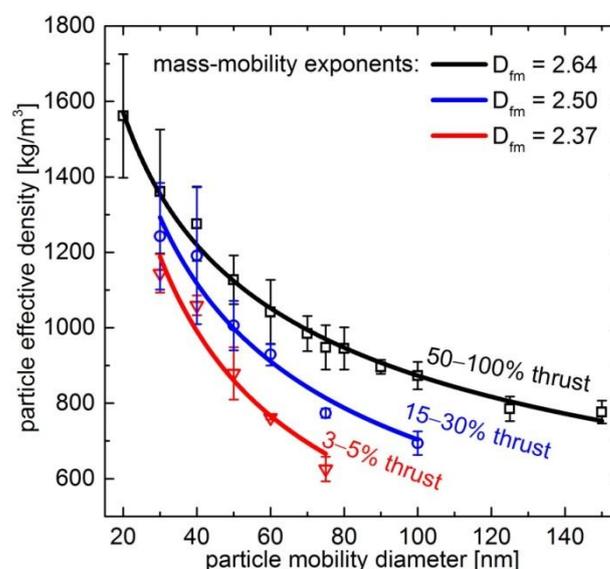


**Figure 5.8: Effective density distributions determined for the various thrust ranges. Error bars represent standard deviation in the experimental data.**

## 5.1.5. Electron microscopic analysis

The morphology and internal structure of soot particles emitted from a turbofan engine were analyzed in an electron microscopic study, down to the nano-scale, for ~100%, ~65% and ~7% static engine thrust as a proxy for take-off, cruising and taxiing, respectively. Sampling was performed directly on transmission electron microscopy grids with a state-of-the-art sampling system designed

for non-volatile particulate matter. The electron microscopy results reveal that for this engine, ~100% thrust produces the highest amount of soot, the highest soot particle volume and the largest and most crystalline primary soot particles with the lowest oxidative reactivity. The opposite is the case for soot produced during taxiing, where primary soot particles are smallest and most reactive and the soot amount and volume are lowest. The microscopic characteristics of proxy cruising conditions soot resemble the ones of the ~100% thrust conditions but are more moderate. Real time online measurements of number and mass concentration show also a clear correlation with engine thrust level, comparable with the TEM study. The results of the present work, in particular the small size of primary soot particles present in the exhaust (modes of 24nm, 20nm and 13nm in diameter for ~100%, ~65% and ~7% engine thrust, respectively) could be a concern for human health and the environment and merit further study. The detailed results are published in Liati et al. 2014.
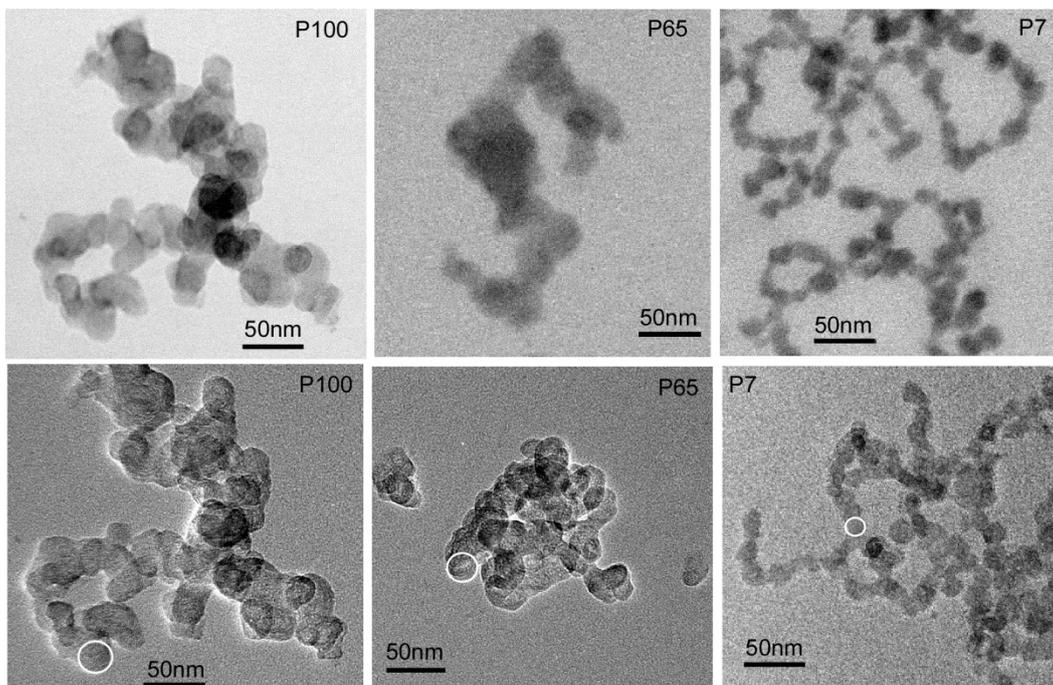


**Figure 5.9. BF-STEM mode (upper row) and TEM mode images (lower row) of soot agglomerates from different engine thrust levels exhibiting a diminishing size of the primary soot particles from the higher to the lower thrust. Note the significantly smaller size of primary soot particles in the ~7% soot as compared to the ~65% and the ~100% thrust samples, as well as the less bulky agglomerates of the ~7% thrust soot. Encircled in the lower row images are examples of primary particles considered for size measurements.**

Low magnification TEM images of soot from the three thrust levels reveal a reduction in the size of the primary soot particle constituents of the agglomerates from the P100, through the P65 to the P7 sample (Figure 5.9). The size of the primary soot particles is given by the diameter of the (nearly)

circular particles (projected spheres) directly measured on the TEM images with the measuring tool of the 'Digital Micrograph' software. Statistical data for the size distribution of primary soot particles for the different engine thrust levels investigated are shown in Figure 5.10. The size of the primary soot particles produced during take-off (312 particles were measured for this thrust level) ranges between 3 and 64 nm (extreme values). About 60% of the primary soot particles are 10-25 nm in size; the most frequently measured particle sizes are between 15 and 20 nm (Figure 5.10), while 52% are >20 nm; the mode is 24 nm and the standard deviation value is 9. The size of the primary soot particles emitted at the ~7% thrust level (321 measurements) ranges between 7 and 21 nm (extreme values). 90% of the primary soot particles are 10-25 nm in size and 99% of them are between 5-20 nm that is significantly smaller than both P100 and P65 soot particles. The maximum percentage of particles is observed for sizes between 10 and 15 nm (Figure 5.10) with a mode of 13 nm and a standard deviation of 3. The lower degree of crystalline order, in combination with the smaller particle size of P7 soot indicates that soot produced during taxiing is more reactive than in the P100 and P65 samples.
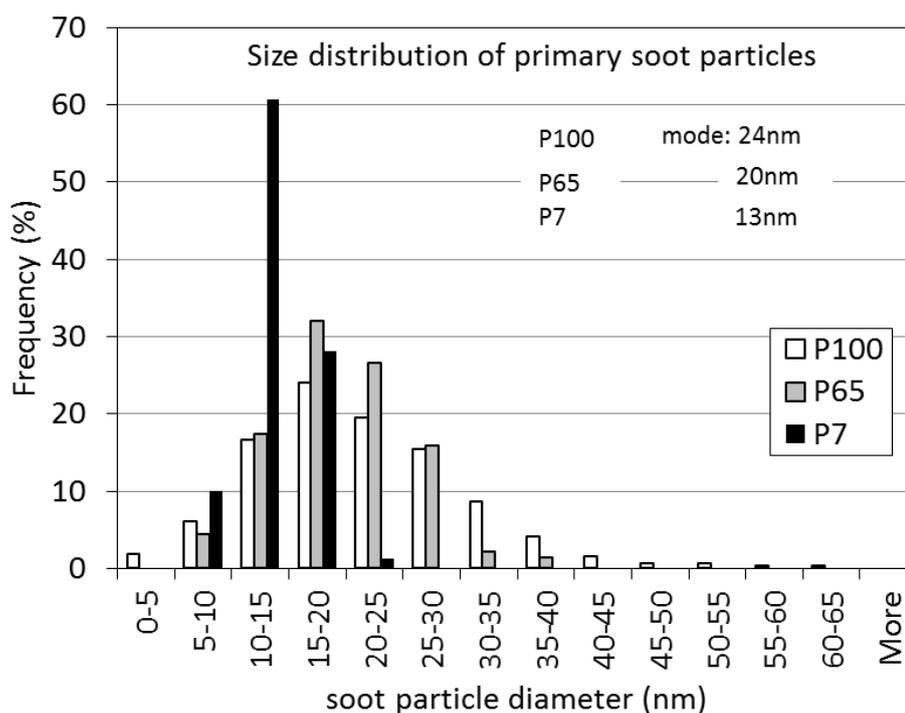


**Figure 5.10. Histogram showing the size distribution of primary soot particles for the different engine thrust levels investigated, as measured on the TEM grids.**

## 5.2. A-PRIDE 6 campaign

The main objective of the A-PRIDE 6 campaign was to intercompare the fixed Swiss reference system with the prototype of a commercial measurement system AVL Sampling System for Aviation (SSA). The measurements were done in the piggy-back mode only on customer engines run in the test cell. Prior to the campaign, both the number and mass instruments from the two systems were

intercompared using the AVL APG soot generator (miniCAST burner with an evaporation tube and a dilution system). The two systems agreed within 5% both in terms of nvPM mass and number.

## 5.3. A-PRIDE 7 campaign preparations

### 5.3.1. Fuel doping

The fuel components, especially the aromatic contents, play significant roles for PM emissions. Because different fuels are used globally, the fuel effects may impact the engine emission certification tests and emission inventory calculation. The study also provides insight for emissions from alternative fuels. A suitable fuel doping approach was investigated in spring 2014. Three different approaches which included a separate external fuel tank, adding the doping to the existing SR Technics tank and injection of the doping into the engine fuel supply were evaluated. The most versatile and at the end also least costly approach was to build an injection system. A technical specification was developed and discussed with SR Technic's safety personnel and dosage pump manufacturers. The following figure provides an overview of the system that was built in collaboration with Peter Beyerle and apprentices from SR Technics. A major effort was made to find a suitable pump that could cover the required flow range. At last a two pump solution was chosen which has one pump for flow rates up to 62 L/hr and one for flow ranges up to 400 L/hr.
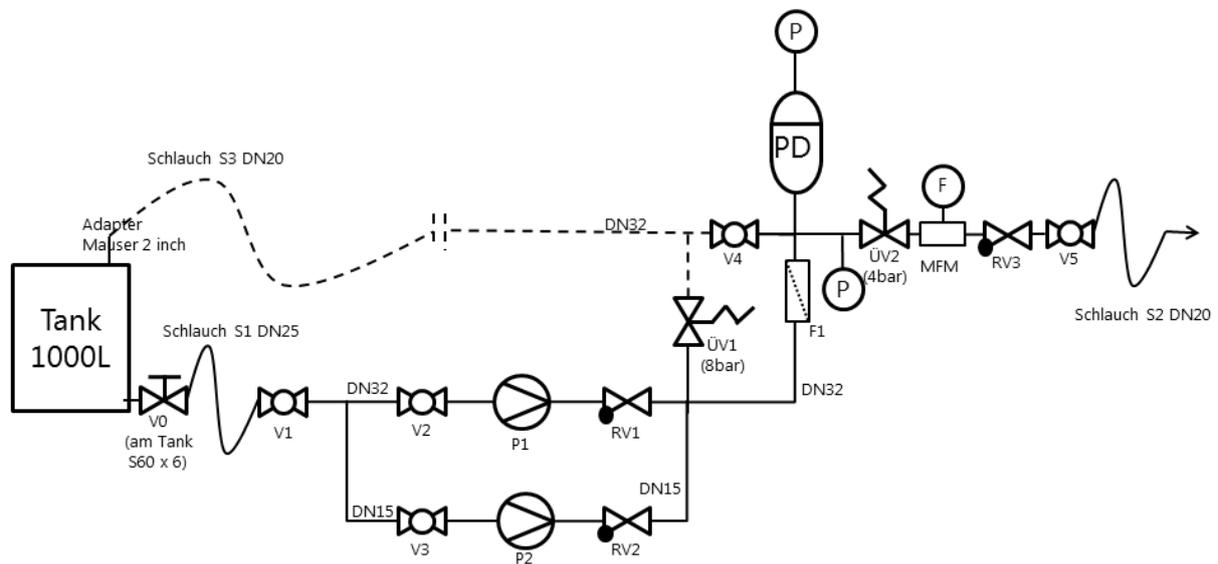


**Figure 5.11. Simplified schematic of the fuel doping apparatus.**

### 5.3.2. Traversable probe

Spatial mapping of the engine emissions is planned for A-PRIDE 7 for which an installation of an additional Z- (horizontal) probe axis is necessary in the test cell at SR Technics. The technical

specifications for such an installation were developed in December 2014 and forwarded to Brunner GmbH Lauterbrunnen. The planned traversable probe design from Brunner is depicted in Figure 5.12.
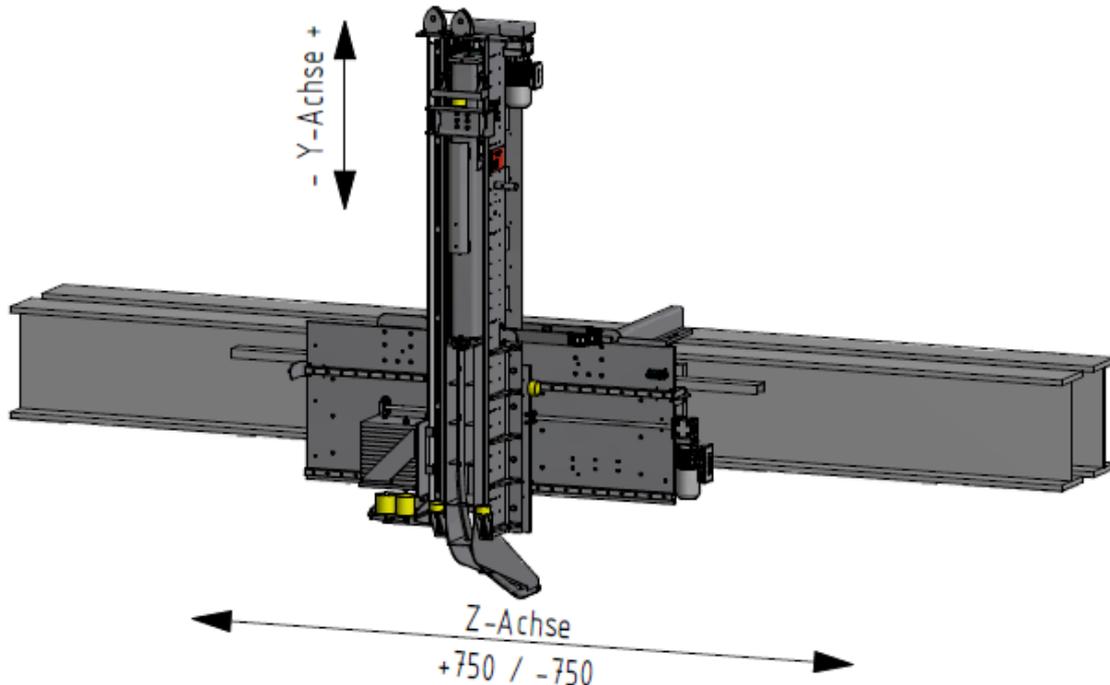


**Figure 5.12. 3D CAD model of the traversable probe.**

## 5.4. Evaluation of particle losses in the sampling system at SR Technics

### 5.4.1. Introduction

Evaluation of particle losses in the sampling system was Empa's effort leading to more accurate estimates of the nvPM number and mass emissions at the engine exit plane. It was also important for assessing the sample line deterioration over time. In April 2013, Empa measured particle losses in the 25 m long PM line using miniCAST 5201C soot generator (Section 4.3). The same methodology was used for measurement of diffusional particle losses in the whole sampling system from the probe tip to the first splitter after the cyclone (see Figure 5.13) on January 24 and 28, 2014. The objective of this study was to compare the results with the previous experiment and the particle transport model.

### 5.4.2. Methods

The monodisperse aerosol generation setup was placed on a trolley allowing us to quickly deploy the instruments in the test cell in the time it was not used for engine testing. When needed, the setup could be removed from the test cell within several minutes. As shown in Figure 5.13, miniCAST exhaust

was classified by electrical mobility using a differential mobility analyzer (TSI DMA 3081). It was then diluted with dry nitrogen (5.0 grade). The upstream and downstream particle concentrations were counted with condensation particle counters (2x TSI CPC 3775). The two CPCs were adjusted in the laboratory to have the same reading using miniCAST for a given particle size and concentration. The adjustment was in the range of 3%. The diluted classified exhaust was fed to the probe tip. Total flow rate was first maintained at 25 slpm during the initial experiment on January 24, but we later decided to use 10 slpm for the whole experiment on January 28 in order to increase the downstream number concentration of the smallest particles. As this high flow rate could not pass through the ejector diluter, it was bypassed using a straight 1 m stainless steel tube with 10 mm OD, as shown in Figure 5.13.
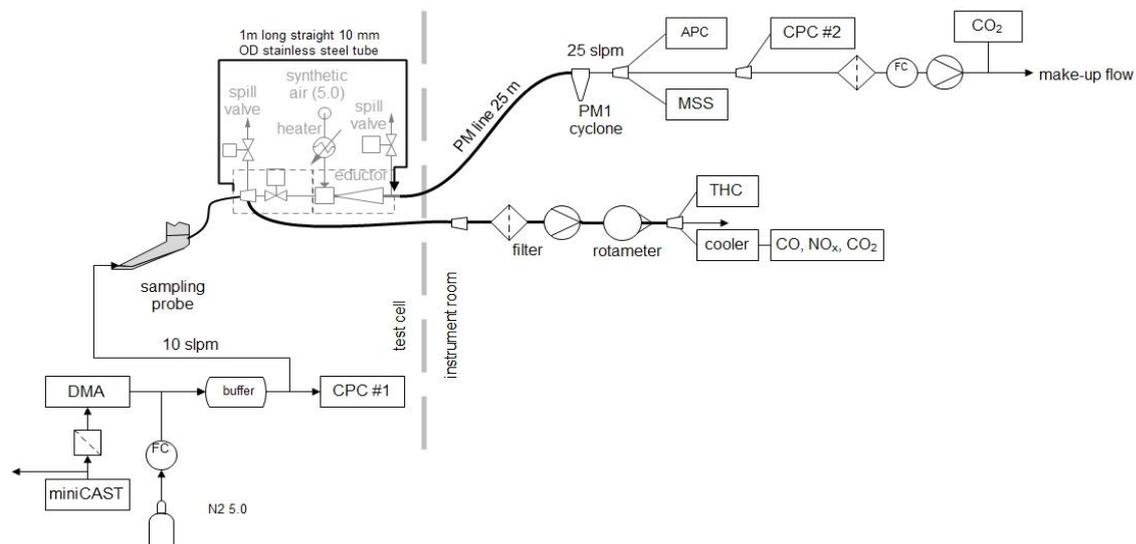


**Figure 5.13. Experimental setup for the sampling system line loss measurement.**

The particle size range covered was 10 to 250 nm. As a single miniCAST setting cannot cover this wide size range, three different settings had to be used. An example of the generated particle size distributions determined with a scanning DMA is shown in Figure 5.14.

The particle transport tool developed by Liscinsky et al. from the United Technologies Research Center (UTRC) was used for modeling the theoretical line penetration. The penetration was modeled for a simplified sampling system as a straight tube with 8 mm ID, neglecting the losses in the cyclone (experimentally evaluated previously to be negligible). No thermophoretic losses were modeled; the gas, particle, and tubing wall temperatures were assumed to have ambient temperature.
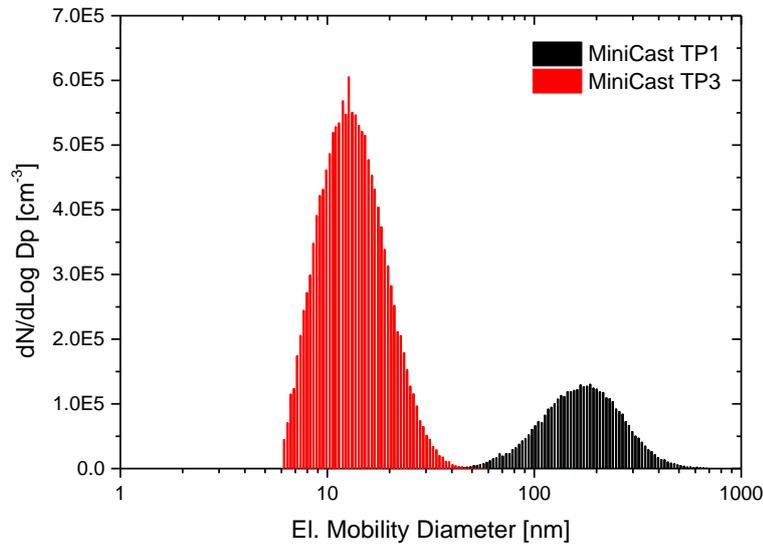
**Figure 5.14. Examples of the particle size distributions generated by miniCAST and used for the experiment.**

### 5.4.3. Results

Overall, the experimental results agreed well with the model. Inspection of Figure 5.15 reveals that the model overestimated particle losses in the size range below 50 nm. It agreed well for all the larger particle sizes.



$$y = A_1 \cdot e^{(-D_p/t_1)} + y_0$$
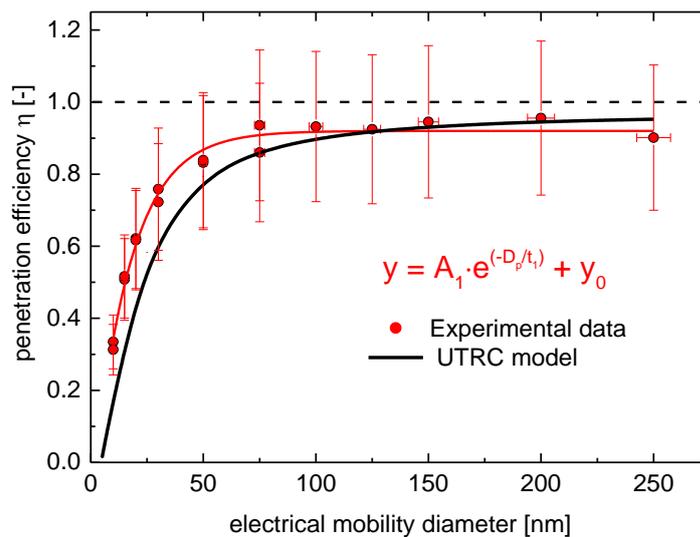
**Figure 5.15. Comparison of the experimental data and the UTRC model for the same conditions. Error bars represent the propagated error assuming 10% counting uncertainty. The assumed particle sizing error is 3%.**

Comparison of the results for the whole sampling system with the previously obtained results for the 25 m long heated PM line is shown in Figure 5.15. Theoretically, particle losses should be lower in the 25 m long line. We hypothesize that the higher losses in the 25 m long line could be due to thermophoresis - temperature gradient in the unheated line connecting the splitter and the downstream CPC. As the results for the 25 m long line were consistently approx. 10% below the model values over the entire particle size range (shown in the previous report), there might have been a systematic error we did not account for in the previous study.
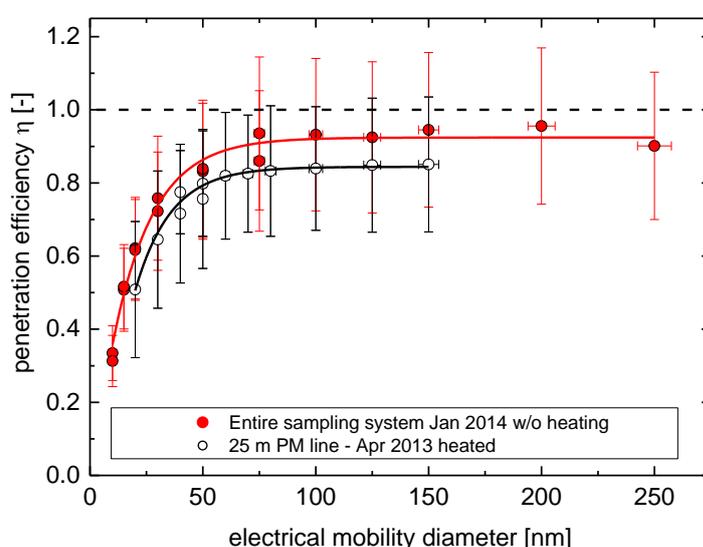


**Figure 5.16. Comparison of the results for the whole sampling system and the heated 25 m long PM line.**

## 5.4.4. Conclusions

The sample line penetration for particles from 10 to 250 nm mobility size was measured and modeled for the entire sampling system at SR Technics from the probe tip to the first splitter after the cyclone. The soot generation and particle size classification system was installed on a trolley parked on the hydraulic platform in the engine test cell. The experimental results agree both quantitatively and qualitatively with the modeled values. Thus, the UTRC model equations implemented in the Empa line loss correction calculation have been experimentally validated for the diffusional losses; thermophoretic losses still have not been well investigated.

A surprising disagreement was found between the results obtained previously for the 25 m long PM line and the current results. The penetration for the heated 25 m line was determined to be higher

than the one for the whole sampling system (not heated) presented here likely due to thermophoretic losses and / or a systematic error.

The future line loss experiments will be likely performed the same way as in this study so that we can assess changes in the sampling system performance. However, given the uncertainty of the technique used, only drastic changes in the sample line performance (e.g. partially clogged sample line) could be determined.

## 5.5. Automated data analysis tool

### 5.5.1. Introduction

Tests at SR Technics produce large amounts of raw data that are merged and stored at FOCA in Excel spreadsheets. Further processing of data is necessary to extract essential information from this raw data such as the nvPM and gaseous emission indices. In the initial phase of the project most of this data processing has been done as labor intensive "spreadsheet crunching" in which stable engine periods were identified visually and the data from these stable periods was further processed.

To save valuable time and also analyze the data in a consistent manner an automated data analysis tool was programmed in MATLAB which currently can perform the following analysis tasks:

- Reading FOCA standard formatted Excel file with a spreadsheets called" sheet1"
- Reading engine parameters and certified gaseous emissions from the EDB data base (based on EDB code)
- Identifying user defined stable periods based on the drift (first derivatives) in the dilution factor, the nvPM mass and nvPM number concentration data
- Averaging all data in the stable periods
- Performing the wet-correction for the dry measured gaseous concentration
- Determining the particle size distribution (PSD) based on engine thrust level
- Determining the actual exhaust gas temperatures for all engines measured at SR Technics
- Performing line loss correction based on the determined PSD, exhaust gas temperature, flow rates etc.
- Calculate line loss corrected and uncorrected emission indices
- Writing all the data for the stable periods including their calculated value in to an added spreadsheet called "ANALYZED"
- Writing all the EDB data for the specific engine model into an added spreadsheet called "EDB_DATA"

## 5.5.2. Implementation and results

The program is implemented as a function in which the argument is the engine data excel file and the output are two added sheets (one for results and one for the EDB data) in the original Excel file (Figure 5.17).
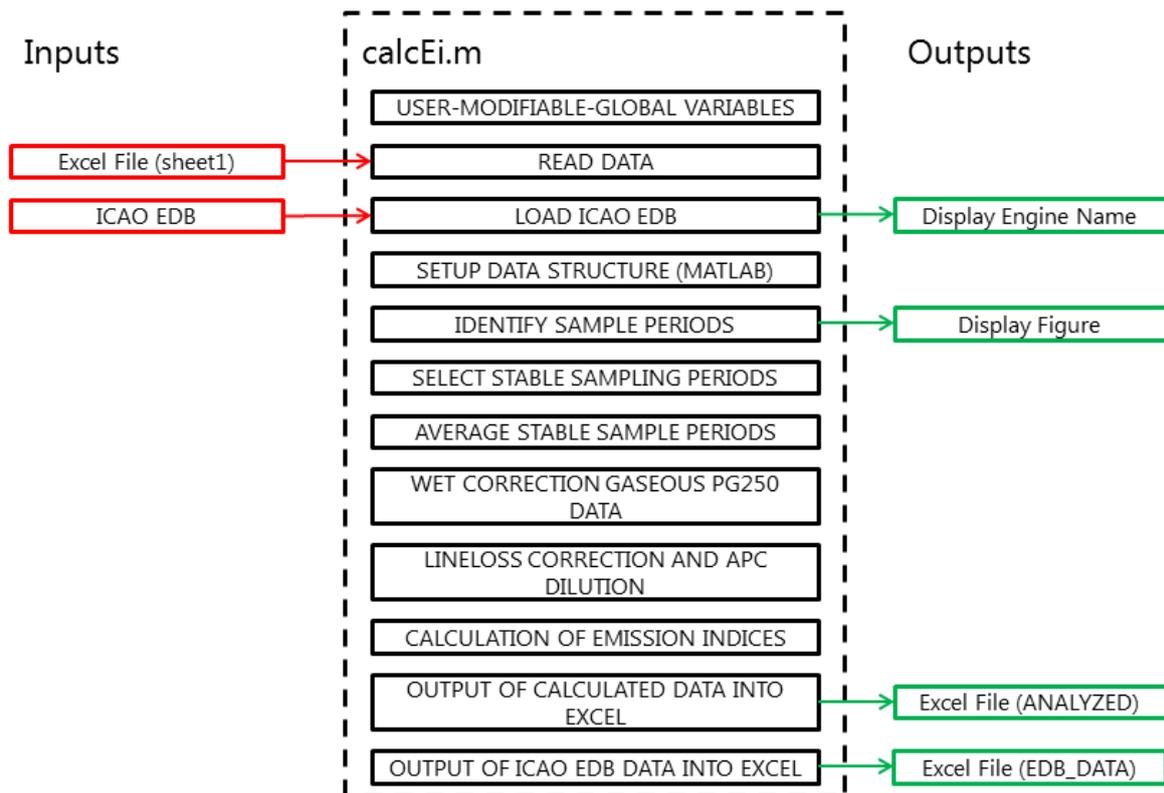


**Figure 5.17. A simplified flow diagram of the data analysis tool.**

The user interface provides a figure with the identified stable sampling point and informs the user about the current program function that is executed. A sample user screen is shown in Figure 5.18.

**Figure 5.18. Snapshot of the user interface.**

All piggy back engine data was analyzed with this program with no major problems besides bringing the data headers in a unified format (the program requires the same headers in all files). A further issue is sometimes the time synchronization of the different instrument which has to be adjusted before the analysis manually.

The automatic stable sample identification using derivatives has worked satisfactory however the best would be if the sample periods would be already identified during sampling at the airport. The newly upgraded sampling system has now this capability and stores a sampling flag into the datafile. The MATLAB code is modified so it can utilize this flag in addition to the derivative method. Another item that should be updated is the prediction of the actual PSD by using more measured engine data. For determining the line losses in terms of mass the size dependent effective density function should be implemented. Currently unit density is assumed.

## 5.6. Upgraded instrumentation rack at SR Technics

Benjamin Brem supervised and helped with the installation of the "upgraded" instrumentation rack in the apprentice shop of Peter Beyerle at SR Technics. The job was finished on 11.7.2014 when Theo Rindlisbacher inspected the installation. Besides the change of the MSS line and splitter port from 3/8" to ¼" diameter only minor details had to be changed to fulfill the contract. The following figure provides a picture of the finished installation.
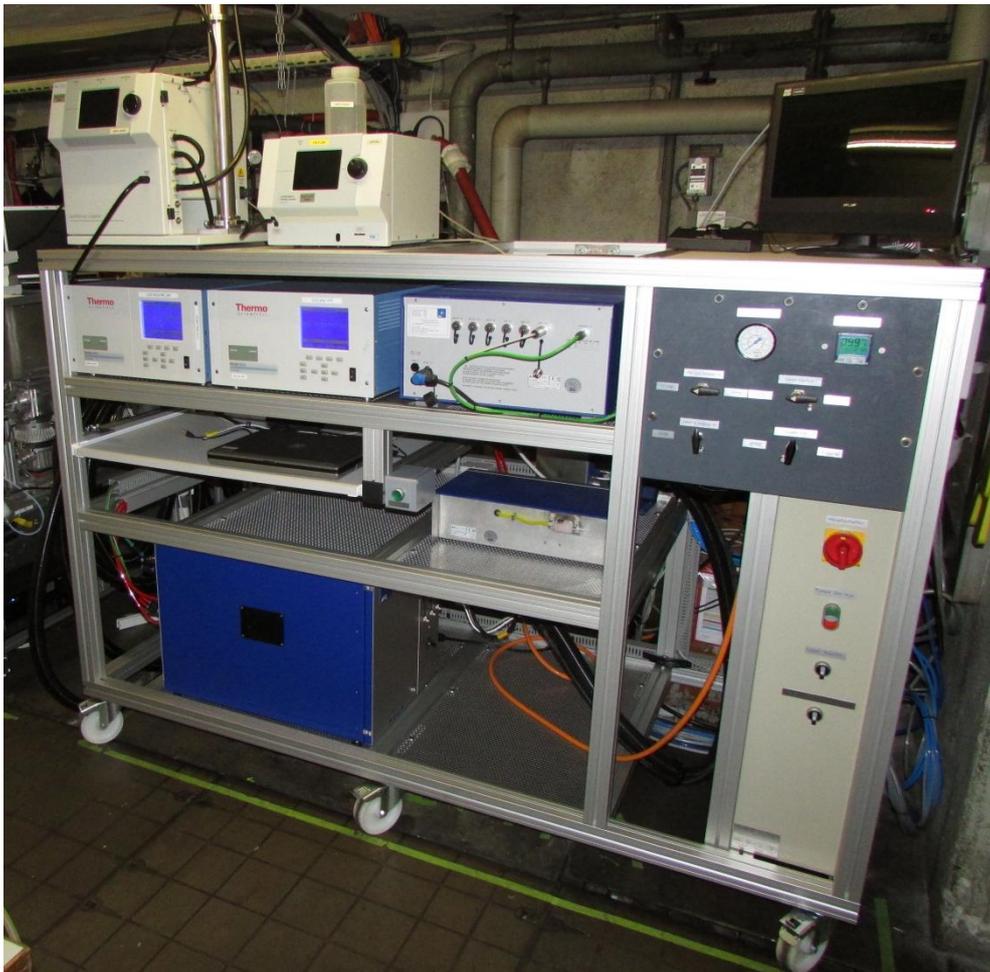


**Figure 5.19. Photo of the new rack in the corridor next to the test cell.**

## 5.7. MiniCAST soot mass and density campaign at Missouri S&T

The miniature combustion aerosol standard (miniCAST) soot generators have been used for intercomparison and calibration of BC mass measurement instruments used in the standardized aircraft exhaust sampling systems. It has been known that different soot generators despite similar

chemical composition of the soot (elemental/organic carbon ratio) lead to different calibration factors. Some of the differences observed in the recent A-PRIDE campaigns between the different mass instruments could be attributed to differences in soot morphology (particle shape and density). To investigate this issue in detail, Lukas Durdina conducted an experimental campaign in collaboration with the Cloud and Aerosol Sciences lab at Missouri University of Science and Technology (MS&T), Rolla, MO where he was active as a visiting research scholar from 15 March to 15 June 2014.
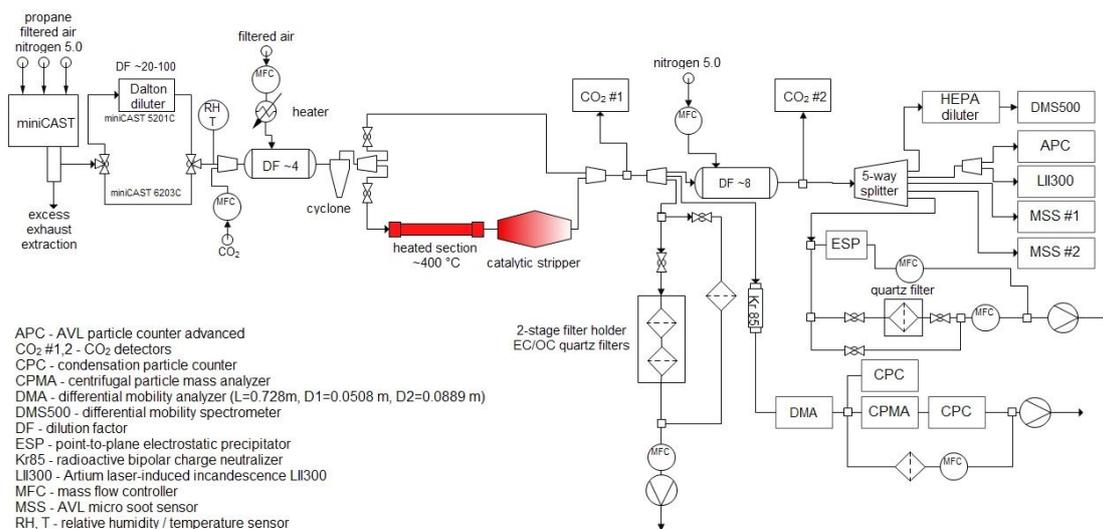


**Figure 5.20. Schematic of the experimental setup used during the mass-density campaign.**

Schematic of the experimental setup is shown in Figure 5.20. In the mass-density campaign, we measured / collected:

- BC mass using two MSS and one LII instrument

- nvPM number using an APC

- particle size distribution using a DMS500

- particle effective density using a DMA and a CPMA

- quartz filter samples for EC/OC analysis

- particle samples for transmission electron microscopic analysis

Two different miniCASTs, 5201C and 6203C were used. These burners normally operate in different AFR ranges so we were able to cover a wide range of conditions from fuel-rich to fuel-lean. We also investigated how a catalytic stripper and nitrogen premix to the fuel affect the particle morphology and composition (28 test points in total). An example result of the effective density analysis shows that

the catalytic stripper in general lowered the mass-mobility exponent and that the two miniCASTs generated particles with different morphology at similar AFR (Figure 5.21).
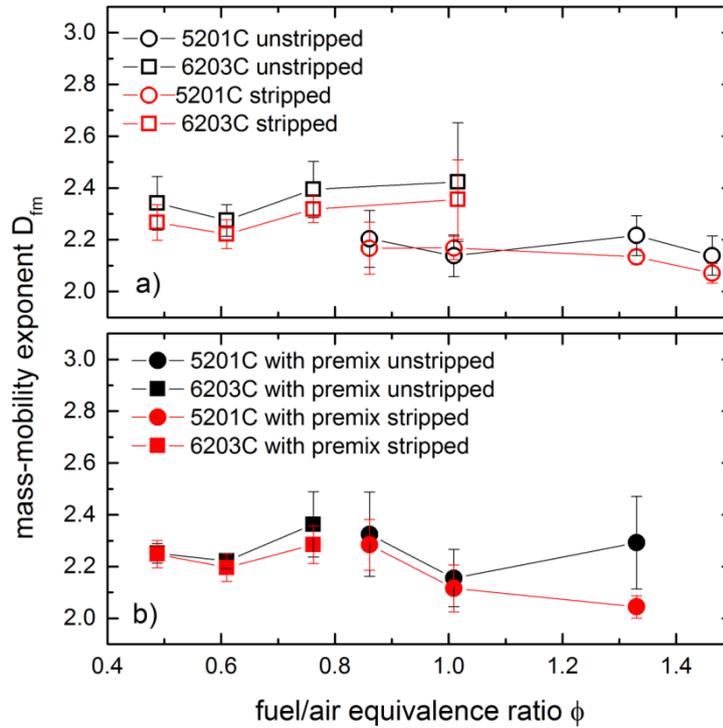


**Figure 5.21. Summary of the mass-mobility exponents for all the investigated test conditions.**

# 6. Activities and results in the period 2014/07 – 2014/12 (including A-PRIDE 7)

## 6.1. Introduction

This chapter describes the progress of the Swiss Federal Office of Civil Aviation (FOCA) sponsored project entitled "Particulate Matter and Gas Phase Emission Measurement of Aircraft Engine Exhaust" during the period from July 2014 to December 2014. This period included joint piggy-back measurements at SR Technics with PSI and the dedicated measurement campaign "A-PRIDE 7" with various partners. The flowing chart (Table 6.1) provides a chronological overview of the major events and tasks during the report period.

**Table 6.1. Major events and task during the report period (7/2014 to 12/2014).**

| ID | Task Name | Start | Finish | 1/7/2014 | | | 1/10/2014 | | |
|---|---|---|---|---|---|---|---|---|---|
| | | | | 1/7/2014 | 1/8/2014 | 1/9/2014 | 1/10/2014 | 1/11/2014 | 1/12/2014 |
| 1 | ⊟ Piggyback campaign with PSI | 1/7/2014 | 31/7/2014 | | | | | | |
| 2 | equipment transport and setup | 1/7/2014 | 4/7/2014 | | | | | | |
| 3 | engine tests | 7/7/2014 | 23/7/2014 | | | | | | |
| 4 | tear-down and transport | 24/7/2014 | 25/7/2014 | | | | | | |
| 5 | data reduction, export, and merging | 28/7/2014 | 31/7/2014 | | | | | | |
| 6 | ⊟ A-PRIDE 7 campaign | 1/8/2014 | 24/10/2014 | | | | | | |
| 7 | ⊟ Campaign preparations | 1/8/2014 | 8/9/2014 | | | | | | |
| 8 | test plan and schedule development, meetings, material orders | 1/8/2014 | 8/9/2014 | | | | | | |
| 9 | old probe dismantling | 7/8/2014 | 7/8/2014 | | | | | | |
| 10 | traversable probe installation | 4/9/2014 | 5/9/2014 | | | | | | |
| 11 | MSS calibration at AVL Graz | 4/8/2014 | 11/9/2014 | | | | | | |
| 12 | equipment transport and setup | 9/9/2014 | 18/9/2014 | | | | | | |
| 13 | engine tests | 19/9/2014 | 13/10/2014 | | | | | | |
| 14 | fuel doping system assembly and shakedown | 11/8/2014 | 22/9/2014 | | | | | | |
| 15 | tear down and cleanup | 13/10/2014 | 15/10/2014 | | | | | | |
| 16 | data reduction, export, and merging | 16/10/2014 | 24/10/2014 | | | | | | |
| 17 | Analysis of A-PRIDE 7 data | 24/10/2014 | 31/12/2014 | | | | | | |
| 18 | Effective density paper revision | 5/8/2014 | 25/8/2014 | | | | | | |
| 19 | AVL APC calibration at AVL | 21/11/2014 | 31/12/2014 | | | | | | |
| 20 | Meeting at GE Munich - presentation of preliminary results | 12/11/2014 | 12/11/2014 | | | | | | |
| 21 | SAE E-31 meeting in Graz, Austria | 1/12/2014 | 5/12/2014 | | | | | | |

## 6.2. Piggy-back measurements

A piggy back campaign was performed with PSI from July 7 until July 23, 2014. This campaign had the following major goals:

- Verify the operation of the constructed sampling rack
- Preparation/ troubleshoot of sampling system for A-PRIDE 7
- Verification of PSI setup

- Preliminary VOC sampling (cartridges for GC-MS analysis)

In total eight engine tests were attempted during the campaign of which six resulted in useful data sets. While ambient pressures remained fairly stable around 965 mbar during the entire campaign, the ambient temperature ranged from 10.8 to 27.5 °C.

Initial performance checks were made by comparing the system pressure values and gaseous (in particular $CO_2$) data as a function of static engine thrust with previously obtained values for the single point probe. The checks at the time indicated that the newly constructed rack, which used the same sampling system components as the original system prototype had indeed the identical performance as the original FOCA system prototype.

## 6.3. Results from VOC samples

VOCs were sampled with adsorbing cartridges, and analyzed after the campaign at Empa by thermal desorption gas chromatography/mass spectrometry (TD-GC/MS). The VOCs sampling system is constituted of a Nafion dryer, a set of two adsorbing cartridges connected in series, a critical orifice to adjust the flow rate (200 ml/min in our case) and a pump. VOCs were sampled on 5 different adsorbing cartridges: Tenax TA, Carbopack C, Carbopack B, Carboxen 569, and DNPH. The use of 5 different sorbents allowed the measurement of a wide range of compounds, such as short- and long-chain alkanes, aromatics, and oxygenated compounds. The total VOCs concentration was also measured with a flame ionization detector (FID), but without any information on the chemical speciation. In addition, fuel samples were also analyzed by GC/MS, and their chemical composition was compared to the VOCs emitted via engine exhaust. During these piggy back measurements, the main goals were to determine the breakthrough of VOCs across the adsorbing cartridges, and to identify which sorbent is the most appropriate for the quantification of each VOC.

The total VOCs concentration was much higher at ground idle (4-7% thrust, >200 ppm C) than at high thrust (<3 ppm C during take-off, 100% thrust). The result at low thrust may be due to lower temperature and poorer air/fuel mixing in the primary combustion zone, and lower fuel/air equivalence ratio at low thrust. All the VOCs identified with the Tenax TA, Carbopack C, Carbopack B, and Carboxen 569 cartridges were either alkanes or aromatics (example of chromatogram shown in Figure 6.1). For a given thrust level, we also observed differences between engine types (but these differences may also be due to different temperatures).
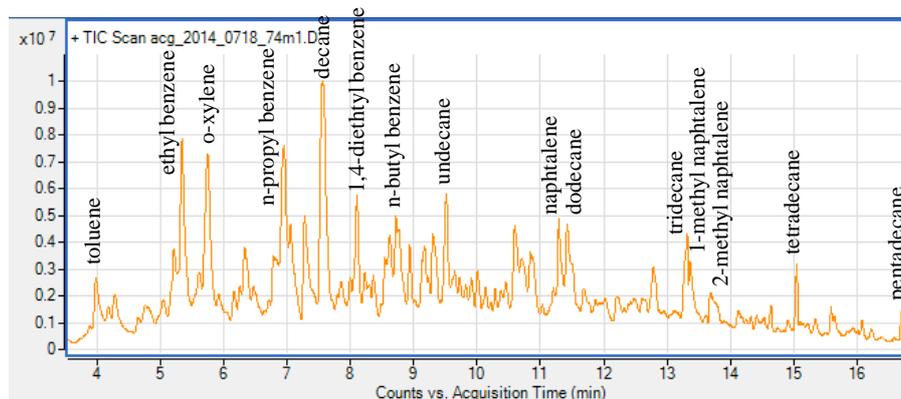
**Figure 6.1. Chromatogram obtained by TD-GC/MS. Thrust: 4-7% (ground idle); sorbent: Carbopack C.**

The comparison between chemical composition of fuel samples and VOCs emitted by aircraft engines showed significant differences. If fuel samples were dominated by alkanes (78%; Figure 6.2, left), VOCs emitted by aircraft engines were mainly comprised of aromatic compounds (64%; Figure 6.2, middle). However, the species identified by GC/MS in the two cases correlated with each other well. We also noticed some significant differences in the aromatic fraction between the fuel and the exhaust. The fractions of C2-, C3-, and C4-benzenes in the exhaust varied substantially compared to their counterparts in the fuel.
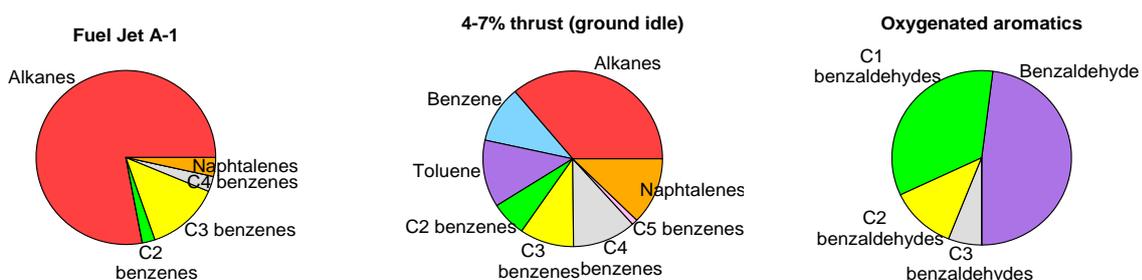


**Figure 6.2. Left: composition of fuel Jet A-1. Middle: composition of VOCs at 4-7% thrust (ground idle, sorbent: Tenax TA). Right: composition of oxygenated aromatics at 4-7% thrust (ground idle, sorbent: DNPH). Only compounds clearly identified by TD-GC/MS are reported in these pie charts. Thus, some VOC families may be overestimated or underestimated by a few percent.**

One of the main issues of the VOCs sampling system was that this technique requested off-line analysis after the campaign, and there was no means to check on-site if the sampling was done

correctly. If there was an issue during sampling (e.g. leak, incorrect flow rate), we could identify it only later, after the analysis of the cartridges by TD-GC/MS. We slightly modified the VOCs sampling system a few months after the piggy back measurements. We replaced the critical orifice by a mass flow controller after the cartridges, and we installed a pressure drop measuring device before the cartridges. Thus, we are now able to immediately notice with these two devices if there is an issue during the sampling.

## 6.4. Commissioning and installation of the traversable probe

### 6.4.1. Commissioning at Brunner GmbH in Lauterbrunnen

The prototype commissioning at the shop in Lauterbrunnen took place on August 15, 2014. Both Empa (Beni Brem) and SR Technics (Frithjof Siegerist) inspected the hardware and software of the prototype in terms of safety and performance. Two minor complaints in the designed system were observed:

1. Center position of Z-axis not visible

2. No software menu and hardware fix for multipoint probe. (Change of position during multipoint operation theoretically possible, which could result in a major accident).

The first complaint was ranked minor and not as a show-stopper whereas it was agreed that the second complaint had to be fixed before probe delivery, which was not a problem for the Brunner GmbH team.

### 6.4.2. Tear down of single point probe and installation of traversable probe

The dismantling of the previous single point probe took place on August 7, 2014. Five people were involved in the operation including Florian Meier and Christian Linder from Brunner GmbH, Frithjof Siegerist and Erwin Roduner from SR Technics, and Beni Brem from Empa. With the custom made jigs that were attached to the back plate of the old probe the uninstallation and lifting of the probe were fairly straightforward and the work could have been finished within 6 hours. The previous single point probe was stored in the old unused engine test cell at SR Technics.

The transport and installation of the traversable probe were performed 10 days before the official start of the A-PRIDE 7 campaign on September 4 and 5, 2014. The same jigs as for the dismantling were used for safely lifting the new probe with the fork lift (Figure 6.3).
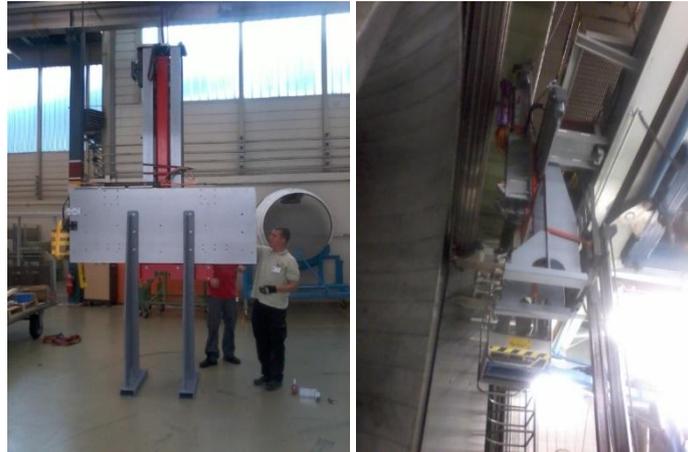
**Figure 6.3. Installation of the y-z traversable probe; (left) attachment of probe to the jigs for the installation with the forklift; (right) installation of the probe in the test cell.**

The attachment to the actual frame in the test cell took some time because all the screws required locking against potential vibrations. Besides the installation of the new probe, the additional z-axis required also the installation of additional wires and of a new electrical cabinet. However, the original touchscreen and process logic control (PLC) from FOCA installed in the engine operators' room were kept and reused for the new system. The total installation including the software update, installation of wires and hoses, and dry performance checks took about 12 hours.

During A-PRIDE 7, thermal stress caused cracking of the newly constructed probe head and small software issues were also found (see descriptions below). All these issues were resolved by the end of 2014. The remaining question is the additional stress on the heated line from the probe to the first splitter that is caused by movements in the two axes. This issue requires permanent attention since it is unknown how flexible and durable the stainless line core is.

## 6.5. Construction of the fuel "doping" system

The fuel doping system was constructed in August and September of 2014. The collaboration with the apprentice shop of Peter Beyerle of SR Technics was the key to success in this endeavor. As with the instrumentation rack that was built in spring 2014, Peter took the responsibility of assembling the provided components in a state-of-the-art manner (Figure 6.4). Planning, selecting, and purchasing the components were the responsibility of Empa/ Beni Brem.

**Figure 6.4. Construction of the fuel doping system in the apprentice shop of SR Technics.**

Two pumps and a Coriolis mass flow meter were selected which allowed adding doping at a rate of up to 10% of the total fuel mass flow of a CFM56 type engine at ISA conditions. The pump manufacturer Prominent provided help in selecting the right components for the nominal fuel system pressures and for dampening the pulsations of the two pumps. Various system safety checks were required by SR Technics before the system was allowed to be installed in the "Pumpenraum". Namely a pressure check of up to 10 bars line pressure without leakage, a scenario where the power was lost and a scenario where air pressure was lost (both in the middle of normal operation. The exceptional planning and PLC programming of Peter Beyerle showed no weakness and all tests could be passed. Overall the excellent teamwork also together with Kevin Bruderer (apprentice) led to an on-time and efficient execution of this project. A better than initially expected world-unique system was built (Figure 6.5) that has great potential for future systematic and controlled aviation fuel research, including the test of alternative aviation fuels.

**Figure 6.5. Photos of the fuel doping system installed at the SR Technics.**

## 6.6. A-PRIDE7 campaign

The A-PRIDE 7 campaign was a dedicated test campaign that took place from September 15 to October 16, 2014. Apart from the established partnership between SR Technics, Empa and FOCA, GE Aviation and SNECMA provided and funded the lease engine and additional expertise to this campaign. PSI and ETH participated as well with their own measurements and goals.

### 6.6.1. Prologue/ Legalities

Partnering with industry is for research institutions not easy in terms of legal and financial aspects. Luckily, Sara Rocci-Denis from GE Munich dedicated a lot of energy into the legal framework and bringing people on board and on the same page. Beni Brem (Empa) took the responsibility for the academic partners. Main hurdle to overcome was at the end not so much the agreement about the collaboration, but the engine lease between CFM and SR Technics, which could only be resolved in the last minute because of various appeals from FOCA, Empa and GE.

### 6.6.2. Summary of Experiments

The campaign included four dedicated weekends (ded) and three piggy-back (pig) tests (Table 6.2). The two major goals of Empa were the exhaust plane mapping and the fuel doping experiments further described below. The exhaust mapping experiments were performed in the beginning of the campaign and the fuel doping experiments at the end, with the single point probe (single) and multipoint probe (multi), respectively. The probe change took up the entire morning of October 9.

**Table 6.2. A-Pride 7 Engine Tests.**

| Date | Test | Time of Day | | Probe | Experiment Description |
|------|------|-------|------|-------|------------------------|
| | | Start | Stop | | |
| 19.09.2014 | ded | 10:25 | 11:10 | single | shakedown traversable probe |
| 22.09.2014 | ded | 14:00 | 19:50 | single | mapping experiment 1 |
| 26.09.2014 | pig | 15:00 | 16:25 | single | seal run-in piggyback |
| 27.09.2014 | ded | 08:15 | 17:45 | single | mapping experiment 2 |
| 29.09.2014 | pig | 12:00 | 13:00 | single | short piggyback without seal run-in |
| 01.10.2014 | pig | 16:25 | 18:15 | single | special piggyback, same engine as on 26.9, long run |
| 02.10.2014 | ded | 13:45 | 19:05 | single | PSI matrix and doping shakedown 1 |
| 04.10.2014 | ded | 07:00 | 16:05 | single | PSI and ETH matrix |
| 05.10.2014 | ded | 08:00 | 16:50 | single | PSI and ETH matrix |
| 09.10.2014 | ded | 08:10 | 19:05 | multi | fuel doping shakedown 2 and PSI matrix |
| 10.10.2014 | ded | 07:45 | 17:45 | multi | fuel doping Solvesso 150 ND |
| 11.10.2014 | ded | 07:15 | 17:10 | multi | fuel doping Solvesso 150 |

The following sections describe the preliminary results from the campaign. Most of these results were also presented during the SAE E-31 PM subcommittee meeting in Graz, Austria in December 2014.

## 6.6.3. Exhaust plane mapping

Two test days during A-PRIDE 7 were dedicated to mapping of the engine exit plane using the traversable probe described above. Preliminary analysis shows that nvPM emissions varied by up to a factor of 2 to 4 at high and low thrust, respectively. For the engine minimum idle condition, the emissions of $CO_2$, UHC, nvPM number and mass at different locations in the engine exit plane are shown in Figure 6.6. The gas emissions are more uniform than the nvPM emissions. It is likely that some of the spatial variability of the nvPM is due to different temperature gradients (and resulting thermophoretic loss) at different locations in the exhaust stream. Therefore, the detailed analysis will focus on this aspect using the measured temperatures at the probe tip and exit to estimate the thermophoretic losses.
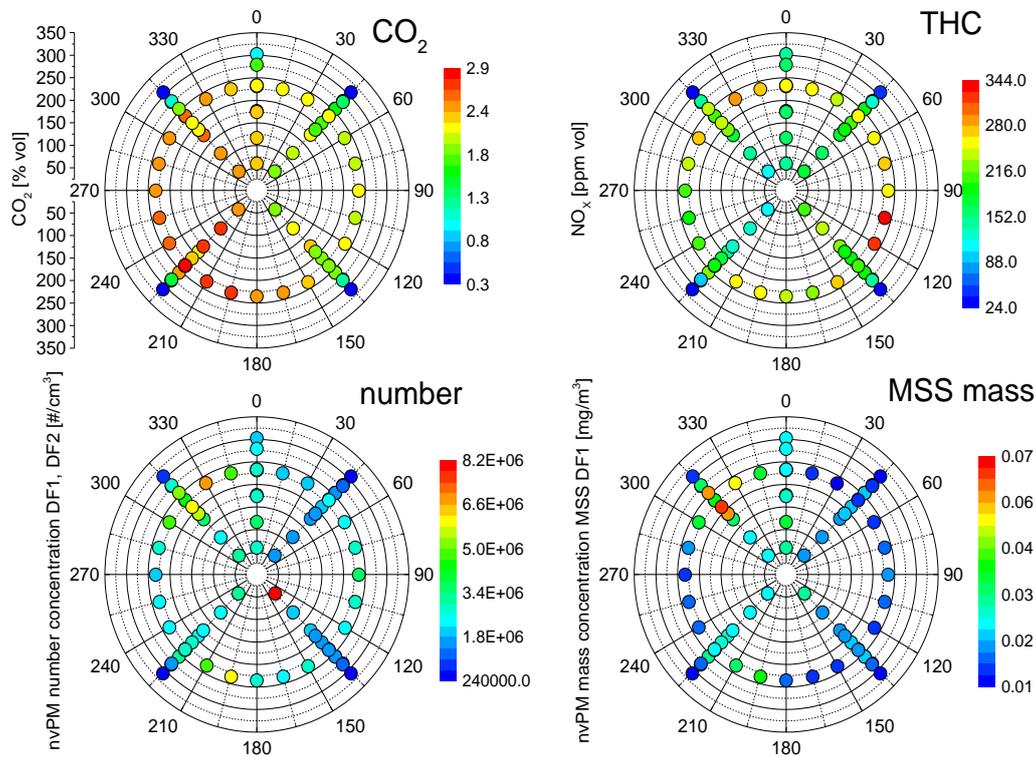
**Figure 6.6. The emissions of CO₂, UHC, nvPM number and mass at different locations in the engine exit plane for the engine minimum idle condition.**

Major issues during the exhaust mapping were the thermal gradients between the hot engine core and cold bypass flows. These gradients caused the probe to crack (Figure 6.7) and resulted in delaying the second campaign day due to repairs.

**Figure 6.7. Cracked welding seam on the sampling probe.**

Due to vibrations and insufficient welding points the first thermocouple installation on the probe tip also failed after three engine runs. Both the welding seam cracks and the thermocouple issue were

fixed by the end of 2014 with some redesigns and additional welding on the sampling head. Ongoing work focuses on analyzing all the measured data including the correction for thermophoresis in the nvPM results as well as on evaluating the previously established fixed sampling head position in the context of these new spatial data.

## 6.6.4. Effects of fuel on engine emissions

The fuel doping system described above was used during two full test days (following 2 earlier shakedown tests) to vary the total aromatics content in the fuel burned. These highly demanding experiments were successful, leading to very interesting and important results. The nvPM mass and number emissions correlate well with fuel hydrogen content and can vary by up to 60% at 6% increase of fuel aromatics content. The offline chemical analysis of more than 100 liquid fuel samples was performed externally by Intertek Schlieren. The detailed results are published in Brem et al. 2015.

### 6.6.4.1. Experimental setup

An in-production, hi-bypass turbofan engine was leased for these measurements. The engine used was considered "well run-in" at approximately half of its expected service life before an overhaul. Experiments were performed on two consecutive test days in October 2014. On both days the fuel total aromatics content was varied with a specifically-built solvent injection system connected to the engine fuel line (Figure 6.8). The tests started with dry motoring followed by a half hour warm-up sequence that included minimum idle, 7%, 65% and 85% relative static sea level thrust levels of 5 minutes each. After the warm-up, an engine thrust matrix that included the proxy static sea level engine thrust levels of take-off (100%), climb out (85%), cruise (65%), approach (30%), taxiing (7%) and minimum idle (3%) running from high to low thrusts was performed. Each thrust level included consecutive measurement of the neat fuel (17.8 % v/v aromatic content), the targeted aromatic content levels and another measurement for the neat fuel to account for potential drifts. Between the different aromatic levels at thrusts below 30%, the thrust was increased to 85% to burn off the previous fuel blend in the fuel line such that the test matrix could be executed more rapidly and the nvPM signals could stabilize more quickly.
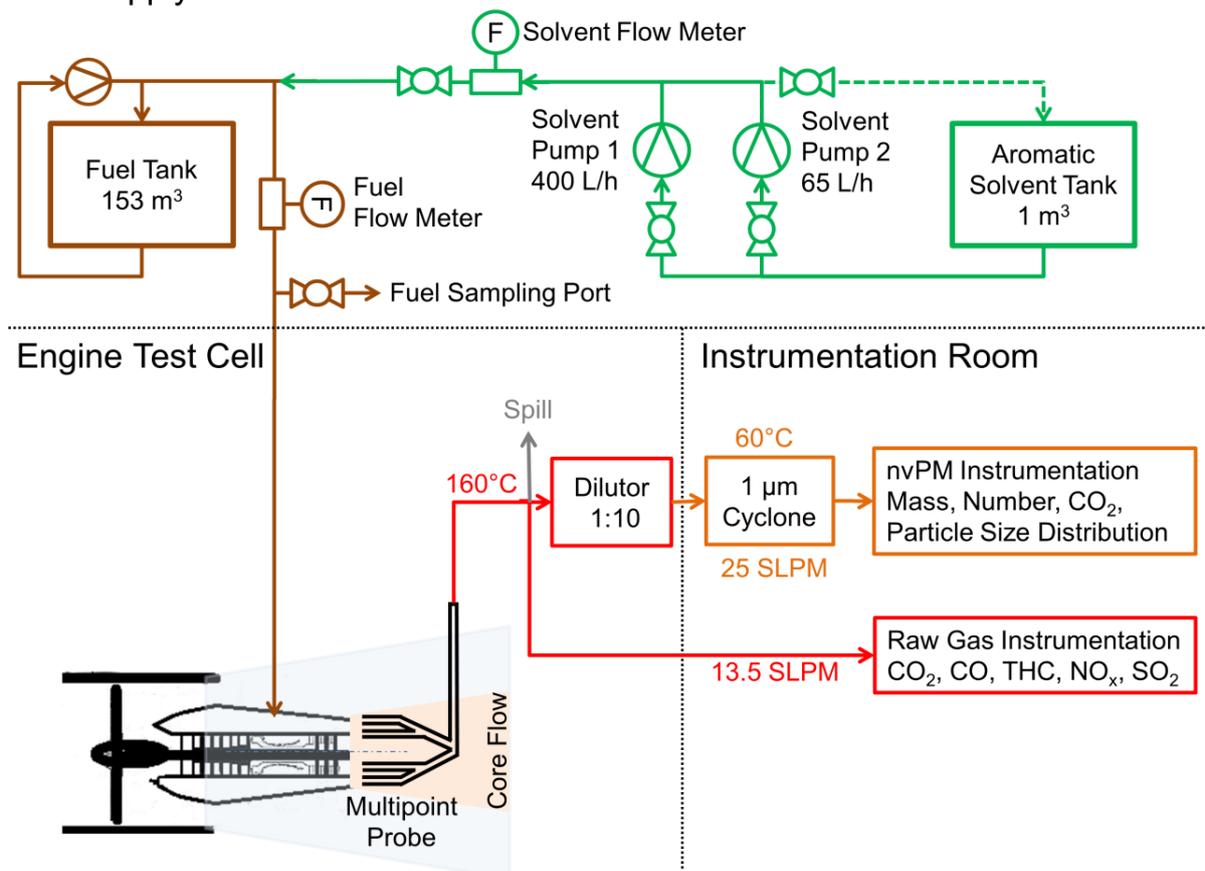
**Figure. 6.8. Overview of the experiment: engine fuel supply components and the specifically built aromatic solvent injection system are shown in brown and green, respectively. The sampling system for nvPM and gaseous pollutants in the core flow of the engine exhaust is indicated in orange and red, respectively. A multi-orifice cruciform sampling probe was used to collect PM laden exhaust.**

To increase the fuel total aromatics content, the neat fuel was blended with two petroleum-derived aromatic solvents, which encompass the boiling point and molecular weight range of the aromatics in Jet A-1. The first aromatic solvent used was the naphthalenes depleted Solvesso 150ND (ExxonMobil Chemical Inc.). The second one, Solvesso 150 (ExxonMobil Chemical Inc.), contained 6 % (v/v) naphthalenes, but otherwise had nearly identical specifications. Two diaphragm metering pumps (Sigma type, Prominent Inc.) with maximum feed rates of 400 L/ h and 65 L/ h (at the fuel line pressure of 3.2 bars) fed the aromatic solvents into the engine fuel supply line from a 1000 L tank (Figure 5.8). The feed rates of the pumps were chosen so that the aromatic solvents could substitute up to 10 % (v/v) of the engine fuel flow at all engine thrusts. A Coriolis type flow meter (Promass 40E, Endress & Hauser) determined mass feed rates of the solvents. The turbine wheel fuel flow gage of the test cell provided the total mass flow of fuel and fuel-solvent mixtures to the engine. Fuel samples for offline chemical analysis were drawn at a sampling port 7.5 m downstream of the injection point (13.5 m

upstream of the engine). For each aromatic level a fuel sample was taken when the nvPM levels were stabilized. All fuel samples were analyzed for total aromatics content (ASTM D1319), naphthalenes (ASTM D1840), and hydrogen mass (ASTM D5291).

We report emission indices (EIs, quantity of species per mass of fuel burned) and normalized emission indices referenced to the neat fuel. The diluted and undiluted $CO_2$ concentrations were used to account for dilution. The change in the fuel hydrogen to carbon ratio when the fuel total aromatics content was varied was also taken into account. Particle losses in the sampling lines are not considered in the results presented.

## 6.6.4.2. Results

The mass and number emission profiles (Figure 6.9), are characteristic of this engine type. Typically, BC mass EIs from this engine type are slightly higher at minimum idle than at 7 % thrust and steadily increase with increasing thrust levels above 30 % (Figure 6.9a, c). In contrast to the mass, the number EIs show distinctly higher emissions at idle and peak in both experiments near the 65 % thrust condition (Figure 6.9 b, d), likely due to particle coagulation at thrust levels greater than 65 % within the engine. The mass and number EIs with neat fuel (blue symbols) have nearly identical profiles, indicating stable ambient conditions and good reproducibility of the measurements on both test days. An increase in both mass and number emissions with increasing fuel total aromatics content is clearly distinguishable for both solvents at thrust levels greater than 7 % where the solvent injection system worked properly. The increased soot formation with higher total aromatics content is in concert with previous studies (Timko et al. 2010; DeWitt et al. 2008; Lobo et al. 2012). This dependence has been explained as follows: parent aromatic molecules in the fuel act as condensation and addition sites for products of incomplete combustion for forming PAHs that subsequently nucleate and carbonize to form soot (Frenklach 2002; Richter and Howard 2000). In contrast to aromatics, aliphatics have to first undergo fragmentation and subsequent aromatic ring formation reactions (Richter and Howard 2000). These additional reaction steps are slower relative to the aromatics pathway, resulting in less soot formation. In contrast to mono-aromatics, naphthalenes should further increase the formation of large PAHs, which subsequently results in additional soot inception. However, the difference in the effect of the two solvents on the emissions is hard to distinguish in Figure 6.9; only slightly higher number EIs are apparent in panel (d).
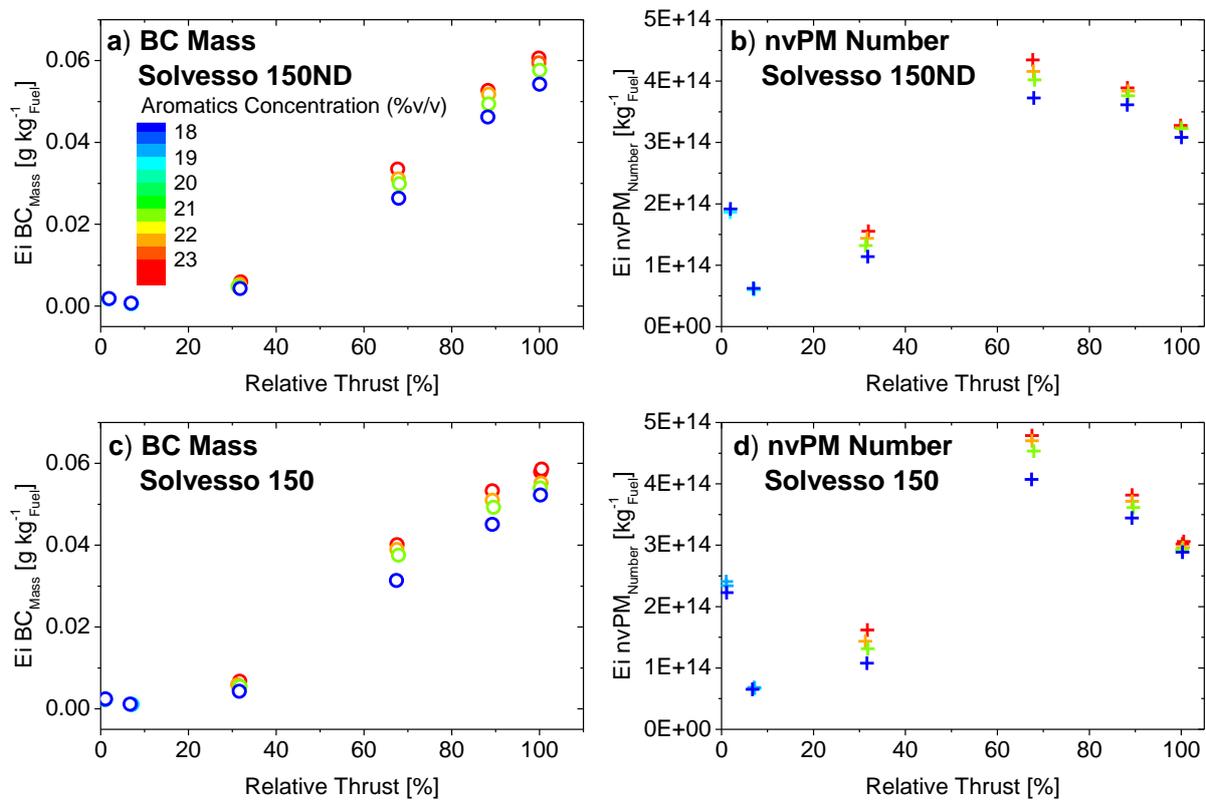
**Figure 6.9. BC mass (circles) and nvPM number (crosses) EIs as a function of sea level static engine thrust and fuel total aromatics content (color coding). The top two panels (a) and (b) correspond to the experiment performed with the naphthalenes depleted solvent (Solvesso 150ND); the bottom two panels show the experiment performed with Solvesso 150 that contained 6 % (v/v) naphthalenes.**

To investigate the effects of different solvent types and correlation parameters, we looked at the relative changes in BC and nvPM number EIs (Figure 6.10). The BC mass and nvPM number EIs increased by up to a factor of 1.59 and 1.51, respectively, due to the 5.8 % (v/v) increased fuel total aromatics content at 30% engine thrust. With increasing engine thrust, the aromatics' influence on soot emissions became less pronounced. At 100 % engine thrust, the EIs increased by a factor of 1.12 for BC mass and 1.06 for nvPM number.

The type of fuel aromatics plays an additional role as shown in Fig. 6.10 (circles vs crosses in (a) and (b)). Substituting mono-aromatics with naphthalenes from 0.78 % (v/v) to up to 1.19 % (v/v) at nearly identical fuel total aromatics content results in up to 40 % higher BC mass and up to 30 % higher nvPM number EIs at the 30 % engine thrust level. The naphthalenes' effect is indistinguishable at 100 % engine thrust. However, some of the difference in the BC mass EI ratio at 30 % engine thrust could be attributed to the loss in precision of the MSS (resolution of 1 µg m$^{-3}$) at the low BC concentrations

(6 to 10 µg m$^{-3}$ at the instrument) at this engine thrust setting. Therefore, further investigation is needed to determine the exact extent of the naphthalenes' effect on BC mass.
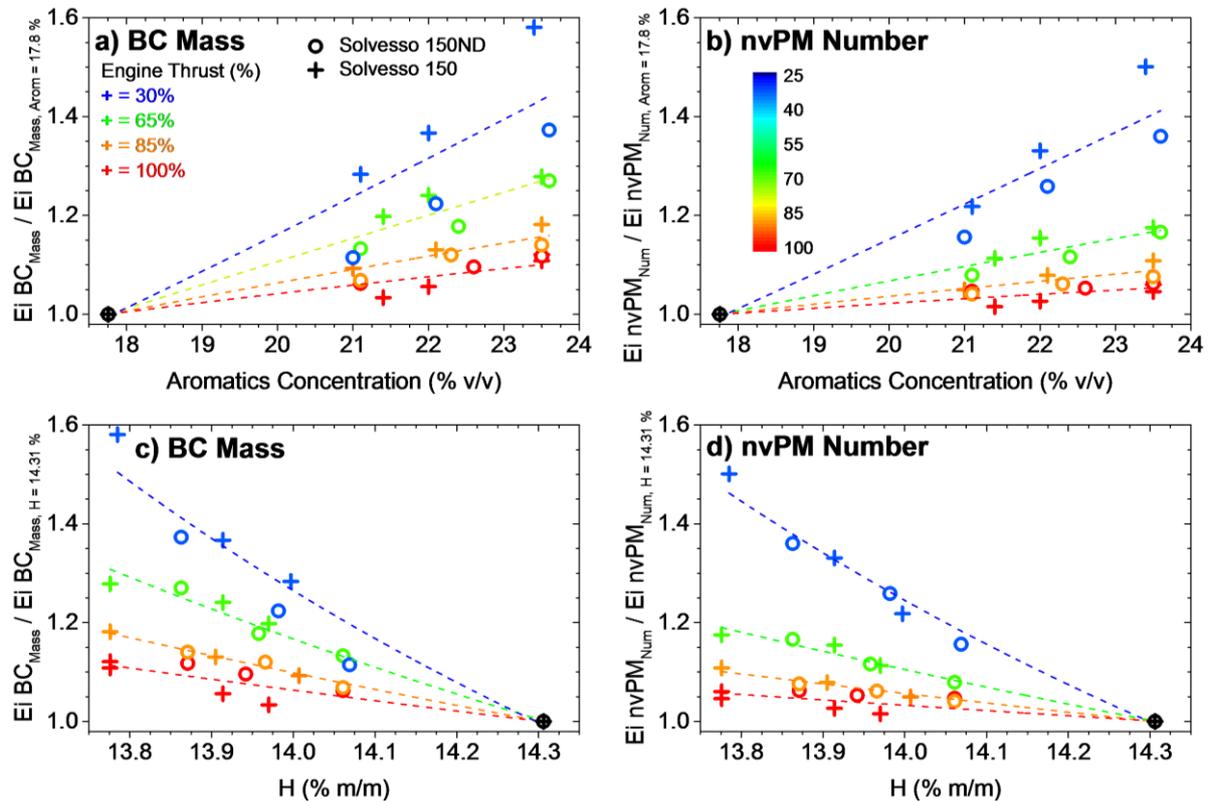


**Figure 6.10. Neat fuel normalized EIs for BC mass and nvPM number concentration as a function of fuel total aromatic concentration (a, b), fuel hydrogen mass concentration (c, d) and engine thrust (color coding in all panels). Solvesso 150ND and Solvesso 150 experiments are depicted as circles and crosses, respectively.**

### 6.6.4.3. Regression Analysis

A simple model (Eq. 6.1) was fitted to the experimental data to predict changes in BC mass and nvPM number EIs as a function of engine thrust and fuel hydrogen mass content.

$$\Delta EI_x = \left( \alpha_0 + \alpha_1 \times \hat{F} \right) \times \Delta H$$
(Eq. 6.1)

In Eq. 6.1 $\Delta EI_x$ corresponds to the percentage change in BC mass or nvPM number EI, $\alpha_0$, $\alpha_1$ are fitting parameters, $\hat{F}$ is the percentage of engine thrust and $\Delta H$ is the change in hydrogen mass content. The method of least squares was applied to determine $\alpha_0$, $\alpha_1$ which are provided in Table 6.3.

**Table. 6.3. Model fitting parameters including their standard errors and coefficients of determination.**

| Variable | $\alpha_0$ | $\alpha_1$ | Adjusted $R^2$ |
|---|---|---|---|
| $\Delta$EI BC$_{Mass}$ | $-124.05 \pm 5.04$ | $1.02 \pm 0.06$ | 0.94 |
| $\Delta$EI nvPM$_{Number}$ | $-114.21 \pm 3.63$ | $1.06 \pm 0.05$ | 0.96 |
| $\Delta$EI Combined | $-119.31 \pm 3.94$ | $1.03 \pm 0.05$ | 0.92 |

The fits were performed for BC mass and nvPM number (indicated as dashed lines in Figure 6.10 (c) and (d) and as surface plots in Fig. 6.11. The model explains the variability in the data, with coefficients of determinations ($R^2$ values) greater than 0.92. It captures the changes in emission indices within $\pm$ 5 % for the BC mass and nvPM number data sets. We anticipate that this model is valid for engines that use similar technology (rich-burn, quick-quench, lean-burn RQL combustors) and burn fuels that are compliant with Jet A-1 specifications. This engine technology is most prevalent in the current fleet. However, the applicability of the model for the engine thrusts below 30 % and changes in hydrogen mass content greater than 0.6 % (m/m) needs further investigation and extrapolations should be done carefully.
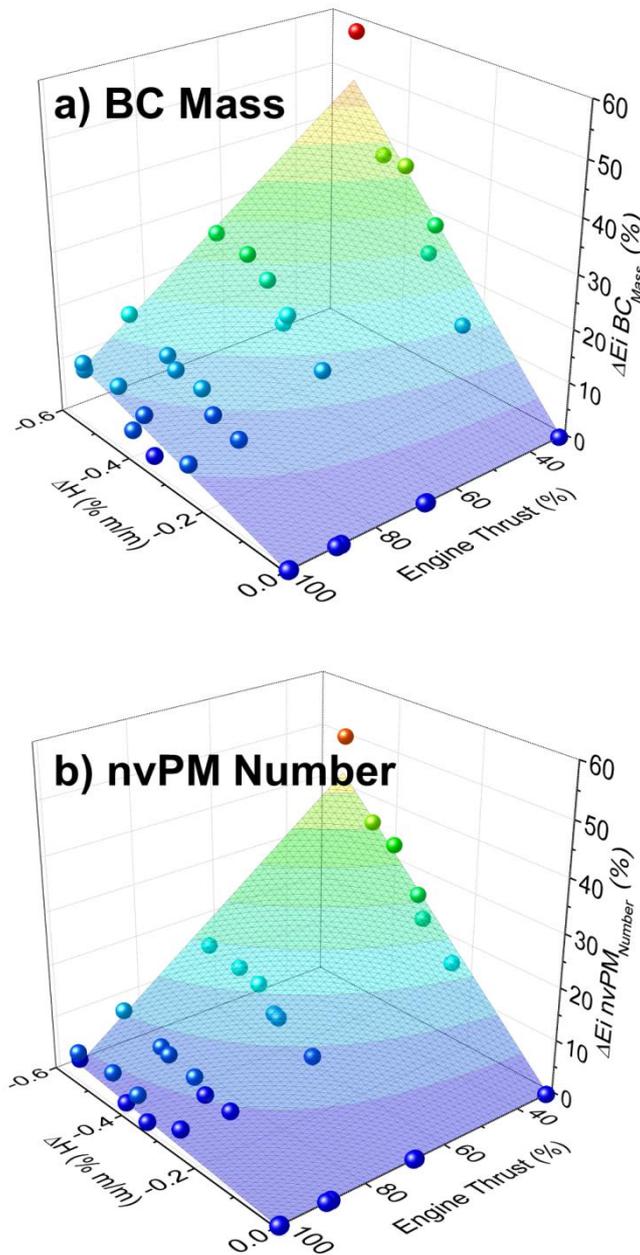
**Figure 6.11. Surface fitted change in (a) BC mass EIs and (b) nvPM number EIs as a function of sea level static engine thrust and change in fuel hydrogen mass content. Spheres represent the data measured.**

### 6.6.4.4. Implications

The fuel study fills an important gap in the understanding of the effects of fuel aromatics on the BC mass and nvPM number emissions of an in-production aircraft gas turbine engine that is representative of the current fleet. The use of a state of the art sampling system allowed us to detect

changes in emissions due to changes in fuel aromatics content that are representative for the variability observed within standard jet fuel that is sold commercially (Hadaller and Johnson 2006). Smoke number measurements which provide the basis of our current inventories are not sensitive enough to detect such changes in emissions and therefore such inventories can be biased significantly by variations in fuel aromatic content. Therefore, the implications of this research are threefold: (1) The environmental nvPM certification of gas turbine aero engines, which is currently under development, could use the model of this paper to correct for changes in BC mass and nvPM mass emissions induced by the variability in the certification fuel. This standardization might also be necessary to set future nvPM emission regulatory levels. (2) Emission inventories relevant for local air quality and climate could be corrected for variation in fuels. For example, the comparison of two ICAO standard landing and take-off (LTO) cycles with the engine measured in this work, one calculated with 14.3 % (m/m) hydrogen content representative of Zürich and the other one calculated with 13.9 % (m/m) representative of Toronto (Hadaller and Johnson 2006), would result in 12 % and 19 % higher LTO BC mass and LTO nvPM number emissions in Toronto compared to Zürich (assuming the model of this study is applicable at 7 % thrust). Assuming that the 65% ground level engine combustor inlet temperature is a valid proxy for the engine combustor condition for cruise (Döpelheuer and Lecht 1999), the BC mass and nvPM number emissions would also be 22% and 15% higher at cruise using the Toronto fuel. Notable reductions in nvPM emissions and potential improvements for local air quality and climate can therefore be made by modestly improving the standard jet fuel refining processes or the oil feedstock used. (3) BC mass and nvPM number emissions from gas turbine engines burning Jet A-1 blended with alternative fuels at low ratios (< 10 % (v/v)) are expected to follow a similar trend with fuel hydrogen mass content as observed in this study and should be investigated. To accurately assess these implications, additional research should cover thrust levels lower than 30 %, use fuel innate aromatics, and other engines equipped with further optimized RQL combustor types. In addition, a complementary investigation should be carried out on engines equipped with novel lean burn combustors which might show a different sensitivity to fuel aromatics and hydrogen content than shown here.

## 6.7. Instrument history and logbook

We have developed a spreadsheet for tracking the calibrations, service, and use of the nvPM instruments. The following tables summarize the calibrations and service from the commissioning of the instruments at the end of 2014.

**Table 6.4. Short summary of the identifiers and actual parameters of the nvPM instruments**

| | nvPM mass | | nvPM number |
|---|---|---|---|
| Instrument model: | Micro Soot Sensor AVL 483 | LII-300 | APC Advanced AVL CS 489 |
| Manufacturer: | AVL Graz, Austria | Artium, CA, USA | AVL Graz, Austria |
| S/N: | 1065 | 418 | 409C |
| Current firmware: | 2.05 | 3.3 | 2.29.4 |
| Current software/ DUI: | 2.7.6.1749 | 4.5 | 2.9.0.2114 |
| Current cal. factor: | 0.554 | 0.801 | N/A |
| Calibrated by: | AVL Graz | NRC Canada | AVL Graz, Austria |
| Calibration date: | 2-Sep-14 | 11-Jul-14 | 15-Dec-14 |

## 6.7.1. APC
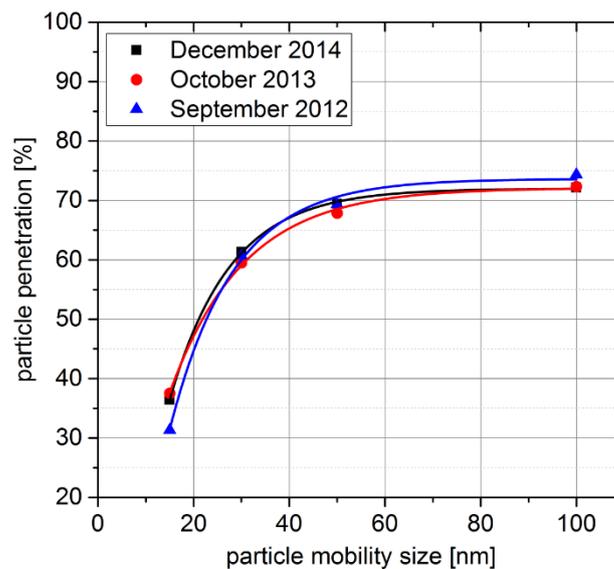


**Figure 6.12. VPR penetration as a function of particle size and date of calibration. No trend in performance deterioration can be observed.**

**Table 6.5. Summary of the APC calibrations and service.**

| Date | Event | Venue | Firmware | Software (DUI) | PCRF | DF | Penetration efficiency 15 | Penetration efficiency 30 | Penetration efficiency 50 | Penetration efficiency 100 | Calibration aerosol |
|---|---|---|---|---|---|---|---|---|---|---|---|
| 10/10/2012 | pre-delivery testing by the manufacturer | AVL Graz, Austria | 2.23 | 2.4.0.636 | 100 | 67 | 31 | 60 | 68 | 73 | miniCAST combustion soot |
| | | | | | 250 | 170 | 32 | 61 | 70 | 75 | |
| | | | | | 500 | 341 | 31 | 61 | 70 | 75 | |
| | | | | | | Average: | 31.33 | 60.67 | 69.33 | 74.33 | |
| 10/7/2013 | annual calibration and service | AVL Graz, Austria | 2.23 | 2.4.2 | 100 | 65 | 38.1 | 59 | 67 | 72.7 | APG combustion soot |
| | | | | | 250 | 166 | 37.8 | 60 | 68.5 | 71.6 | |
| | | | | | 500 | 333 | 36.7 | 59.5 | 68.1 | 72.7 | |
| | | | | | | Average: | 37.53 | 59.50 | 67.87 | 72.33 | |
| 12/15/2014 | annual calibration and service | AVL Graz, Austria | 2.29.4 | 2.9.0.2114 | 100 | 66 | 35.4 | 59.3 | 68.3 | 70.8 | APG combustion soot |
| | | | | | 250 | 169 | 37.4 | 61.5 | 69.1 | 72.9 | |
| | | | | | 500 | 343 | 36.4 | 63.2 | 70.9 | 72.8 | |
| | | | | | | Average: | 36.40 | 61.33 | 69.43 | 72.17 | |

| Date | CPC linearity | counting efficiency 10 nm | counting efficiency 15 nm | Replacement / upgrade |
|---|---|---|---|---|
| 10/10/2012 | 0.945 | 76 | 91.8 | |
| 10/7/2013 | 0.97 | 52.3 | 91.3 | catalytic stripper heating element upgrade to 350 degC upgrade CPC mount plate for faster CPC unistallation upgrade interface board - new wiring |
| 12/15/2014 | 0.9452 | 62.1 | 91.1 | Chopper diluter motor upgrade - no jamming PCRF 250 to 100 Firmware upgrade |

## 6.7.2. MSS

**Table 6.6. Summary of the calibrations and service of the MSS.**

| Date | Event | Venue | Calibration factor | Firmware | Software (DUI) | Soot source |
|---|---|---|---|---|---|---|
| 29/6/2012 | AVL factory calibration | AVL Graz | 0.475 | 1.31 | 3.0.7 | AVL Matter CAST |
| 9/11/2012 | A-PRIDE 4 miniCAST | SR Technics | 0.396 | 1.31 | 3.0.7 | miniCAST 5201C |
| 13/1/2013 | NIOSH 5040 calibration | Empa | 0.475 | 1.31 | 3.0.7 | miniCAST 5201C |
| 4/2/2013 | MSS comissioning | Empa | 0.4062 | 1.31 | 3.0.7 | no |
| 25/3/2013 | NIOSH 5040 calibration | Empa | 0.475 | 1.31 | 3.0.7 | miniCAST 5201C |
| 26/7/2013 | pre-APRIDE 5 calibration | NRC Canada | 0.4616 | 2.05 | 2.7.6.1749 | inverted flame burner |
| 2/9/2014 | AVL factory calibration | AVL Graz | 0.554 | 2.05 | 2.7.6.1749 | AVL Matter CAST |

| Date | Comment |
|---|---|
| 29/6/2012 | initial calibration before commissioning |
| 9/11/2012 | "normalization factor" applied - LII300 calibrated according to NIOSH 5040 was used as a reference |
| 13/1/2013 | changed to factory settings prior to calibration, results not obtained |
| 4/2/2013 | obtained from the absorption window span check - its value was changed during A-PRIDE 4 by M. Arndt (AVL) |
| 25/3/2013 | correction factor 1.16*0.4062=0.471; factory calibration factor was applied instead, but the phase angle was changed according to instructions in MSS manual, section 7.2, page 116 |
| 26/7/2013 | correction factor obtained from NRC calibration 0.9718 applied and phase angle changed to factory setting -61 degrees; new firmware installed by M. Arndt |
| 2/9/2014 | calibration and maintenance at AVL Graz using their Matter CAST as a soot source |

### 6.7.3. LII-300 (TC-NRC)

**Table 6.7. Summary of the calibrations and upgrades/service of the TC-NRC LII-300 used by Empa.**

| Date | Event | Venue | Calibration factor | Firmware | Software | Soot source |
|---|---|---|---|---|---|---|
| 1/7/2013 | mass instruments calibration prior to A-PRIDE 5 | NRC Canada | 0.618 | 3.00 | 4.2 | inverted flame burner |
| 3/6/2014 | Upgrade at Artium after a campaign at Cardiff | Artium | 0.618 | 3.3 | 4.5 | no NIOSH cal |
| 11/7/2014 | calibration at NRC Canada prior to A-PRIDE 7 | NRC Canada | 0.801 | 3.3 | 4.5 | inverted flame burner |

| Date | Comment |
|---|---|
| 1/7/2013 | new instrument delivered by Artium, EC/OC analysis done by Concorde analytical services |
| 3/6/2014 | 1. PMT boards did have the direct high voltage feed back but lacked kapton tape to prevent arcing. 2. Channel two PMT board replaced. 3. Painted outside edge of filter wheel for more reliable homing. Pitch and catch sensor will have better reflective surface. 4. Changed wiring for pressure transducer to sampling card to increase updated from 1 per second to laser shot rate. 5. Changed test cell seals on windows(softer) and purge apertures(harder). 6. Reduced gain from pyroelectric to analog input on sampling card. Pyroelectric has an output of 17.0V per J into a 1M ohm resistor which is double the average of other units. This would rail the input circuitry. 7. Reduced the laser probe volume to 3.1mm set power which includes the first window loss to 2.25mJ/mm2. Energy 4.00 Q-Switch Dly 140uS. 8. Calibrated for dichroic out or high sensitivity. 9. Performed Optical calibration. 10. Firmware upgrade |
| 11/7/2014 | new Aalborg MFC was installed on the sampling plate |

# 7. Activities and results in the period 2015/01 – 2015/10 (including A-PRIDE 8)

## 7.1. Introduction

This chapter describes the Swiss Federal Office of Civil Aviation (FOCA) sponsored project entitled "Particulate Matter and Gas Phase Emission Measurement of Aircraft Engine Exhaust" during its final period from January 2015 to October 2015. This period included piggyback measurements at SR Technics and a dedicated measurement campaign "A-PRIDE 8". This report presents preliminary findings of this campaign together with a more detailed analysis and summary of the results obtained in the previous campaigns. The following chart (Table 7.1) provides a chronological overview of the major events and tasks during the reporting period.

**Table 7.1. Overview of the main activities during the reported period.**

| ID | Task Name | Start | Finish |
|----|-----------|-------|--------|
| 1 | Experimental and technical work | 13/1/2015 | 13/10/2015 |
| 2 | PM sampling probe repair | 13/1/2015 | 30/1/2015 |
| 3 | measurement system upgrades and piggyback measurements | 13/5/2015 | 29/5/2015 |
| 4 | A-PRIDE 8 preparations | 20/8/2015 | 4/10/2015 |
| 5 | A-PRIDE 8 measurements | 5/10/2015 | 13/10/2015 |
| 6 | Data / samples processing and analysis | 16/2/2015 | 18/12/2015 |
| 7 | engine exit plane mapping (A-PRIDE 7) | 15/4/2015 | 20/6/2015 |
| 8 | mini-CAST study at MS&T | 16/2/2015 | 2/6/2015 |
| 9 | VOC samples analysis - piggyback measurements | 30/5/2015 | 1/9/2015 |
| 10 | fuel sensitivity study (A-PRIDE 7) - detailed analysis | 1/4/2015 | 30/6/2015 |
| 11 | A-PRIDE 8 data reduction and export | 1/11/2015 | 13/11/2015 |
| 12 | A-PRIDE 8 data processing and analysis | 22/11/2015 | 18/12/2015 |
| 13 | VOC samples analysis - A-PRIDE 8 | 13/10/2015 | 18/12/2015 |
| 14 | Writing projects | 17/2/2015 | 25/11/2015 |
| 15 | A-PRIDE 4 overview paper | 17/2/2015 | 10/4/2015 |
| 16 | BAZL proposal 2016-2018 | 2/3/2015 | 30/3/2015 |
| 17 | Fuel sensitivity study paper | 1/4/2015 | 26/7/2015 |
| 18 | mini-CAST study paper | 1/7/2015 | 25/11/2015 |
| 19 | Meetings and conferences | 10/2/2015 | 25/9/2015 |
| 20 | ICAO CAEP Aviation Environmental Impacts Seminar, Virginia, USA | 10/2/2015 | 12/2/2015 |
| 21 | ICAO MESG Meeting, Belfast, Ireland | 11/5/2015 | 13/5/2015 |
| 22 | Aerosol Technology conference, Tampere, Finland | 15/6/2015 | 17/6/2015 |
| 23 | TAC-4 conference, Bad Kohlgrub, Germany | 21/6/2015 | 25/6/2015 |
| 24 | ETH combustion-generated nanoparticles conference | 28/6/2015 | 1/7/2015 |
| 25 | ICAO MESG Meeting, Rolla, MO, USA | 13/9/2015 | 18/9/2015 |
| 26 | European Aerosol Conference 2015, Milan, Italy | 6/9/2015 | 11/9/2015 |
| 27 | ANERS 2015, La Rochelle, France | 22/9/2015 | 25/9/2015 |

## 7.2. A-PRIDE 8 campaign overview

The A-PRIDE 8 campaign took place from October 5th to October 13th 2015. It consisted of one piggyback engine test and four dedicated engine tests. Summary of the engine tests performed together with the objectives of the individual test days are shown in Table 7.2. The campaign was performed using the Empa/FOCA sampling system only with ancillary LII and MSS instruments from

Cardiff University. The campaign guests were Andrew Crayford, Elliot Durand from Cardiff, Gregory Smallwood from the National Research Council of Canada and Mark Johnson from Rolls Royce.

**Table 7.2. A-PRIDE8 overview.**

| Date | Ancillary measurements | Objective |
|---|---|---|
| 6 October 2015 | Effective density, SMPS, CAPS, Cardiff MSS, Cardiff LII, SVOC cartridges | Measurement and sampling system shake down |
| 7 October 2015 | Effective density, SMPS, CAPS, Cardiff MSS, Cardiff LII, EC/OC filters, SVOC cartridges | Fuel doping shakedown, EC/OC measurement, LII fluence check |
| 8 October 2015 | Effective density, SMPS, CAPS, Cardiff MSS, Cardiff LII, EC/OC filters, SVOC cartridges, | Mass instrument - EC/OC intercomparison |
| 9 October 2015 | Effective density, SMPS, CAPS, SVOC cartridges | Fuel doping at low thrust levels |
| 12 October 2015 | Effective density, SMPS, CAPS, SVOC cartridges | Circumferential mapping and mapping with fuel doping |

Table 7.2 indicates the major objectives of A-PRIDE 8 which included:

1. Characterize engine thrust resolved volatile organic compound (VOCs) emissions
2. Assess nvPM and VOC emissions sensitivity to fuel aromatic content at engine thrusts below 30%
3. Perform a LII instrument applicability check as described in the draft ICAO Annex 16 Appendix 7
4. Perform mapping measurement to verify spatial nvPM heterogeneity in exhaust observed in A-PRIDE 7. Also investigate if heterogeneity is affected by fuel aromatic content.

The following sections of this report include the currently analyzed A-PRIDE 8 data in comparison to previous campaigns. However major data analysis in particular for the VOC analysis and the OC/EC filters is still ongoing.

## 7.3. Size distributions of aircraft turbine nvPM

This section summarizes the current knowledge about the particle physical properties, determined from measurements at SR Technics. The size distributions data are a compilation form A-PRIDE 8 and previous campaigns.

Particle size is a vital parameter for estimating the PM emissions at the engine exit plane and understanding nvPM losses within the sampling system. Particle size measurements are not part of the standardized nvPM measurement system. The currently developed particle loss correction method (Annex 16, Appendix 8) infers the relevant particle distribution data solely from the measured nvPM mass and nvPM number concentrations. Measured particle size distributions are critical for validating this method. Since aircraft PM distributions are nearly lognormal and therefore parameterized using a count median or geometric mean diameter (GMD) and a geometric standard deviation (GSD).
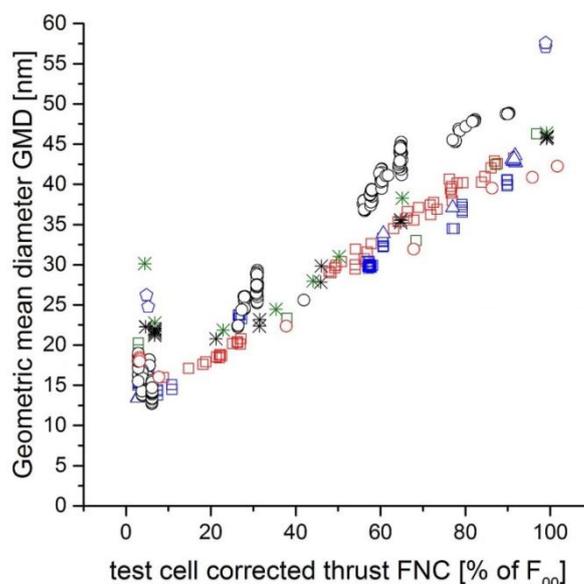


**Figure 7.1. GMD as a function of thrust measured using the single point probe and the multi-point probe (A-PRIDE 7). Symbol colors correspond with the campaigns as follows: green – A-PRIDE 4, red – A-PRIDE 5, blue – A-PRIDE 7, and black – A-PRIDE 8.**

The GMD for the single annular combustor (SAC) engines increases linearly with engine thrust (Figure 7.1). Given that the data shown were taken with a different particle mobility analyzer in each campaign (DMS500 in A-PRIDE 4 and 5; TSI SMPS 3938 and 3936 in A-PRIDE 7 and 8, respectively), the GMDs of most of the CFM engines measured show small variability at a similar relative thrust. However, the situation is different for the Pratt and Whitney (PW) engine variants. These engines tend to produce

larger GMD at idle (higher soot mass concentration), which then decreases and later on increases linearly with increasing thrust, similar to the CFM series engines.

Using a fit function to predict GMD as a function of thrust for one engine type does not take the emissions variability into account. Therefore, particle size distributions should be measured during each engine test for the most accurate emissions estimates. The relationship between the GMD and $EI_m$ was found to be logarithmic, and a larger database could potentially help to improve the prediction of GMD based on the measured $EI_m$.

The GSD for most engines was in a narrow range from 1.6 to 1.9 with a weighted average of 1.76 (Figure 7.2). These data suggest increasing GSD (broadening PSD) with increasing engine thrust. This broadening could be due to the lower tail of the distribution which is typically truncated near 7 to 10 nm in most standardized sizing methods. At higher thrust, the entire distribution including the lower tail can be accurately measured resulting in a more accurate determination of the GSD.
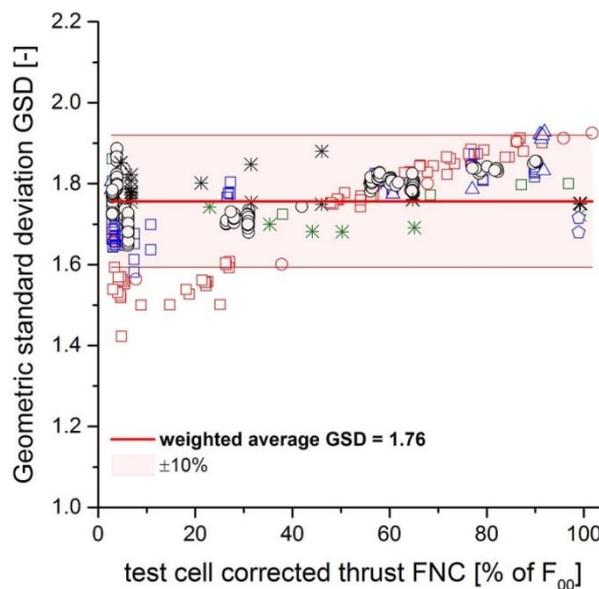


**Figure 7.2. GSD as a function of thrust measured using the single point probe and the multi-point probe (A-PRIDE 7). Colors correspond with the campaigns as follows: green – A-PRIDE 4, red – A-PRIDE 5, blue – A-PRIDE 7, and black – A-PRIDE 8.**

These GSDs are measured more than 30 m downstream of the sampling probe and are therefore not representative of the aerosol at the engine exit plane.

The PSDs are expected to be significantly altered after passing through the sampling system. Using the UTRC line loss model the PSDs at the exit plane can be estimated (Figure 7.3). The most noticeable influence of the system losses are at low thrust levels with the smallest GMD. Since the smallest particles are most affected, one can expect the GMD measured to be larger than that of the aerosol at the engine exit plane.
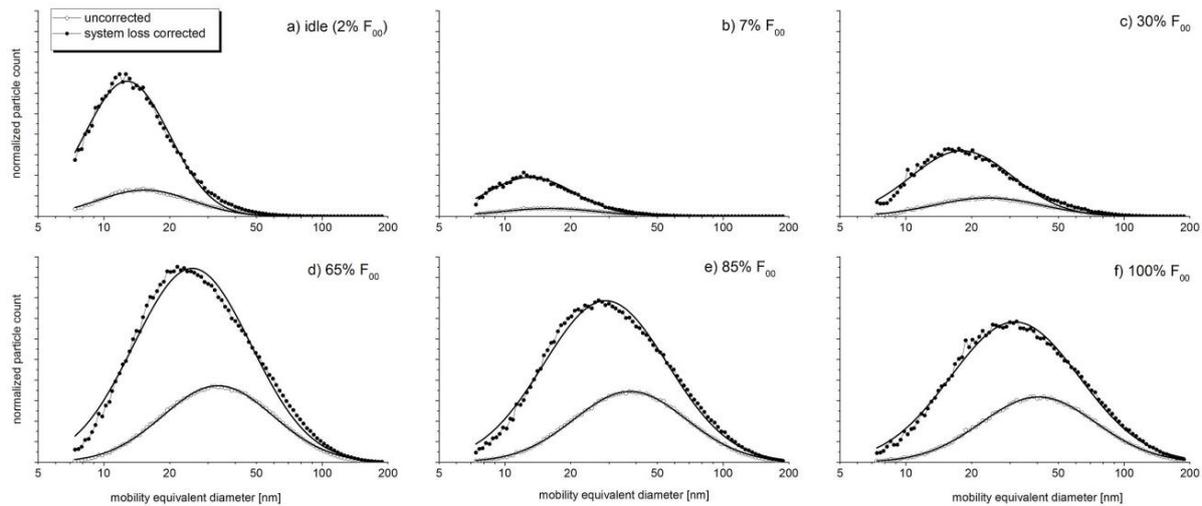


**Figure 7.3. Particle size distributions in the exhaust (A-PRIDE 7) measured and corrected for particle loss in the sampling system.**

The predicted system loss corrected lognormally parameterized PSD indeed have smaller GMD (Figure 7.4). For example, the measured 40 nm GMD at 100% thrust then corresponds to approx. 30 nm GMD at the engine exit plane. The system loss corrected distributions also exhibit broadening with engine thrust, with GSD of 1.6 at idle, linearly increasing up to 1.95 at maximum thrust.
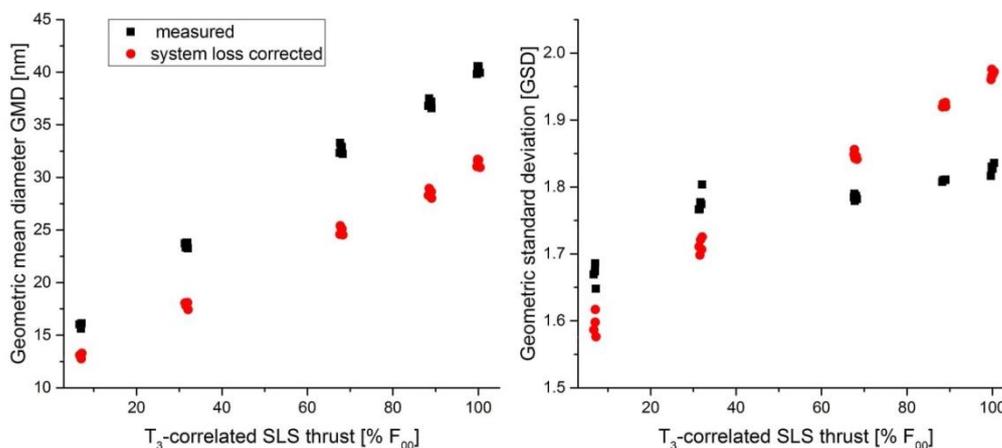


**Figure 7.4. GMD (left) and GSD (right) (A-PRIDE 7) of the measured and system loss corrected particle size distributions.**

## 7.4. nvPM mass instruments

The LII technology for determining nvPM mass has issues with its applicability to aircraft engine soot, if a laboratory soot source is used for calibration. A significant effort has been made in the lab and behind engines to investigate and solve this ongoing issue with SAE-E31 collaborators.

### 7.4.1. Mini-CAST soot study

Calibration of the nvPM mass measurement instruments MSS and LII has been an ongoing topic for the last couple of years. The community has addressed the guidance for showing conformity of nvPM mass instruments to the specifications, such that correct response of nvPM mass instruments to aircraft gas turbine soot is guaranteed in principle. However, the LII instrument currently has to be calibrated using an aircraft gas turbine to achieve this, which is very costly. Therefore, research is ongoing to find a suitable laboratory soot source, which would work for the calibration of all nvPM mass instruments. If a laboratory soot source is used, the only known requirement of the laboratory diffusion flame soot used for calibration is its EC content, which must be ≥80%, as determined using the NIOSH 5040 thermal-optical method. Therefore, in the spring of 2014, we designed and conducted a study at Missouri S&T looking at the response of the real-time BC mass measurement instruments MSS and LII using two different mini-CAST soot generators operated over a wide range of conditions, producing soot with various morphology, EC content, effective density, and GMD. The results of this study can be found in Durdina et al. 2016.

### 7.4.2. Mass instrument applicability check with engine exhaust

One dedicated day was spent in A-PRRIDE 8 to compare the real time mass instruments with EC filter mass collected on the diluted sampling line. It was a so called "mass instrument applicability check" as described in the ICAO Annex 16 Appendix 7, which will become effective around 2019. The OC/EC filters were not analyzed when this report was written so no conclusions can be made. Issue in the whole effort was also the calibration of the two LII instruments for which the data has also not been made available by NRC yet.

## 7.5. Speciation and quantification of volatile organic compounds

The measurement of VOCs emitted by aircraft engines is very important, because previous studies showed that engines emit very high concentrations of VOCs when they are operated at low power, so typically when the aircraft is on the ground. Thus, people who are in the airports, such as workers and travelers, and people living in the vicinity of airports, are potentially exposed to high concentrations of VOCs. Moreover, some VOCs are known to have adverse health effects. For instance, benzene,

formaldehyde, acetaldehyde, and 1,3-butadiene are in the group I of the IARC, and thus are known as carcinogenic to humans. Finally, VOCs play also an important role in climate. They can act as precursors in the ozone formation, and they can also participate in the new particle formation and growth. Therefore, it is important to have a better insight into the chemical composition of the VOCs emitted by aircraft engines.

Within the framework of this study, two different techniques have been used to measure unburned hydrocarbons. The first one is a flame ionization detector (FID) to measure online and in real time the total concentration of hydrocarbons, without any information on the chemical speciation. The second one is the use of adsorbing cartridges to sample VOCs, followed by the analysis of these VOCs by chromatography. Three different sorbents have been used: Carboxen 569 for the sampling of compounds with low molecular weight and high volatility (hydrocarbons C2-C5), Tenax TA for less volatile compounds (hydrocarbons C6-C20), and 2,4-dinitrophenylhydrazine (DNPH) for carbonyl compounds. With these three sorbents, a very large set of VOCs can be sampled and analyzed. Carboxen 569 and Tenax TA are analyzed by thermal desorption-gas chromatography/mass spectrometry (TD-GC/MS), while DNPH cartridges are analyzed by high performance liquid chromatography (HPLC). Results presented in this section come from piggy-back measurements performed in May 2015. VOCs have also been sampled and analyzed during A-PRIDE 8, but the data treatment is still ongoing.

Results obtained with the FID for all the engines are shown in Figure 7.5. The trend observed for all the engines is the same, and as expected. Indeed, at low thrust, we have a high emission of VOCs, due to the fact that at low thrust, the combustion is less efficient. Then, at high thrust, the combustion is much more efficient, and the VOCs are almost completely burned. We also notice that at ground idle, there is an important variability between the engines, with a ratio of 3 between the lowest and highest emission. These differences may be due to the status of the engines (e.g. refurbished engines, used engines being repaired, etc.).
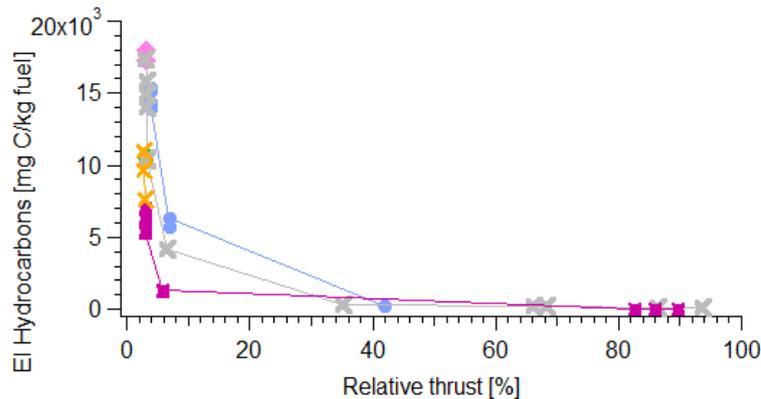
**Figure 7.5. Emission indices of total hydrocarbons measured by the FID as a function of the relative engine thrust.**

The comparison between adsorbing cartridges and the FID is shown in Figure 7.6. The FID gives the total concentration of hydrocarbons in ppm of carbon. For this comparison, we converted that unit in emission index (mass of carbon per kilo of fuel), and we converted the adsorbing cartridges data into the same unit as the FID. "VOCs cartridges" correspond to the sum of the VOCs sampled with Tenax TA and those with Carboxen 569. First, we notice an excellent agreement between the two methods ($r^2$ = 0.97). Then, the slope indicates that the sum of the VOCs sampled with Tenax TA and Carboxen 569 corresponds to 53% of the VOCs measured by the FID.
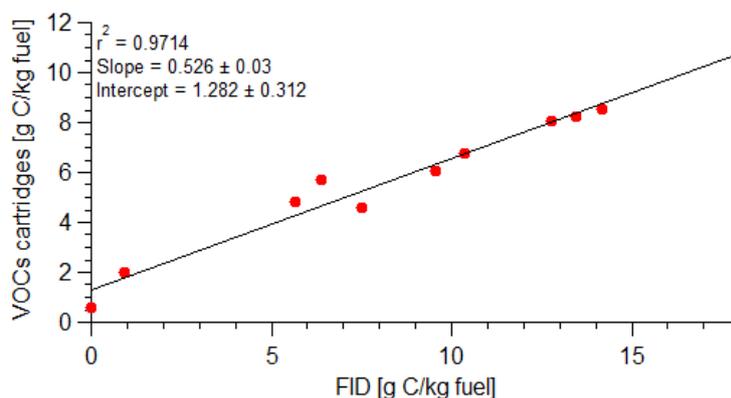


**Figure 7.6. Scatterplot of the sum of VOCs measured with adsorbing cartridges vs FID.**

Figure 7.7 shows the comparison between the chemical composition of the fuel and the VOCs in the exhaust. The exhaust corresponds to the average of all the ground idle periods for all the engines. The fuel samples have been analyzed by GC/MS in the same conditions as the VOCs cartridges. The fuel Jet A-1 is one of the most widely used in aviation, especially outside of the U.S. The Jet A-1 is

conventional kerosene, which is obtained by distillation of crude oil. Kerosene corresponds to the middle fraction, between gasoline and Diesel. The Jet A-1 is mainly constituted of alkanes, which account for roughly 80% of the total mass, and the rest is aromatics. The aromatic fraction contains mainly C2- to C4-benzenes, and traces of naphthalenes. Naphthalene and its 1-methyl and 2-methyl derivatives are the only PAHs that we found in the fuel, while heavier PAHs should be in the Diesel fraction. The composition of the exhaust is very different. We notice that a lot of compounds are present in the exhaust, but not in the fuel: alkenes, oxygenated compounds, benzene, and toluene. These compounds were supposedly formed either in the engine during the combustion or in the exhaust.
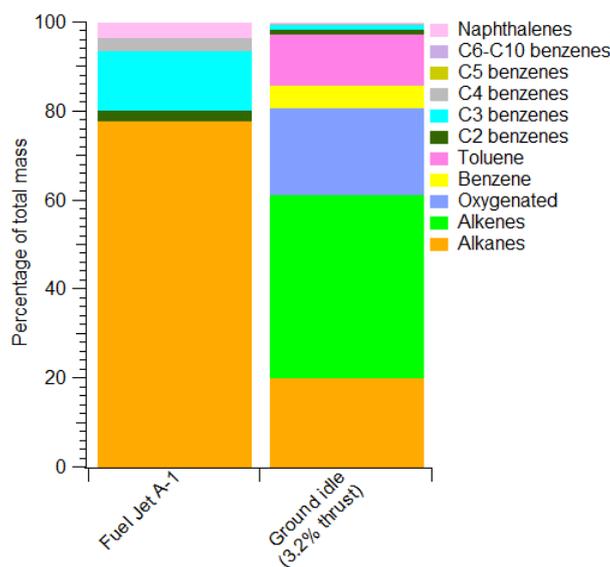


**Figure 7.7. Chemical composition of the fuel Jet A-1 (left) and of the VOCs in the exhaust (right, average for all the engines at ground idle).**

# 8. Project related activities and outreach

## 8.1. SAE-E31 Meetings

Empa has been an active contributor to the SAE E-31 committee meetings. Empa organized the SAE-E31 meeting that took place from January 22 to 25 2013 on the Empa campus in Dübendorf. The meeting was a success with a positive feedback from the participants.

Benjamin Brem attended the E-31 PM subcommittee meeting in Tullahoma TN on 3-5 December 2013. Lukas Durdina attended the annual E-31 committee meeting at Aerodyne in Boston MA on 2-6 June 2014 where he presented the results of the effective density and line loss correction analysis. Benjamin Brem and Lukas Durdina attended the SAE-E31 meeting in Graz at the beginning of December 2014.

## 8.2. Airport excursions ETH Zürich

Empa organized excursions for fourth semester students in the program of environmental engineering at ETH Zürich. The excursions occurred on May 8$^{th}$ 2013, April 9$^{th}$ 2014, and March 25$^{th}$ 2015. Special thanks belong to Frithjof Siegerist for helping in organizing the facility access and presenting SR Technics company background. In total, these excursions provided over 100 students the opportunity to visit our engine testing facilities, look closely at an airport and even visit the cockpit of an aircraft.

## 8.3. Tours of the testing facility

Empa participated actively in the BAFU excursion organized by FOCA on June 18, 2013. We had the opportunity to have Nadine Harivel and Delphine Lottin from SNECMA as visitors on one weekend during A-PRIDE7 besides Olivier Penanhoat SNECMA and Sara Rocci-Denis who were actively involved in the joint campaign. On April 24, 2015 a tour was given to Cercl'Air in collaboration with FOCA and SR Technics.

## 8.4. Public presentations

We actively presented the results from the BAZL project in many academic conferences and invited speeches. A list of the presentations is as follows.

Kilic, Dogushan, Rujin J. Huang, Benjamin Brem, Lukas Durdina, Imad El-Haddad, Felix Klein, Simone M. Pieber, Jing Wang, Theo Rindlisbacher, Jay Slowik, Urs Baltensperger and Andre S Prevot (2015) Direct emissions and oxidative processing of aircraft turbine engine exhaust, AGU fall meeting, San Francisco, December 14 – 18, 2015. (oral presentation)

Kilic, D., Huang, R-J., Brem, B., Durdina, L., El Haddad, I., Klein, F., Lavi, A., Pieber, S., Rindlisbacher, T., Rudich, Y., Wang, J., Slowik, J., Baltensperger, U., Prévôt, A. (2015) Secondary Organic Aerosol Formation from Aircraft Turbine Engine Exhaust, 34th annual conference of American Association for Aerosol Research (AAAR), October 12 – 16, 2015, Minneapolis. (oral presentation)

Wang, J., Brem, B., Durdina, L., Setyan, A., Kuo, Y-Y. (2015) Aircraft engine emission measurement in Zürich and comparative assessment, Aircraft Noise and Emission Reduction Symposium (ANERS), Sept. 22 – 25, 2015, La Rochelle, France. (oral presentation)

Setyan, A., Kuo, Y-Y., Brem, B.T., Durdina, L., Gerecke, A.C., Heeb, N.V. and Wang, J. (2015) Chemical characterization of volatile organic compounds emitted by aircraft engines, European Aerosol Conference, Sept 6 – 11, 2015, Milan. (oral presentation)

Wang, J. (2015) Particulate Matter and Gas Phase Emission Measurement of Aircraft Engine Exhaust, Federal Office for the Environment (BAFU), Bern, Sept 2nd, 2015. (invited talk)

Brem, B., Durdina, L., Rindlisbacher, T., Siegerist, F., Rocci-Denis, S., Penanhoat, O., Andac, G., Zelina, J. and Wang, J. (2015) Sensitivity of aircraft gas turbine non- volatile particulate matter mass and number emissions to fuel aromatic content. 19th ETH-Conference on Combustion Generated Nanoparticles, Zurich, June 28 – July 1, 2015. (poster)

Abegglen, M., Sierau, B., Brem, B., Wang, J., Rindlisbacher, T. and U. Lohmann (2015) Chemical characterization of particulate matter aircraft turbine engine exhaust using single particle mass spectrometry. 19th ETH-Conference on Combustion Generated Nanoparticles, Zurich, June 28 – July 1, 2015. (oral presentation)

Durdina, L., Brem, B., Rindlisbacher, T., Siegerist, F., Rocci-Denis, S., Penanhoat, O., Andac, G., Zelina, J. and Wang, J. (2015) Spatial variability of PM and gaseous emissions at the exit plane of an in-service commercial aircraft turbine engine. 19th ETH-Conference on Combustion Generated Nanoparticles, Zurich, June 28 – July 1, 2015. (oral presentation)

Durdina, L., Lobo, P., Black, E., Trueblood, M.B., Hagen, D.E., Whitefield, P. and Wang, J. (2015) Suitability of two mini-CAST generators as laboratory surrogate sources for black carbon mass measurements in the aircraft engine exhaust, Aerosol Technology Conference 2015, June 15 – 17, Tampere, Finland. (oral presentation)

Wang, J. (2014) Sino-Swiss Cooperation on Air Quality and Pollution Control Technologies, College of Environmental Sciences and Engineering, Peking University, Sept 3rd, 2014. (invited talk)

Wang, J. (2014) Sino-Swiss Cooperation on Air Quality and Pollution Control Technologies, China Meteorological Administration, Sept 4th, 2014. (invited talk)

Wang, J. (2014) Release of nanomaterials into the environment: examples from nanocomposites to aircraft engines, invited keynote speaker for International Aerosol Conference, Busan, Korea, Aug 28 – Sept 2, 2014. (keynote presentation)

Huang, R-J., Kilic, D., Wolf, R., Slowik, J., Durdina, L., Brem, B., Rindlisbacher, T., Wang, J., Baltensperger, U. and Prévôt, A.S.H. (2014) Secondary aerosol formation from aircraft exhaust. International Aerosol Conference, Busan, Korea, Aug 28 – Sept 2, 2014. (poster)

Brem, B., Durdina, L., Suri, A., Rindlisbacher, T., Siegerist, F. and Wang, J. (2014) Variability in non-volatile particulate matter mass and number emissions of aircraft gas turbine engines: a piggy-back study. 18th ETH-Conference on Combustion Generated Nanoparticles, Zurich, June 22nd – 25th 2014. (oral presentation)

Durdina, L., Brem, B., Abegglen, M., Sierau, B. and Wang, J. (2014) Improved determination of soot PM emissions from aircraft turbine engines using effective density. 18th ETH-Conference on Combustion Generated Nanoparticles, Zurich, June 22nd – 25th 2014. (poster)

Brem, B., Durdina, L., Liati, A., Wichser, A., Rindlisbacher, T. and Wang, J. (2014) Thrust Dependent Metal Particle Emissions from an Aircraft Gas Turbine Source. Aerosol Technology Conference 2014, June 16 – 18, Karlsruhe, Germany. (oral presentation)

Durdina, L., Brem, B. and Wang, J. (2014) Techniques for estimation of non-volatile particulate matter mass in aircraft turbine engine exhaust. Aerosol Technology Conference 2014, June 16 – 18, Karlsruhe, Germany. (oral presentation)

Abegglen, M., Durdina, L., Brem, B., Rindlisbacher, T., Wang, J., Lohmann, U. and Sierau, B. (2014) Effective density measurements of aircraft exhaust. European Geosciences Union General Assembly 2014, Vienna, Austria, 27 April – 02 May, 2014. (poster)

Abegglen, M., Sierau, B., Mensah, A., Wang, J., Durdina, L., Gysel, M., Lohmann, U. (2013) Effective density measurements of different fresh soot types, European Aerosol Conference, Sept 1-6, 2013, Prague (poster).

Brem, B., Durdina, L. and Wang, J. (2013) Measurement of Non-Volatile Particulate Matter Mass Emission Indices of Aircraft Gas Turbine Sources, European Aerosol Conference, Sept 1-6, 2013, Prague (poster).

Durdina, L., Brem, B., Abegglen, M., Sierau, B. and Wang, J. (2013) Effective density of particulate matter emitted from aircraft gas turbine engine sources, European Aerosol Conference, Sept 1-6, 2013, Prague (poster).

Brem, B., Durdina, L. and Wang, J. (2013) Non-Volatile Particulate Matter Mass and Number Emission Indices of Aircraft Gas Turbine Sources, 17th ETH-Conference on Combustion Generated Nanoparticles, June 23th – 26th 2013 (oral presentation).

Durdina, L., Abegglen, M., Brem, B., Sierau, B. and Wang, J. (2013) Effective Density Characterization of Soot Particles Emitted from Aircraft Gas Turbine Engine Sources, 17th ETH-Conference on Combustion Generated Nanoparticles, June 23th – 26th 2013 (poster).

# 9. Summary

During the project "Particulate and gas phase emission measurement of aircraft engine exhaust", we in collaboration with FOCA have built up a world unique system in an engine test cell near the Zürich airport which allows measurement of commercial aircraft engines. The sophisticated sampling system and state-of-the-art instruments are applied to measure the size, number and mass concentrations, elemental and organic carbon fractions, and chemical composition of the emitted particles. Gas-phase hydrocarbon and volatile organic compounds are measured. The accurate measurement of aircraft emissions is crucial for the establishment of emission inventories and for the assessment of aviation impacts on human health, the environment and climate. The project contributes significantly to the international standard passed in 2016 for aircraft emission of particulate matter under the auspices of the International Civil Aviation Organization. The Zürich system serves as the reference system for the standard. The European Aviation Safety Agency, US Federal Aviation Administration and Environmental Protection Agency, and Transport Canada have committed significant support for the project in addition to the FOCA grant.

To date we have measured a large number in-service aircraft engines, and obtained emission indices for particulates and gases (Lobo et al. 2015; Boies et al. 2015). The particle size distribution, primary particle size and morphology, particle crystalline structure and reactivity have been analyzed at different thrust levels (Liati et al. 2014). The effective density and fractal structure of the particles have been quantified (Durdina et al. 2014, Johnson et al. 2015, Abegglen et al. 2015) and used to determine the mass emissions (Durdina et al. 2014). The metal components of the emissions have been analyzed (Abegglen et al. 2016) and we are indentifying and quantifying the organic chemicals.

In addition to the standard system, we built up advanced capabilities for the Zürich system. The installation of a sampling probe that is capable of traversing the vertical and horizontal directions of the engine exhaust plane was completed with additional support by a Swiss National Science Foundation grant (SNF award ID: 206021_157663). It improves the emission measurement by providing vastly improved spatial resolution over the previously fixed probe. A fuel doping system was constructed. This automated system enables mixing of fuels with different compositions and controls the flow rates accurately to ensure that the result is within the specifications of the jet fuel standard. We investigated the correlations between fuel aromatic compositions and emissions (Brem et al. 2015). These infrastructures further strengthen our capabilities in the field of aircraft emission studies.

Empa is continuing the research on aircraft engine emissions. As an extension of the project "Particulate and gas phase emission measurement of aircraft engine exhaust", a second project

"EMissions of Particulate and gaseous pollutants in AIRcraft engine Exhaust (EMPAIREX)" sponsored by FOCA has started. We look forward to contributing more results to better understand the environmental and health impacts of civil aviation and to facilitate the impact reduction in the long term.

# References:

Boies, A.M., Stettler, M.E.J., Swanson, J.J., Johnson, T.J., Olfert, J.S., Johnson, M., Eggersdorfer, M.L., Rindlisbacher, T., Wang, J., Thomson, K., Smallwood, G., Sevcenco, Y., Walters, D., Williams, P.I., Corbin, J., Mensah, A.A., Symonds, J., Dastanpour, R. and Rogak, S.N. (2015) Particle emission characteristics of a gas turbine with a double annular combustor, *Aerosol Science and Technology*, 49 (9), 842-855, DOI:10.1080/02786826.2015.1078452.

Bond, T.C., et al., *A technology-based global inventory of black and organic carbon emissions from combustion.* Journal *of Geophysical Research: Atmospheres*, 2004. 109(D14): p. D14203.

Brem, B., Durdina, L., Siegerist, F., Beyerle, P., Bruderer, K. Rindlisbacher, T., Rocci-Denis, S., Andac, M.G., Zelina, J., Penanhoat O. and Wang, J. (2015) Effects of fuel aromatic content on non-volatile particulate emissions of an in-production aircraft gas turbine, *Environmental Science & Technology*, 49, 13149 – 13157, DOI: 10.1021/acs.est.5b04167.

Corbin, J. C., B. Sierau, M. Gysel, M. Laborde, A. Keller, J. Kim, A. Petzold, T. B. Onasch, U. Lohmann, and A. A. Mensah. "Mass spectrometry of refractory black carbon particles from six sources: carbon-cluster and oxygenated ions." *Atmospheric Chemistry and Physics* 14, no. 5 (2014): 2591-2603.

Crayford, A., Johnson, M., Marsh, R., Sevcenco, Y., Walters. D., Williams, P., Petzold, A., Bowen, P., Wang, J., Lister, D. (2012) Studying, sAmpling and Measuring of aircraft ParticuLate Emissions III – Specific Contract 02 SAMPLE III – SC.02, final report for European Aviation Safety Agency, project EASA.2010.FC.10, Specific Contract 02. http://www.easa.europa.eu/safety-and-research/research-projects/environment.php .

DeWitt, M. J.; Corporan, E.; Graham, J.; Minus, D., Effects of aromatic type and concentration in Fischer− Tropsch fuel on emissions production and material compatibility. *Energy & Fuels* 2008, *22*, (4), 2411-2418.

Döpelheuer, A.; Lecht, M. In *Influence of engine performance on emission characteristics*, RTO Meeting proceedings, 1999.

Durdina, L., Brem, BT, Abegglen, M., Lobo, P., Rindlisbacher, T., Thomson, K, Smallwood, GJ, Hagen, D.E., Sierau, B. and Wang, J. (2014), Determination of PM mass emissions from an aircraft turbine engine using particle effective density, *Atmospheric Environment*, 99, 500–507, DOI:10.1016/j.atmosenv.2014.10.018.

Durdina, L., Lobo, P., Trueblood, M.B., Black, E.A., Achterberg, S., Hagen, D.E., Brem, B.T., Wang, J. (2016) Response of Real-Time Black Carbon Mass Instruments to Mini-CAST Soot, *Aerosol Science and Technology*, accepted.

Frenklach, M., Reaction mechanism of soot formation in flames. *Physical Chemistry Chemical Physics* 2002, *4*, (11), 2028-2037.

Hadaller, O.; Johnson, J., World fuel sampling program. *Coordinating Research Council, Inc., CRC Report* 2006, (647).

Johnson, T.J., Olfert, J.S., Symonds, J.P.R., Johnson, M., Rindlisbacher, T., Swanson, J.J., Boies, A.M., Thomson, K., Smallwood, G., Walters, D., Sevcenco, Y., Crayford, A., Dastanpour, R., Rogak, S.N., Durdina, L., Bahk, Y.K., Brem, B. and Wang, J. (2015) Effective density and mass-mobility exponent of aircraft turbine particulate matter, *Journal of Propulsion and Power*, 31(2), 573 – 582, DOI: 10.2514/1.B35367.

Liati, A., Brem, B., Durdina, L., Vögtli, M., Arroyo Rojas Dasilva, Y., Dimopoulos Eggenschwiler, P., and Wang, J. (2014) Electron microscopic study of soot particulate matter emissions from aircraft turbine engines, *Environmental Science & Technology*, 48 (18), 10975–10983, DOI:10.1021/es501809b.

Liscinsky, D. S., Bhargava, A., Colket, M. B., Hautman, D. C., Hollick, H. H., and True, B. (2010). Effect of Particle Sampling Technique and Transport on Particle Penetration at the High Temperature and Pressure Conditions Found in Gas Turbine Combustors and Engines. NASA/CR-2010eNNC07CB03C. NASA/Glenn Research Center, Cleveland, OH.

Lobo, P., Durdina, L., Smallwood, G.J., Rindlisbacher, T., Siegerist, F., Black, E.A., Yu, Z., Mensah, A.A., Hagen, D.E., Miake-Lye, R.C., Thomson, K.A., Brem, B.R., Corbin, J.C., Abegglen, M., Sierau, B., Whitefield, P.D. and Wang, J. (2015) Measurement of Aircraft Engine Non-volatile PM Emissions: Results of the Aviation - Particle Regulatory Instrument Demonstration Experiment (A-PRIDE) 4 Campaign. *Aerosol Science and Technology*, 49:472 – 484, DOI: 10.1080/02786826.2015.1047012.

Lobo, P.; Rye, L.; Williams, P. I.; Christie, S.; Uryga-Bugajska, I.; Wilson, C. W.; Hagen, D. E.; Whitefield, P. D.; Blakey, S.; Coe, H.; Raper, D.; Pourkashanian, M., Impact of Alternative Fuels on Emissions Characteristics of a Gas Turbine Engine – Part 1: Gaseous and Particulate Matter Emissions. *Environmental Science & Technology* 2012, *46*, (19), 10805-10811.

Masiol, M. and R.M. Harrison, *Aircraft engine exhaust emissions and other airport-related contributions to ambient air pollution: A review. Atmospheric Environment*, 2014. 95: p. 409–455.

Richter, H.; Howard, J. B., Formation of polycyclic aromatic hydrocarbons and their growth to soot—a review of chemical reaction pathways. *Progress in Energy and Combustion science* 2000, *26*, (4), 565-608.

Schürmann, G., et al., *The impact of NOx, CO and VOC emissions on the air quality of Zurich airport. Atmospheric Environment*, 2007. 41(1): p. 103–118.

Timko, M. T.; Yu, Z.; Onasch, T. B.; Wong, H.-W.; Miake-Lye, R. C.; Beyersdorf, A. J.; Anderson, B. E.; Thornhill, K. L.; Winstead, E. L.; Corporan, E.; DeWitt, M. J.; Klingshirn, C. D.; Wey, C.; Tacina, K.; Liscinsky, D. S.; Howard, R.; Bhargava, A., Particulate Emissions of Gas Turbine Engine Combustion of a Fischer–Tropsch Synthetic Fuel. *Energy & Fuels* 2010, 24, (11), 5883–5896.

Yim, S.H.L., et al., *Global, regional and local health impacts of civil aviation emissions. Environmental Research Letters*, 2015. 10(3): p. 034001.

Yim, S.H.L., M.E.J. Stettler, and S.R.H. Barrett, *Air quality and public health impacts of UK airports. Part II: Impacts and policy assessment.* Atmospheric Environment, 2013. 67: p. 184–192.